

UNIVERSITY OF OKLAHOMA

GRADUATE COLLEGE

DESIGN AND SYNTHESIS OF NEW CLPP ACTIVATORS:

TOWARDS THE DEVELOPMENT OF A
COMPUTATIONALLY GUIDED APPROACH

A THESIS

SUBMITTED TO THE GRADUATE FACULTY

in partial fulfillment of the requirements for the

Degree of

MASTER OF SCIENCE

By

QUENTIN P. AVILA
Norman, Oklahoma
2016

DESIGN AND SYNTHESIS OF NEW CLPP ACTIVATORS:
TOWARDS THE DEVELOPMENT OF A
COMPUTATIONALLY GUIDED APPROACH

A THESIS APPROVED FOR THE
DEPARTMENT OF CHEMISTRY AND BIOCHEMISTRY

BY

Dr. Adam S. Duerfeldt, Chair

Dr. Robert H. Cichewicz

Dr. Daniel T. Glatzhofer

Dr. Pascal De Sainte Claire

Dr. Isabelle Ripoché

© Copyright by QUENTIN P. AVILA 2016
All Rights Reserved.

Acknowledgements

I would like first to thank Dr. Adam Duerfeldt for his support from the first day I arrived in Oklahoma. I could not hope to have a better mentor, he transmitted his passion for medicinal chemistry to me through his teachings and his encouragements. Not every supervisor would have let me follow my own path and I could always count on his guidance and friendship in difficult times.

I wish to thank the Department of Chemistry and Biochemistry and particularly my committee members, Dr. Glatzhofer and Dr. Cichewicz, for giving the keys to success as a graduate student, an organic chemist and a scientist. Furthermore, I would like to thank the OU-Blaise Pascal program for giving me the opportunity to travel, to learn, and to experience such an adventure. I hope that this program will carry on because it is proof that travel broadens the mind. I wish to express my gratitude to Dr. Ripoché and Dr. De Sainte Claire for their help and support, not only during the past year, but also when I was in Clermont-Ferrand.

I wish to thank the Duerfeldt lab, Nate, Dinesh, Yangxiong, Jessi and Xiaoxheng, for their friendship and team spirit. Coming from another country is not easy and I found some true friends within the Department who helped me feel more at home. Finally, I want to thank my parents and my sister for their support and their love no matter how far I am from them.

Table of Contents

Acknowledgements	iv
List of Figures.....	viii
List of Tables	xii
Chapter 1	1
Bacterial Caseinolytic Protease P: A Promising Target for Antibacterial Development	1
1. Antibiotic Resistance	1
1.1. Current State of Antibiotics	1
1.2. Resistance in Bacteria	2
1.3. Addressing Resistance.....	5
2. Bacterial Caseinolytic Protease P	6
2.1. Background.....	6
2.2. ClpP Chemo-modulation: A New Antibacterial Strategy	10
Chapter 2	15
Computational Assessment of Small Molecule ClpP Activators	15
1. Structure-Activity Relationships of the ACP4/5 Scaffold	15
1.1. Introduction	15
1.2. ACP4/5 Structure-Activity Relationship Summary	18
2. Computational Analysis of the ACP4/5•EcClpP Interactions	27
2.1. Docking Study of ACP4/5 on EcClpP	28
2.1.1. Introduction.....	28
2.1.2. Methods	31
2.1.3. Results and Discussion	32

2.2. The Frontier Molecular Orbital Theory: A Tool to Enhance	
Molecular Recognition	49
2.2.1. Introduction.....	49
2.2.2. Methods	53
2.2.3. Results and Discussion	53
2.2.3.1. Phenyl Moiety Analysis	53
2.2.3.1.1. Halogen Bonding.....	53
2.2.3.1.2. Phenyl Ring	56
2.2.3.2. Dihalovinyl Moiety	61
2.2.3.3. Ester Moiety	63
3. Future Directions	64
Chapter 3	67
Design and Synthesis of ACP Analogues	67
4. Rationale Design of New ACP Analogues.....	67
4.1. Introduction	67
4.2. Rationale and Design of New Phenyl Substituted ACP Analogues ..	68
4.2.1. Design of ADEP-inspired Analogues	68
4.2.2. Design of ACP1-Inspired Analogues.....	69
4.3. Rationale and Design of New Dihalovinyl Substituted ACP	
Analogues	71
4.4. Rationale and Design of New Ester Substituted ACP Analogues	71
5. Synthesis of ACP Analogues	73
5.1. Robinson Annulation	73
5.2. Dichlorovinyl Chalcone Synthesis.....	78
5.3. Synthesis	79
5.4. Alternate Route to Dichlorovinyl Chalcone.....	82

6. Determination of ACP4/5 Binding Pocket via Photo Affinity

Labelling 84

6.1. Introduction	84
6.2. Results and Discussion	87
6.2.1. Synthesis of Azido-ACP4/5 Analogues.....	87
7. Future directions.....	88
8. Experimental Section.....	89
8.1. Synthesis of ACP4/5 Analogues.....	89
8.2. Synthesis of Dichlorovinyl Chalcones and Precursors.....	96
References.....	101
Appendix.....	113
Compound key	113
Spectral Data for All Identified Compounds and Intermediates	115

List of Figures

Figure 1. Antibiotic introduction and first detection of resistance.	4
Figure 2. Structure of tetradecameric <i>Escherichia coli</i> ClpP.	7
Figure 3. X-ray structure of <i>E. coli</i> ClpP monomer.....	8
Figure 4. Model for natural co-chaperone-mediated ClpP activation.....	9
Figure 5. Chemical structures of ClpP activators.	11
Figure 6. Chemical structures of ClpP inhibitors.....	13
Figure 7. Chemical structures of ACP4 (left) and ACP5 (right).	16
Figure 8. Minimized structure of ACP5.	16
Figure 9. Predicted EcClpP binding pockets (PDB: 3MT6).....	17
Figure 10. Plot of <i>para</i> -substituent electronegativity versus ClpP activation.	20
Figure 11. SAR summary of ACP4/5 scaffold.	26
Figure 12. Co-crystal of ADEP1 (green/yellow) bound to EcClpP (grey) (PDB: 3MT6).	31
Figure 13. Superimposition of ADEP1 (green) and ACP5 (7) (orange) bound to EcClpP.	33
Figure 14. Experimentally determined ClpP activation activity of ACP4/5 analogues.	34
Figure 15. Predicted binding affinities of ACP4/5 analogues calculated by Glide (grey) and AutoDock (black).....	34
Figure 16. Predicted binding conformation of ACP5 (7) in EcClpP•ADEP binding pocket, calculated by Glide.....	36
Figure 17. Close up view of superimposed phenyl ring moieties of compounds 6, 7, 11, 12, 13, 15, 16 and 18, and the surrounding residues.....	37

Figure 18. Close up view of superimposed phenyl ring moieties of compounds 6, 7, 11, 12, 13, 15, 16 and 18, and surrounding residues.....	38
Figure 19. Predicted binding interactions of 6, 7, 11, 12, 13, 15, 16 and 18 with the surrounding residues Thr79 and Met92.	39
Figure 20. Traditional (left) and current (right) electrostatic representation of a halobenzene.....	40
Figure 21. Close up view of superimposed dihalovinyl moieties of compounds 7 and 23, and the surrounding residues Phe112, Ser88 and Tyr60.....	44
Figure 22. Superimposition of predicted docking conformations of 7 (orange) and 23 (green).	44
Figure 23. Binding conformation of compounds 7 and 23, and surrounding residues Phe112, Ser88 and Tyr60.....	45
Figure 24. Close up view of the superimposed ester moieties of compounds 7, 27, 28 and 29, and the surrounding EcClpP residue Tyr60.	47
Figure 25. Predicted binding conformation of compounds 7, 27, 28 and 29.....	47
Figure 26. Docking studies summary of ACP5.	48
Figure 27. Diagram of frontier molecular orbital interactions.....	52
Figure 28. Electrostatic potential (ESP) isosurfaces of fluorobenzene, chlorobenzene, bromobenzene and iodobenzene.	54
Figure 29. LUMOs of the phenyl portion of analogues 13, 7 and 15.....	54
Figure 30. HOMO of threonine.	54
Figure 31. Relative EcClpP activation of compounds 13, 7 and 15.	56
Figure 32. Correlation of LUMO energy and halogen electron density for 13, 7 and 15.....	56

Figure 33. Favorable aromatic stacking arrangements and schemes representing the partial negative charge (blue) and the partial positive charge (red).....	57
Figure 34. ACP5 (7) phenyl ring and predicted interactions with (a) Phe82 and (b) Tyr62.....	58
Figure 35. HOMOs and LUMOs of ACP5 (7) phenyl ring.	58
Figure 36. a. RD ₂₅ of ACP4/5 analogues; b. phenyl ring LUMO energies of ACP4/5 analogues.....	61
Figure 37. Different geometries of halogen(X)-aromatic interactions.	62
Figure 38. HOMOs of compound 7 and 23.	63
Figure 39. Energies of HOMOs of compounds 27, 7, 28 and 29.	64
Figure 40. Chemical structure of ADEP4.	68
Figure 41. ADEP-inspired ACP analogues.....	69
Figure 42. ACP1-Inspired ACP analogues.	71
Figure 43. Difluorovinyl ACP analogue.	71
Figure 44. Keto-, amido- and carboxyl ACP analogues.	72
Figure 45. Synthetic route to ACP4/5 analogues.....	73
Figure 46. Expected enantiomers of synthesized ACP4/5 analogues.....	73
Figure 47. ¹ H NMR spectra of compounds (a) 34, (b) 59, (c) 72, (d) 73.	74
Figure 48. Analysis of Michael addition of 50 with 51 via steric approach control..	76
Figure 49. Cyclisation analysis via steric approach control and chelation control....	78
Figure 50. Synthetic route to dichlorovinyl chalcones.	79
Figure 51. Synthetic routes to dichlorovinyl chalcones (a) 58, (b) 61.....	80
Figure 52. Synthetic routes to compounds (a) 34, (b) 47 and (c) 59.	81
Figure 53. Dichlorovinyl chalcone synthesis via β-ketosulfoxide addition.	82
Figure 54. Dichlorovinyl chalcone generation via Heck coupling reaction.	83

Figure 55. Retrosynthetic scheme of compound 35.....	83
Figure 56. Photoactivation mechanism of aryl azides.	85
Figure 57. Target ACP4/5 azido-analogues.....	86
Figure 58. Synthetic route to analogues 3/4-azido ACP4/5 analogues.....	87
Figure 59. Generation of azido-acetophenones via proline-promoted CuI-catalyzed coupling reaction.....	88

List of Tables

Table 1. Relative ClpP activation of <i>para</i> -phenyl substituted ACP4/5 analogues.	21
Table 2. Relative ClpP activation of altered dihalovinyl ACP4/5 analogues.	23
Table 3. Relative ClpP activation of alkyl ester ACP4/5 analogues.	24
Table 4. Cyclohexanone modification and associated activities.	26
Table 5. Calculated distance between ACP5 phenyl ring moiety and surrounding residues.	37
Table 6. Calculated distance between ACP4/5 analogues <i>para</i> -substituent and surrounding residues.	38
Table 7. Standard distances between halogen and halogen bond acceptors (Å).	41
Table 8. Calculated distances and angles between dihalovinyl moiety of compounds 7 and 23, and Ser88.	45
Table 9. Calculated distances between ACP4/5 ester moiety and Tyr60.	47
Table 10. Calculated energy differences between <i>cis/trans</i> ester conformation.	48
Table 11. Subset of ACP1 analogues and ADEP derivative.	69
Table 12. Conditions explored to synthesize dichlorovinyl <i>para</i> -bromochoalcone 58.	79
Table 13. Linear and non-linear volumes of atom/group of atoms in Å ³	87

Chapter 1

Bacterial Caseinolytic Protease P: A Promising Target for Antibacterial Development

1. Antibiotic Resistance

1.1. Current State of Antibiotics

“The time may come when penicillin can be bought by anyone in the shops. Then there is the danger that the ignorant man may easily underdose himself and by exposing his microbes to non-lethal quantities of the drug make them resistant.”

These words were spoken by none other than Alexander Fleming at his Nobel Prize acceptance speech in 1945 for the discovery of penicillin. Seventy years later, it is clear that it was a prediction rather than a warning. Even though penicillin, and antibiotics that followed, revolutionized the way bacterial infections are treated, the unfortunate result of their (mis)use, however, is the emergence of antibiotic resistant bacteria.

With his discovery of penicillin, Fleming put in motion a new avenue of drug discovery aimed at developing drugs capable of killing, or at least inhibiting the growth of microorganisms (e.g. bacteria, fungi, etc) to treat infection. By definition, antibiotics are secondary metabolites isolated from microorganisms or synthetic derivatives thereof. Current antibiotics affect the survival of bacteria through different mechanisms of action, all of which operate through inhibition or disruption of key bacterial processes. The most common mechanisms exploited by clinical antibiotics include the disruption of cell wall synthesis, inhibition of protein biosynthesis, or the interference of bacterial DNA replication or transcription.¹ Efforts to expand the scope of mechanism of action have been relatively unsuccessful over recent years and efforts have instead focused on the development of derivatives of known antibiotics. In fact, since 1998, only four antibacterial drugs

with novel mechanisms of action have been approved by the FDA, and between 1980 and 2005, 34 of the 59 approved antimicrobials, were β -lactams derivatives.^{2,3}

Global antibiotic consumption is estimated to exceed 70 billion doses per year. Unfortunately, 20–50% of antibiotic use suffers from poor patient compliance and/or inappropriate treatment selection (e.g. use for viral infections, unnecessary selection of broad spectrum agents).⁴ Despite the effectiveness of modern antibiotics, the emergence of bacterial resistance continues to outpace the development of new therapeutics and represents a serious threat to public health.

Historically, high-throughput screening of natural products has been a major resource for the discovery of new antibiotics. However, rediscovery of known compounds has prompted researchers to explore uncultured microorganisms, new cultivation conditions, and biosynthetic manipulation to increase chemical diversity. In addition to novel discovery approaches, medicinal chemistry programs have employed methods such as structure-activity relationship (SAR) studies, which have been pivotal in advancing the understanding of ligand-receptor interactions and allowing a more rational design of pharmaceuticals with optimized properties.⁵ Even with the advancements in discovery and design methods, our ability to address antibacterial drug resistance will only be possible through the exploitation of novel targets.

1.2. Resistance in Bacteria

Resistance in bacteria is a natural process that occurs through spontaneous mutation, gene regulation, and/or horizontal gene transfer.⁶ Exposure to antibiotics results in a selective pressure that often drives the emergence of resistant phenotypes. Common mechanisms of resistance include target modification (e.g.

upregulation, downregulation or structural modification), efflux pump overexpression, and enzymatic drug inactivation. Microbial evolution is rapid and robust. By employing these mechanisms, bacteria evade antibiotic intervention, leading to microbial populations that are unresponsive to therapeutic intervention.

As shown in Figure 1, most mechanistically distinct antibiotics were discovered during the “golden era of antibiotics” (1950–1980).^{7,8} Not until 2000, with the FDA approval of the oxazolidinones (linezolid), was a new antibiotic class discovered. This “intermission” testifies to the mindset of researchers at the time who declared a premature victory over infectious disease: *“It is time to close the book on infectious disease, declare the war on pestilence won and shift national resources to such chronic problems as cancer and heart disease.”* (William Stewart, U.S. Surgeon General, 1969).⁹ Therefore, their approach to address resistance was to optimize existing antibiotic chemotypes, by creating effective “quick-fix” therapeutics, but it has led to an innovation gap. Even with the introduction of new antibiotic classes, the time span between the introduction and identification of a resistant strain is strikingly short due to the adaptive flexibility of bacteria (Figure 1).

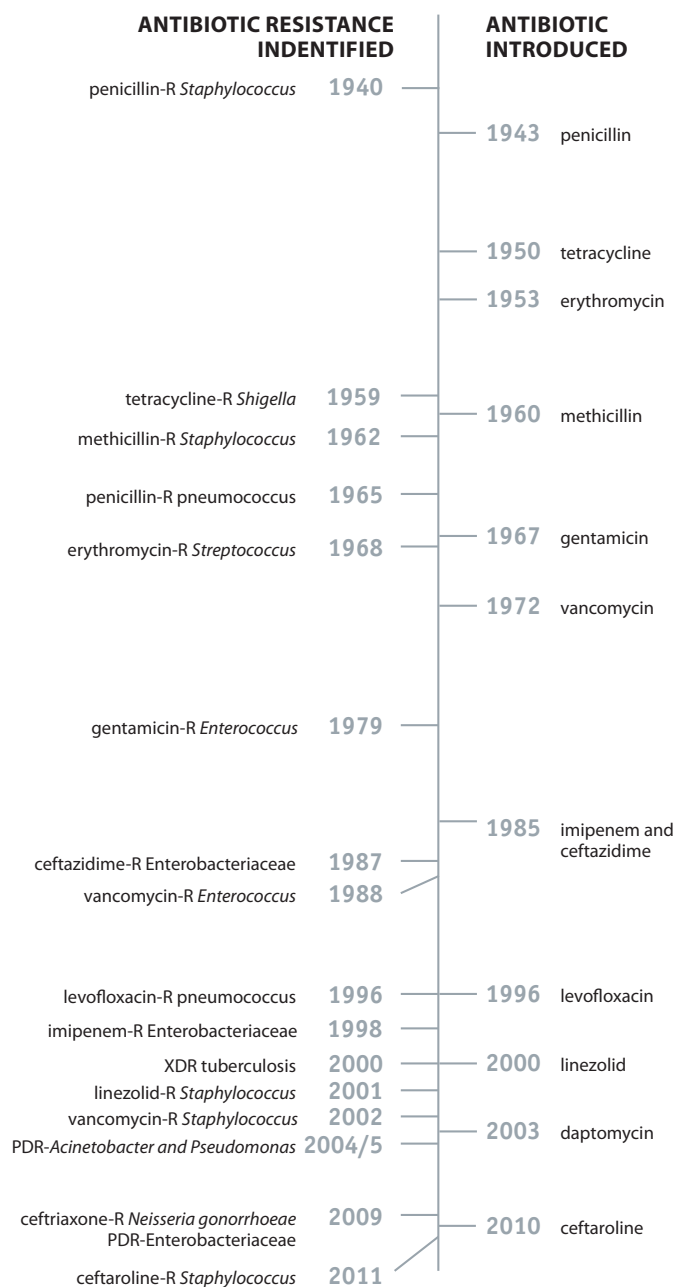


Figure 1. Antibiotic introduction and first detection of resistance.^a

With resistance outpacing the development of new antibiotics, a number of historically useful antibiotics are now irrelevant. β -lactams, the most commonly prescribed antibiotics (60% of total consumption), now have limited utility, as resistant strains like Methicillin-resistant *Staphylococcus aureus* (MRSA) have

^a Figure from <https://www.cdc.gov/drugresistance/pdf/5-2013-508.pdf>.

emerged and can circumvent the β -lactam mechanism of action of cell wall synthesis inhibition.¹⁰ This resistant strain of *S. aureus* represents a serious threat to hospitals and communal settings, due to its ability to enzymatically inactivate traditional β -lactams. However, MRSA is not the only “superbug”, as Vancomycin-resistant *Enterococci* (VRE), Carbapenem-resistant *Enterobacteriaceae* and multidrug-resistant *Mycobacterium tuberculosis* have emerged and are also unresponsive to most antibiotics. As such, there is a concern that society may find itself with no defense against the developing superbugs, prompting society to address this issue. Unfortunately, this concern is quickly becoming reality, as more than 700,000 people died due to antibiotic resistance in 2014 and by 2050 this number is expected to reach 10,000,000.¹¹

1.3. Addressing Resistance

In an effort to slow resistance emergence, the Centers for Disease Control (CDC) recently released a recommendation report that suggests an increase in funding for antibacterial research and a global public awareness campaign focused on reducing the unnecessary use and dissemination of antibiotics in environmental/agricultural settings.

In addition to more stringent regulations, new directions in research should also be pursued in order to break the cycle of perpetual bacterial resistance. One promising avenue is to develop antibiotics with new mechanisms of action that exhibit no observed cross-resistance to clinical options. New antibiotic classes are expected to have a longer delay of resistance emergence than new generations of current antibiotics. Therapeutics that exploit new targets provide unfamiliar challenges to bacteria; and thus require the development of completely new resistance regimes, potentially lengthening the duration of action.

In addition to developing mechanistically distinct bactericidal compounds, focus has also shifted to methods of restoring the efficacy of available drugs. Examples of such approaches include co-administration of antibiotics with efflux pump inhibitors and β -lactamase inhibitors.¹² Another contemporary strategy to combat resistant pathogenic microbes is to attenuate virulence and bacterial communication in hopes of neutralizing infectivity. Suppressing aspects of pathogenicity (e.g. quorum sensing, adherence, and biofilm formation) may not affect the bacterial growth but may render bacteria susceptible to clearance by the immune system.¹³

2. Bacterial Caseinolytic Protease P

2.1. Background

Abnormal gene expression and protein denaturation are common effects of environmental stressors on bacteria. Bacteria have a variety of robust regulatory mechanisms at their disposal to handle stressors, including, but not limited to, pH alterations, changes in salt concentrations, extreme temperature fluctuations, and the presence of various antibacterials. One example of a key regulatory mechanism is intracellular proteases, which play a critical role in cellular homeostasis by degrading obsolete or denatured polypeptides. Proteases responsible for the turnover of intracellular proteins include the AAA+ proteases (ATPases associated with various cellular activities) ClpP, FtsH, Lon, and HslUV.¹⁴

Evolutionary conservation and involvement in a variety of cellular processes make proteases promising yet challenging targets in drug discovery.¹⁵ In theory, disruption of the normal physiological function of proteases leads to either over-degradation or accumulation of protein substrates in the bacterial cell and results in growth impairment, virulence alteration, or in many instances, cell death.

In the last decade, bacterial caseinolytic protease P (ClpP) has attracted a lot of attention as a promising new antibacterial drug target. The interest surrounding ClpP arises from the fact that either inhibition or activation of this protease leads to detrimental effects on bacterial survival and virulence. This ability to investigate two orthogonal targeting approaches represents a unique opportunity in drug discovery and thus has attracted the attention of the antibiotic research community as a promising new target.

ClpP is a serine protease comprised of 14 subunits (Figure 2). In its tetradecameric form, ClpP exhibits a cylindrical structure, arising from two heptameric rings that dimerize to form a barrel. The proteolytic activity of ClpP resides inside of the oligomeric complex, which encompasses 14 catalytic sites (Ser-His-Asp catalytic triads, Figure 3).¹⁶

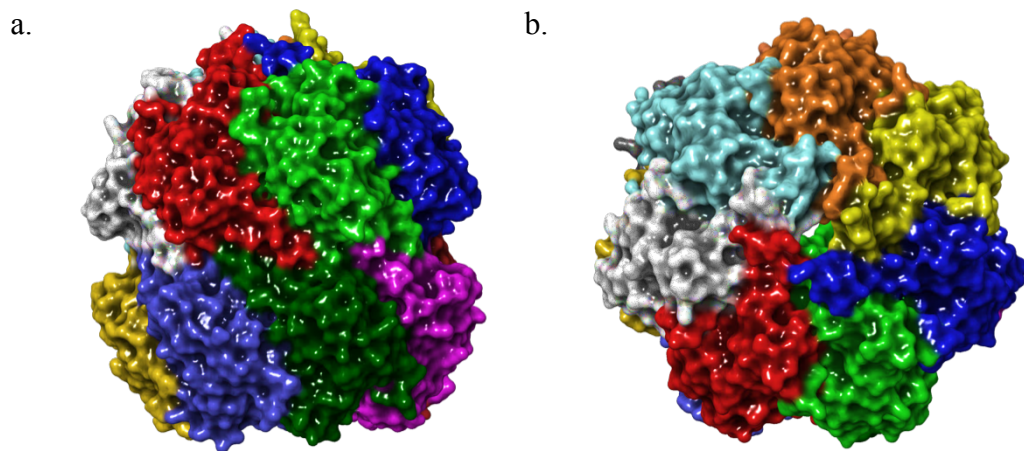


Figure 2. Structure of tetradecameric *Escherichia coli* ClpP. (a) Distal and (b) apical views (PDB: 1YG6).

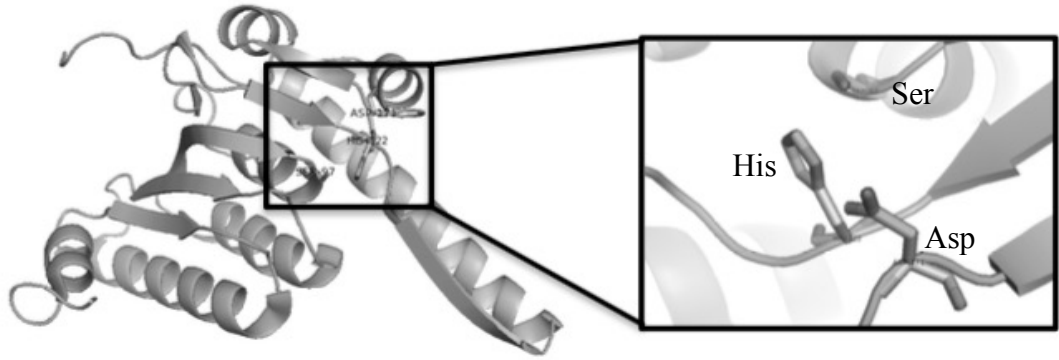


Figure 3. X-ray structure of *E. coli* ClpP monomer. Inset: catalytic triad (PDB: 1YG6).

Although ClpP is conserved throughout prokaryotes and eukaryotes, distinct differences between the homologs provide a means for selective modulation. For example, human ClpP is localized to the mitochondrial matrix and exists as a single heptameric ring with an exposed and inactive catalytic triad.¹⁷ The cellular location and latent state suggest that drugs targeting bacterial ClpP should not have adverse effects on human ClpP. Confirmation of the ability to selectively target bacterial ClpP over eukaryotic ClpP has been demonstrated experimentally, as targeting bacterial ClpP eradicates *Enterococcus faecalis*, *S. aureus*, and *Streptococcus pneumoniae* infections in rodents. To date, low toxicity profiles for targeting ClpP have been observed in both mice and dogs, paving the way for future human studies.¹⁸

In normal biological circumstances, proteolytic activity of ClpP is highly regulated by several factors. First, protein substrates must pass through small entrance pores at the apical surface, in the center of each heptameric ring. The N-terminal region of each ClpP subunit (red in Figure 4) acts as a gatekeeper, controlling substrate entry through a narrow channel of 10-12 Å in diameter. The disposition of the axial pore residues restricts folded proteins or large polypeptides from entering the chamber. Second, ClpP activity requires a pre-organized

tetradecamer, which upon activation, results in the alignment of the catalytic triad into an active state. Therefore, the proteolytic activity of ClpP is only possible when the catalytic triads are securely shielded from cytoplasmic environment.¹⁹

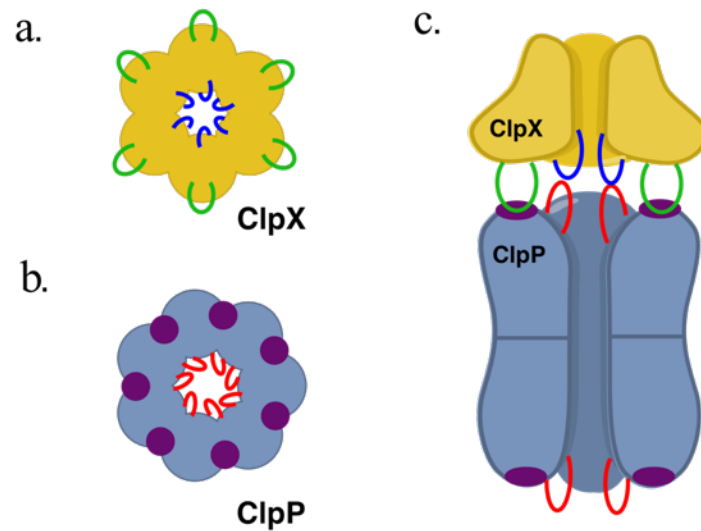


Figure 4. Model for natural co-chaperone-mediated ClpP activation.

ClpP alone can only degrade small peptides (<5 amino acids) and requires association with Clp-ATPases to handle larger substrates.²⁰ The co-chaperones (e.g. ClpA and ClpX) belong to the AAA+ protein family and exhibit a hexameric structure as presented in Figure 4a. Proteins flagged by the specific SsrA degradation tag, are recognized by co-chaperones as substrates that require ClpP-mediated degradation. This tag-based mechanism results in high substrate selectivity and, thus, protects non-substrate cytoplasmic proteins from undesired proteolysis.²¹ Besides substrate recognition, Clp-ATPases are responsible for unfolding and translocating substrates through ClpP axial pores and into the proteolytic chamber in an ATP-dependent process.²²

Upon binding, ClpP co-chaperones interact with the proteolytic core in two different ways. First, six co-chaperone L/IGF loops (green in Figure 4) bind into six of the seven hydrophobic pockets of ClpP (purple in Figure 4). The flexibility of these loops allows a strong and static interaction despite the asymmetry.²³

Second, the N-terminal loops of ClpP (red in Figure 4) and the pore-2 loops of the co-chaperone interact weakly, but the flexibility of these loops allows a dynamic interaction.²⁴ These two interactions are not only critical for the stability of the ClpXP or ClpAP complex but also induce the opening of the axial pore in ClpP to allow substrate access to the proteolytic chamber.

2.2. ClpP Chemo-modulation: A New Antibacterial Strategy

In the last decades, small molecule and natural product ClpP modulators (activators and inhibitors) have been reported. Specifically, ClpP activators have captured researchers' attention, as enzyme activation represents a new paradigm for the development of antibiotics, which has traditionally revolved around pathway inhibition or disruption. This so-called chemo-activation of ClpP results in the unselective degradation of essential polypeptides, leading to cell death. The bactericidal effect of ClpP chemo-activation has led to screening campaigns that have produced a limited number of activating chemotypes, the most active of which contains an acyldepsipeptide (ADEP) core, exemplified by ADEP4 (**1**) in Figure 5.

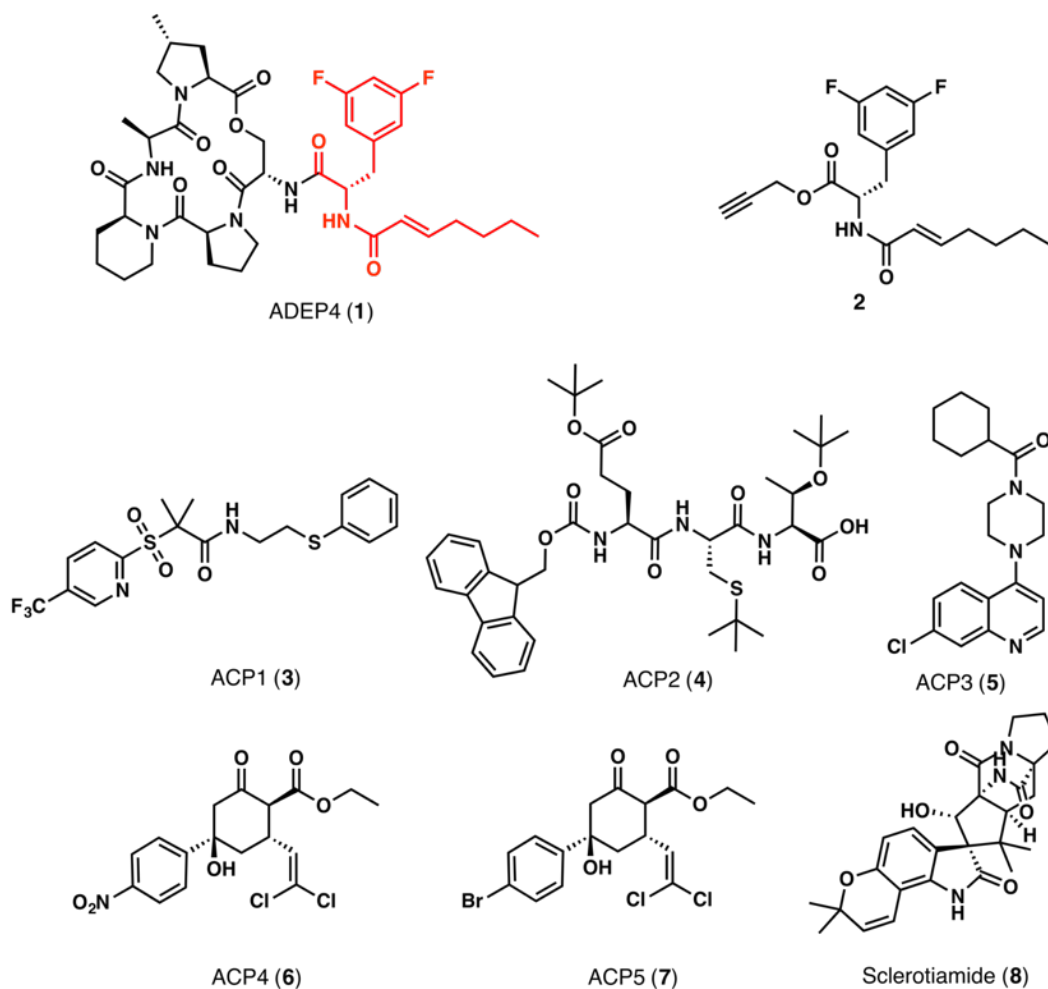


Figure 5. Chemical structures of ClpP activators.

X-ray crystallography studies have shown that ADEPs bind in the same hydrophobic pocket between ClpP monomers (purple in Figure 4) as the L/IGF. In addition, Gersch and co-workers have shown that full occupation of tetradecameric ClpP induces activation.²⁵ ADEPs do not only activate the tetradecameric complex, but also disrupt the interaction of ClpP with natural co-chaperones. Thus, ADEPs affect bacterial fitness via two mechanisms of action; 1) by inducing an uncontrolled degradation of flexible cytoplasmic polypeptides and 2) by preventing co-chaperone docking; thus, disrupting the necessary degradation of normal substrates. As such, ClpP chemo-activation inherently includes a mode of inhibition simply through the competitive binding of activators to the natural co-chaperone site.²⁶ Furthermore, no cross-resistance to marketed antibiotics has been

detected, indicating that ClpP is the major target of the ADEP family. *In vitro*, ADEPs are active against a variety of Gram-positive bacteria, but lack effectiveness against Gram-negative bacteria due to their susceptibility to efflux pump excretion, limited outer membrane penetration, or a combination of the two.²⁷ The N-acylphenylalanine fragment (red in Figure 5) was identified as both the ADEP pharmacophore and the motif recognized by efflux pumps in *Mycobacterium tuberculosis*,²⁸ *Streptomyces lividans*, *Streptomyces coelicolor*,²⁹ thus limiting ADEPs' spectrum of action and prohibiting any significant alteration of the moiety due to its essential role in ADEP activity.

Recently, small molecule ADEP derivatives have been identified (e.g. **2**, Figure 5) and despite the lower potencies for ClpP, they display submicromolar minimum inhibitory concentrations (MICs) for Gram-positive species such as *S. aureus*, *S. pneumoniae* and *Enterococcus faecium*, including multi-resistant clinical isolates (i.e. MRSA, VRE, and Chloramphenicol-resistant *Neisseria gonorrhoeae*).³⁰ This provides proof-of-concept that small molecule fragments are capable of inducing chemo-activation *in vitro*, thus establishing both complex natural products and small molecules as viable leads.

ADEPs and simplified ADEP fragments are not the only known chemotypes capable of activating ClpP. In two separate screening campaigns, small molecules ACP1-5 (**3-7**) (activators of cylindrical proteases), and the natural product sclerotiamide³¹ (**8**) have been identified as additional ClpP-activating scaffolds; however, no further optimization of these compound classes has been reported.

As previously mentioned, ClpP is not only involved in bacterial homeostasis, it also maintains significant roles in bacterial virulence. Several

mutation studies have demonstrated that *clpP* deletion attenuates virulence in pathogenic bacteria (e.g. *Listeria monocytogenes*, *S. pneumoniae*, *S. aureus*).^{32,33,34} Therefore, disruption or chemo-inhibition of ClpP is expected to cause a decrease in the production of bacterial virulence factors.³⁵ β -lactones such as lactone D3 or U1 (**9** and **10**, Figure 6) inhibit ClpP activity by covalently binding to the conserved serine residue in the Ser-His-Asp catalytic triad. Studies on the inhibitory activity of lactone D3 and U1 against *L. monocytogenes* and *S. aureus* illustrates the downstream effect of ClpP inhibition on bacterial virulence. In *L. monocytogenes*, lactone U1 decreased intracellular bacterial survival by inhibiting the ClpP dependent production of virulence factors.³⁶ In *S. aureus* and MRSA, lactone U1 reduced the extracellular hemolytic and proteolytic activities as a consequence of ClpP inhibition.³⁷

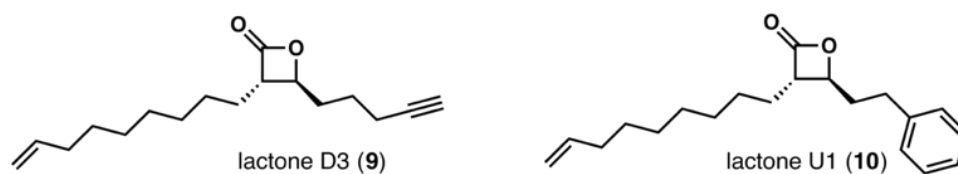


Figure 6. Chemical structures of ClpP inhibitors

With the rise of antibiotic-resistant bacteria, there is an urgent need to develop antibacterials with new mechanisms of action. Considering its essential role in bacterial survival, fitness, and virulence, ClpP represents a target worthy of further investigation. Chemo-modulation of ClpP offers two possible approaches, 1) inhibition via covalent binding to the catalytic triad inducing reduction of bacterial virulence, and 2) activation of unselective substrate degradation. We chose to pursue the activation approach because of its deviation from traditional antibacterial strategies and because of the multi-modal mechanism of action: 1) induction of ClpP oligomerization, 2) inhibition of the natural co-chaperone operation, and 3) induction of unselective degradation. In addition, large and small

molecules have been shown to activate ClpP at submicromolar MICs in Gram-positive bacteria including multi-resistant clinical isolates.

Furthermore, given the small number of chemotypes known to target ClpP and the limited understanding of protein-ligand interactions involved in the binding, an opportunity to enrich the field of ClpP biology through the development of new tools exists. Only a few crystal structures of ClpP activators are available (all ADEP derivatives bound to ClpP) and no extensive docking studies have been reported. Thus, we intend to utilize computational approaches to provide insight into specific ligand•ClpP interactions and thus address some of the structure optimization issues in the field.

Chapter 2

Computational Assessment of Small Molecule ClpP Activators

1. Structure-Activity Relationships of the ACP4/5 Scaffold

1.1. Introduction

In efforts to identify small molecule ClpP activators, Leung and co-workers screened a library of 60,000 commercially available drug-like compounds.³⁸ The screen revealed five activators of *Escherichia coli* ClpP (EcClpP), two of which, ACP4 and ACP5, exhibited high structural similarity (Figure 7). Although the ACP4/5 scaffold has been subjected to a brief SAR study, the authors chose to pursue a more synthetically tractable hit.

Unlike other small molecules identified in the screen, ACP4/5 exhibits a three-dimensional architecture around the cyclohexanone core, which allows functional groups to interact with a large surface area of the binding pocket. Woznesensky's X-ray diffraction analysis of ACP5 demonstrated that the structure adopts a chair conformation (Figure 8) with the bulky substituents (i.e. phenyl, ester and dichlorovinyl moiety) in the equatorial position. An equilibrium between the two possible chair conformations is unlikely since the energy barrier is 10.43 kcal/mol.^b Consequently, the flexibility of the scaffold is low, despite the important three-dimensional character of the core. The inflexibility of this molecular family suggests there is little entropic penalty imposed during ClpP binding. As such, the SAR relationships produced for this class are more directly correlated to ligand-protein interactions than other ClpP activating scaffolds, which exhibit more flexibility for the design of new analogues. ACP4/5, therefore, represents a good

^b Energy barrier between the two chair conformations was calculated with Schrödinger.

scaffold to utilize for computational studies, which are often complicated by molecular flexibility.

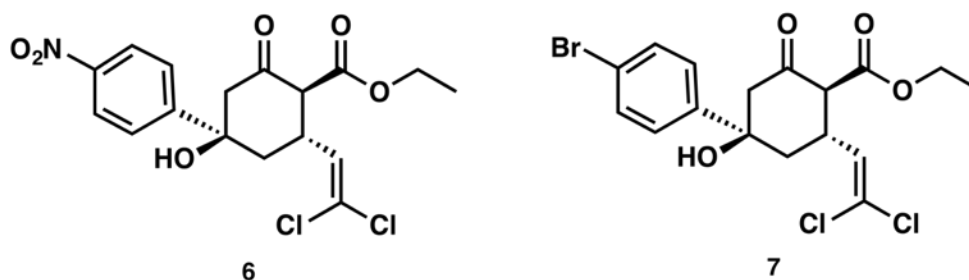


Figure 7. Chemical structures of ACP4 (left) and ACP5 (right).

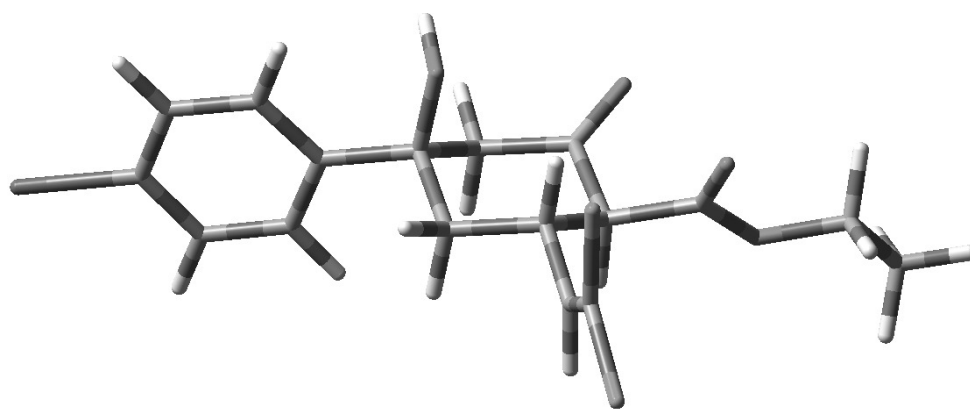


Figure 8. Minimized structure of ACP5. The structures were minimized with the basis set M06-2X/Def2-TZVP in Gaussian 9.

In Leung's study, the binding of ACP4/5 was first investigated by docking analysis. The docking studies were limited to the docking of ACPs (3-7) to EcClpP and did not provide a thorough analysis of ACPs•EcClpP interactions, as the ligands were overlaid into the pocket. Interestingly, ACP4/5 were predicted to not only bind to the same pocket as ADEPs (H-pocket, red in Figure 9a), but also to a newly identified adjacent pocket (C pocket, green in Figure 9a). Mutations of the putative binding sites were utilized to validate the docking predictions (Figure 9b). Single mutations of the ADEP binding site residues were performed to assess the effect on the activity of ACP4/5. Residue mutations, Phe112Ala, Leu189Glu and Phe112Ala/Leu189Glu (H pocket mutations) decreased both ADEP and ACP4/5 activity, suggesting the compounds bind to a same pocket. Furthermore, mutations

of residues in the C pocket, Gln81Ala and Asp86Ala, only affected ACP4/5 activity, providing evidence of a potential dual binding mode for ACP4/5.

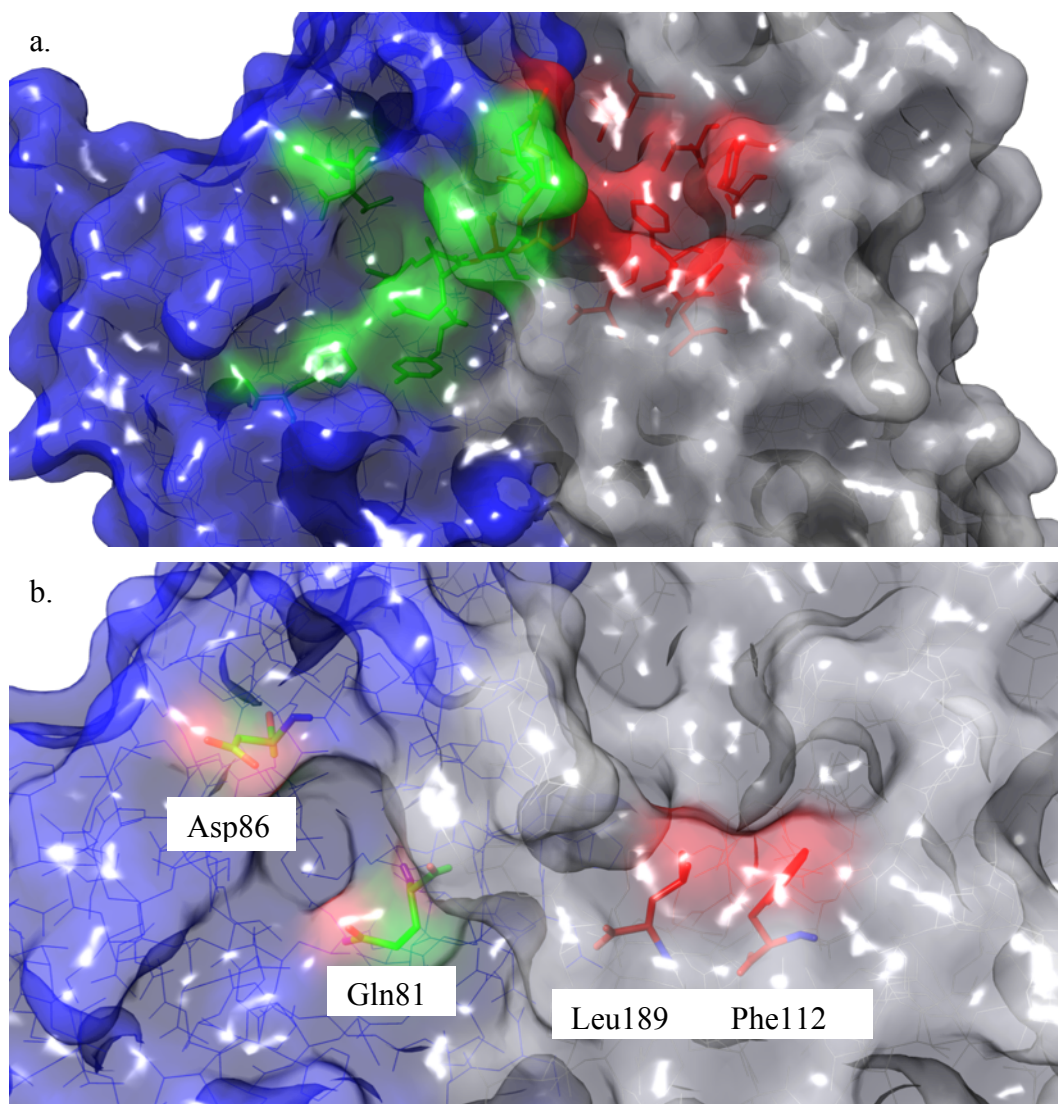


Figure 9. Predicted EcClpP binding pockets (PDB: 3MT6). (a) View of C pocket (green) and H pocket (red) on two EcClpP subunits (blue/grey). (b) Highlighted residues were subjected to mutation.

Although ACP4/5 were not the most potent ClpP activators to arise from the *in vitro* screen, these two analogues exhibited some of the most efficacious activity against a number of pathogenic bacteria. Against *N. gonorrhoeae* and *Neisseria meningitidis*, ACP4 showed better minimum bactericidal concentration (MBC) than other hits, and was comparable to an ADEP derivative against *E. coli* when co-administered with the membrane permeabilizing agent polymyxin B.

ACP4 even surpassed ADEP derivatives against *Haemophilus influenzae* (+ polymyxin B), *S. pneumoniae* and *Mycobacterium smegmatis*. These results further demonstrate that the ACP4/5 cyclohexanone exhibits good ligand efficiency and provides a great core for further medicinal chemistry initiatives.

As previously discussed, few structurally distinct ClpP activators are known and an even smaller number have been subjected to extensive studies. Thus, enrichment of the ClpP activator arsenal and/or scaffold development is necessary to assess the validity of ClpP as an antibacterial target. ACP4/5 is an interesting starting point to develop new ClpP activators. Although structurally more complex than the amino acid ADEPs, the synthesis of ACP4/5 is considerably more tractable. Moreover, the highly substituted nature and three-dimensional character of the ACP4/5 core provides an opportunity to explore multiple avenues towards the optimization of this family. In addition, ACP4/5 is a non-peptide-based scaffold, making it less susceptible to enzymatic inactivation (e.g. through peptide bond cleavage) compared to ADEPs.

1.2. ACP4/5 Structure-Activity Relationship Summary

Although ACP4/5 analogues were eventually abandoned by Leung *et al.* in favor of another hit, 31 analogues were synthesized and assessed for EcClpP activation capabilities. To evaluate these analogues, a well-established degradation assay was utilized, which measures the ability of compounds to activate the EcClpP tetradecamer and induce EcClpP-mediated degradation of a substrate protein, fluorescein isothiocyanate-labeled casein (FITC-casein). FITC-casein is not fluorescent in its globular state and must be hydrolyzed in order to fluoresce. To quantify fluorescence resulting from the degradation of FITC-casein, a relative

degradation (RD₂₅) index, in the presence of 25 μM compound, was calculated as follows:

$$RD_{25} = \frac{(\Delta\phi_{ClpP} + \text{compound})_{\text{after 6hrs}} - (\Delta\phi_{ClpP})_{\text{after 6hrs}}}{(\Delta\phi_{EcClpAP})_{\text{after 6hrs}} - (\Delta\phi_{EcClpP})_{\text{after 6hrs}}}$$

- $\Delta\phi$ is the change in fluorescence after 6 hours of reaction;
- *E. coli* ClpAP is used as a benchmark for ClpP proteolytic activity since ClpAP is responsible for inducing natural substrate degradation in bacteria.

Parallel synthesis produced 31 ACP4/5 analogues in which each substituent of the ACP4/5 scaffold was subjected to a brief preliminary SAR evaluation.^{39,40} This small, yet structurally rich, collection of compounds provides a good basis set for us to analyze, in hopes of providing insights to enable the development of computational tools for structure-guided design of ClpP activators. Prior to embarking on computational studies, we conducted a detailed analysis of the analogues generated by Leung and coworkers.

Derivatization of the aromatic ring revealed that a *para*-substituent is required for activity, as demonstrated by the inability of **14** to activate EcClpP (Table 1). To rationalize the effect of this substitution on the activity, we considered several properties of the substituents. First, the effect of electronegativity was analyzed to see if any correlation to the activity could be identified. A plot of electronegativity versus RD₂₅ values (Figure 10) reveals no obvious correlation.⁴¹ Notably, analogues containing *para*-electron donating groups, **12**, **16** and **17** display weaker activity compared to those with electron withdrawing groups **6**, **7**, **11**, and **13**, with **18** being the exception (Table 1). Therefore, an electron-poor phenyl ring appears to be more favorable than an electron-rich system. Interestingly, the presence of a halogen provides a drastic improvement in ClpP

activation with **7**, **13** and **15**, showing a direct correlation to the size of the halogen and the EcClpP activation potency. As such, the *para*-iodo derivative **15** is the most active of the analogues synthesized.

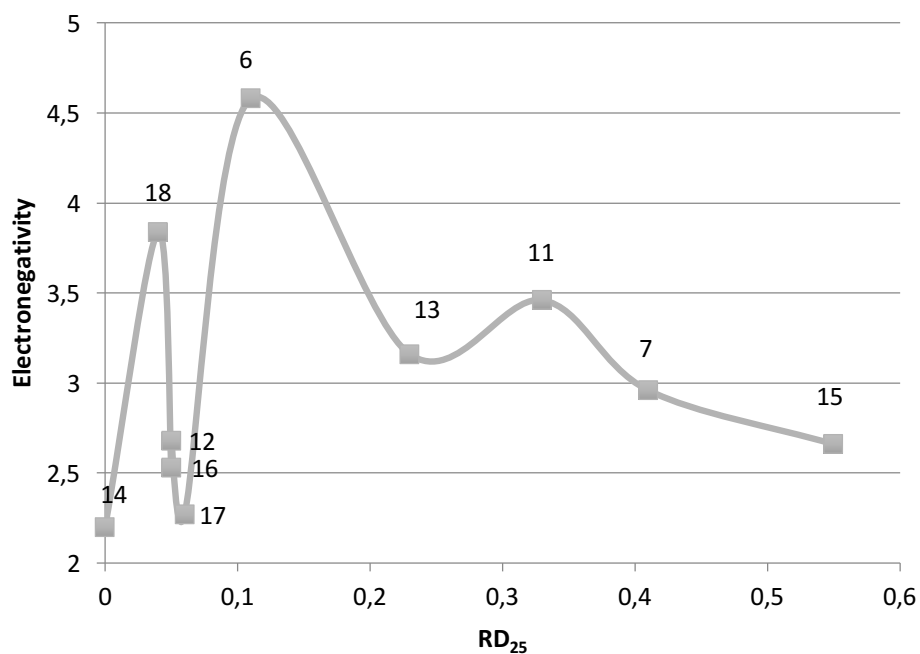


Figure 10. Plot of *para*-substituent electronegativity versus ClpP activation.

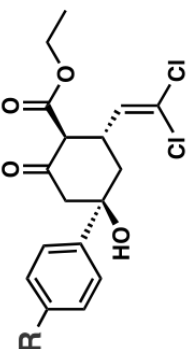
Structure	Analogue	-R	RD ₂₅	Electronegativity	Van der Waals volume ^a (V _{vdw}) (Å ³)
	6	-NO ₂	0.11 (± 0.03)	4.58	32.21
	7	-Br	0.41 (± 0.07)	2.96	30.88
	11	-CF ₃	0.33 (± 0.06)	3.46	30.74
	12	-OCH ₂ CH ₃	0.05 (± 0.06)	2.53	49.18
	13	-Cl	0.23 (± 0.02)	3.16	25.16
	14	-H	0	2.2	7.24
	15	-I	0.55 (± 0.02)	2.66	40.17
	16	-OCH ₃	0.05 (± 0.01)	2.68	30.75
	17	-CH ₃	0.06 (± 0.01)	2.27	15.98
	18	-CN	0.04 (± 0.02)	2.66	27.07

Table 1. Relative ClpP activation of *para*-phenyl substituted ACP4/5 analogues.

^a Values from *Chemical Physics Letters*, 116(5), 1985.

Considering the important involvement of hydrogen bonding in ligand-receptor interactions, the hydrogen acceptor capacity of the *para*-substituent was also evaluated. However, available compounds bear functional groups only known to be weak or moderate hydrogen bond acceptors.⁴² Furthermore, nitro (**6**), ethoxy (**12**), methoxy (**16**), and nitrile (**18**) analogues display weak or moderate activity. Therefore, we can either assume that that hydrogen bond formation weakly contributes to ligand-induced activity or that a stronger H-bond acceptor is required at this position.

Finally, the size of the substituent was taken into consideration since the binding affinity of a ligand can be significantly affected by steric interactions with the pocket. A bulky substituent can displace the molecule from its favored position and then disrupt any interactions involved in the binding. To describe the size of the substituent, we chose to use van der Waals volumes (V_{vdW}), as presented in Table 1. The V_{vdW} consists of the sum of the volume of intersecting spheres representing single atoms and takes into account bond distances, bond angles and intermolecular van der Waals radii.⁴³ Although the low activity of **12** may initially be attributed to the sizeable V_{vdW} of ethoxy group, 49.18 Å³, the activity of other analogues does not seem to be impaired by the substituent size, as compounds bearing large groups are active (e.g. **6** and **15**). On the contrary, analogues with small groups (**14**, **17**) have limited activity. Thus, the steric interactions alone are not the sole contributor of activity abolishment and further computational studies are required to better understand the contribution of steric factors in ligand binding.

The SAR surrounding the dihalovinyl moiety (Table 2) reveals a rather strict pattern of functionality, as any deviation from the dichloro derivative results in a decrease or abolishment of activity. Both incorporation of an aromatic moiety

19, 20, 21, 24 and 25, and deletion of functionalization 26 resulted in abolishment of activity. Interestingly, although analogues with the dihalovinyl moiety 7 and 23 activate ClpP, analogue 22 with the dimethyl vinyl moiety fails to exhibit meaningful activation at the same concentration. Therefore, only electron withdrawing substituents seem to induce activity. Closer analysis of 7 and 23 suggests that smaller halogens are more favored and a difluoro derivative is certainly worth assessment.

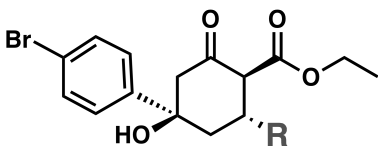
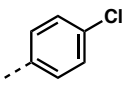
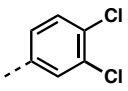
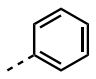
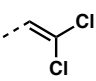
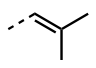
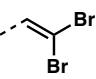
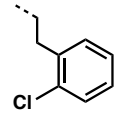
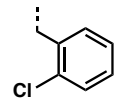
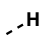
Structure	Analogue	-R	RD ₂₅
	19		0
	20		0
	21		0
	7		0.41 (± 0.07)
	22		0.04 (± 0.02)
	23		0.15 (± 0.01)
	24		0.06
	25		0
	26		0.03 (± 0.01)

Table 2. Relative ClpP activation of altered dihalovinyl ACP4/5 analogues.

As shown in Table 3, manipulation of the ester reveals a bell-curve-type size-dependent SAR profile with the ethyl ester exhibiting optimal activity with either an increase or decrease in size lowering activity. When rationalizing this SAR, sterics and ester conformation should be considered. The *cis/trans* conformation of esters is known to exist in a sterically driven equilibrium with the *cis* conformation generally predominating.⁴⁴ As such, bulky groups are locked in *cis* conformation (**7**, **28**, **29**), whereas *cis/trans* transition for smaller substituents is more facile. As a result, the activity profile of ester analogues may result from both entropic-based and space-filling components.

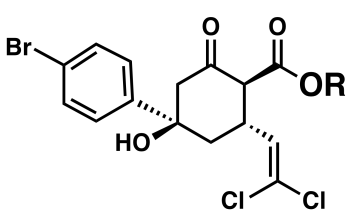
Structure	Analogue	-R	RD ₂₅	V _{vdW}
	7	-CH ₂ CH ₃	0.41 (± 0.07)	28.92
	27	-CH ₃	0.06 (± 0.01)	16.15
	28	-C(CH ₃) ₃	0.26 (± 0.03)	54.47
	29	-CH(CH ₃) ₂	0.22 (± 0.02)	41.7

Table 3. Relative ClpP activation of alkyl ester ACP4/5 analogues.

Modifications of the cyclohexane core have also been reported and are shown in Table 4. Although discussed previously, compounds **7** and **15** have been included in Table 4 to allow for direct comparison with analogues **30** and **31-33**, respectively. First, elimination of the hydroxyl group led to the formation of the α,β -unsaturated analogue **30**. Loss of activity indicates that the chair conformation is essential to correctly orient the other functionalities in the binding pocket. Although the elimination may suggest an important interaction is made with the hydroxyl, methylation of the hydroxyl group (**33**) only slightly affected the activity, providing evidence that an H-bond donor is not required at this position. Moreover, the minor effect of hydroxyl methylation on the activity implies that the binding pocket may accommodate larger substituents at this position. Reduction of the

cyclohexanone ketone to the alcohol also resulted in the abolishment of activity (**31**). Transformation of the ketone (**7**, hydrogen-bond acceptor) to an alcohol (**31**, hydrogen-bond donor) is detrimental to activity, suggesting that an H-bond acceptor at this position is necessary. Furthermore, reduction of the ketone results in a change of hybridization of the carbon, from sp^2 to sp^3 , inducing geometric modification, and potentially altering the binding orientation within the pocket. Chlorine substitution of the single β -ketoester α -hydrogen (**32**) did not significantly affect activity (compared to **15**) and thus suggests structural modification of this position may be worth investigating.

Structure	Analogue	RD ₂₅
	7	0.41 (± 0.07)
	30	0
	15	0.55 (± 0.02)
	31	0.02 (± 0.01)
	32	0.52 (± 0.01)
	33	0.45 (± 0.03)

Table 4. Cyclohexanone modification and associated activities.

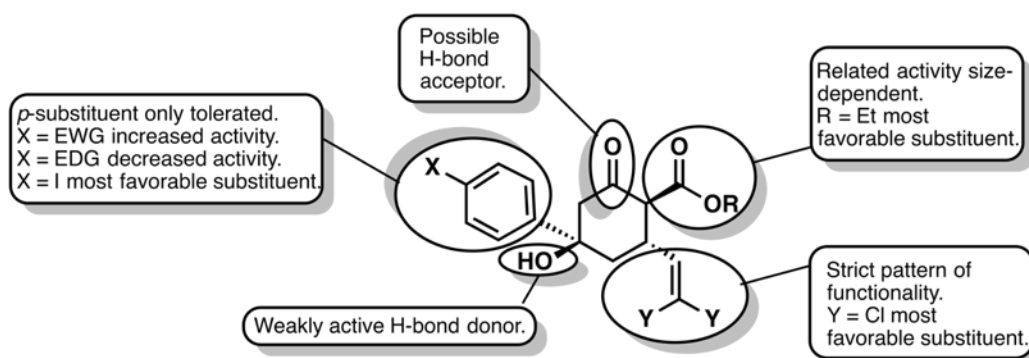


Figure 11. SAR summary of ACP4/5 scaffold.

In summary, the chair conformation of the cyclohexane core is essential along with the ketone involved in a putative hydrogen bond. The dichlorovinyl moiety, ethyl ester and the hydroxyl group are certainly prone to optimization and further study could unveil more optimal substituents. The preliminary SAR study provided some insights into the substituents favored for activity; however, like other ClpP activator studies, this is only a ligand-based analysis and does not take the receptor into consideration. However, we believed that the diversity in the library of ACP4/5 analogues represents an opportunity to develop a computational platform for analyzing ligand•ClpP interactions. Computational assessment of ACP4/5 analogues will contribute to a better understanding on how the compounds interact with the pocket and may lead to the design of more potent and efficacious analogues.

2. Computational Analysis of the ACP4/5•EcClpP Interactions

To date, no computational platform exists to perform *in silico* analysis of ClpP activation. This is not surprising as general docking methods are well-known to have many limitations, one of which is accurately assessing ligand-protein interactions of oligomeric targets that exhibit cooperative ligand binding (e.g. ClpP). Indeed, we have seen this disconnect in our own laboratory, in which we have executed *in silico* screens for novel ClpP activators and were unable to experimentally validate any computational hits. As such, a critical barrier exists in the field of ClpP modulator optimization, as it is currently not possible to carry out structure-based optimization of ligands, due to the lack of computational tools. Until this barrier is addressed and computational methods are available, it is our opinion that the field of ClpP modulation will rely on empirical and incremental advancements. In this chapter, we utilized the ACP4/5 basis set provided by Leung

and co-workers towards the development of a computational platform to allow for structure-based optimization of ClpP small molecule analogues. Specifically, we aimed to combine molecular docking protocols with frontier molecular orbital (FMO) theory, to provide a new level of insight to activator•ClpP interactions. We hypothesized that FMO-docking experiments will provide insight on a per-residue level of detail.

First, the docking studies provided the binding conformation of compounds in the EcClpP binding site, second, calculations of the electronic structure allowed for per-residue assessment. By simultaneously assessing FMO and docking predictions, we hope to better interpret the activity of ACP4/5 analogues, identify different interactions involved in EcClpP binding site, and use this information to rationally design new analogues.

2.1. Docking Study of ACP4/5 on EcClpP

2.1.1. Introduction

Intermolecular interactions are key elements in biological processes, whether it is between an enzyme and its substrate, a receptor and its ligand or between proteins, the binding of these entities triggers biological responses. Mutual molecular recognition is a result of non-covalent interactions that contribute to high affinity and specificity in binding.⁴⁵ In biological systems, it is understood that ligands and receptors do not exist in a single rigid conformation, but rather in a distribution of conformations coexisting in a dynamic equilibrium. Therefore, the binding of a ligand to the target-protein occurs with each component undergoing structural compromise to allow for the maximum number of favorable interactions.^{46,47}

These non-covalent interactions vary in nature and strength, and depend on the geometry of atoms or group of atoms that interact. The most studied of these interactions is hydrogen bonding; it consists of an interaction between a polar hydrogen and an electronegative atom (e.g. oxygen or nitrogen). Proteins are essentially made of carbon, hydrogen, oxygen and nitrogen atoms, so it is easy to understand the predominant role of hydrogen bonds (H-bonds) in molecular recognition. However, other structure-specific interactions exist. For instance, ionic bonds can occur between cations or anions and π -systems. Additionally, a wide range of hydrophobic interactions take place between a ligand and a protein, such as π - π stacking, London dispersion forces, or van der Waals interactions.^{48,49}

In medicinal chemistry, the optimization of molecular recognition is a major focus, since the objective is generally to develop therapeutics that specifically bind to a desired target but fail to interact with others of similar architecture. However, discovery of a ligand that tightly binds to a specific target is challenging and experimentally expensive.⁵⁰ In the past decade, the rise of computer-aided drug design has provided powerful tools to predict ligand-receptor binding affinity. Docking is certainly the most used tool in computational drug design, as it allows the screening and scoring of a large collection of ligands against a target of interest.⁵¹ From docking results, target compounds can be prioritized and analogue synthesis can be pursued strategically, making medicinal chemistry even more so efficient. In order to quantify the relationship between a ligand and the binding site, docking programs approximate the protein-ligand potential energies (e.g.: van der Waals interactions, Coulomb energies, hydrogen bond potentials) for the scoring function to determine the Gibbs free energies of the system.^{52,53} Docking methods also provide valuable qualitative visual insights into ligand-receptor interactions

(i.e. the three-dimensional representation of the bound compound) similar to a co-crystal structure. However, calculation of ligand-protein affinities can only afford a prediction and cannot replace experimental data. This is the reason why docking analysis should be combined to other methods, such as experimental SAR and co-crystal structures, to rationalize and verify docking results.

Fortunately, extensive literature on ClpP and the ADEP family provides crystallographic analysis of ADEP•ClpP binding. As mentioned, ADEPs bind to the hydrophobic pocket between ClpP subunits. It is noticeable in Figure 12 that the N-acylphenylalanine moiety (yellow) is anchored in a subpocket constituted of hydrophobic residues, such as Val144, Tyr62, Thr79, Phe82, Ile90, Met92, Leu114 and Leu189. Compton *et al.* identified the N-acylphenylalanine fragment as the ADEP pharmacophore. Thus, we can consider the residues interacting with this fragment as critical for the activation of ClpP.

Although ACP4/5 scaffolds are structurally different from ADEPs, they have a phenyl ring in common. Therefore, we hypothesized that ACP4/5 phenyl ring binds in the same subpocket as the ADEP phenylalanine and interacts with the aforementioned residues. For this reason, and the lack of data on the other pocket identified in the Leung paper, this study focused only on the interactions of ACP4/5 with the ADEP binding pocket in ClpP. To assess this hypothesis, ACP4/5 analogues were docked to EcClpP and the docking results were analyzed in order to identify the interactions involved in the binding of ACP4/5 scaffold.

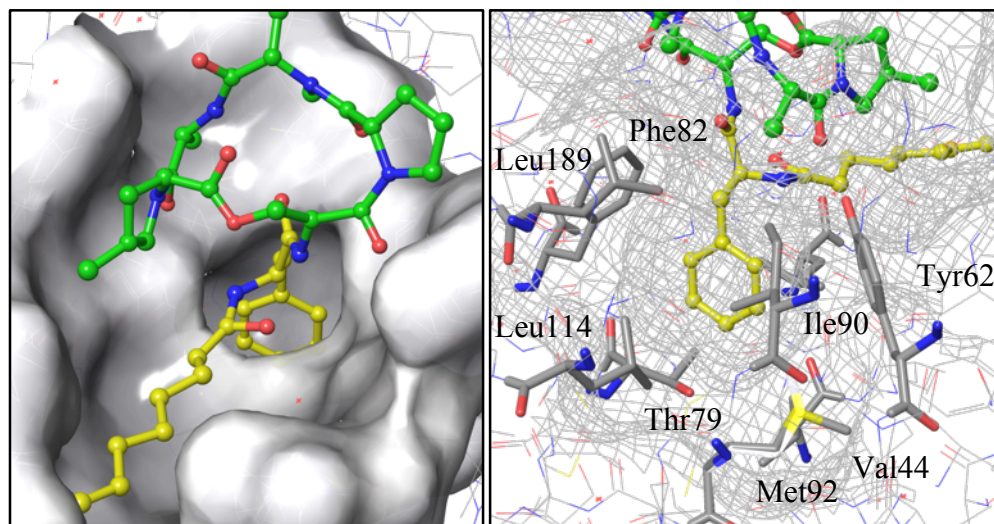


Figure 12. Co-crystal of ADEP1 (green/yellow) bound to EcClpP (grey) (PDB: 3MT6). (left) Global view of ADEP1 into the binding pocket, (right) close-up view on ADEP1 pharmacophore and surrounding residues.

2.1.2. *Methods*

The docking studies were carried out using two programs in order to allow for comparison of results between AutoDock 4.2.6 (freeware)⁵⁴ and Schrodinger's Glide version 7.1 (subscription).^{55,56,57} The binding energies calculated by both software packages represent the gain of stability of the ligand-protein complex compared to the two entities alone. The more negative the energy difference is, the higher the affinity is predicted to be between the ligand and the protein.

In efforts to assess the accuracy of the predicted binding energies, compound RD₂₅ was used. As discussed previously, RD₂₅ is representative of compound potency and reflects the degree of EcClpP activation induced by 25 μM of the compound of interest. We will consider that high binding affinity generates high activation, since more favorable ACP4/5•EcClpP interactions result in stronger binding. Therefore, a change in the predicted binding energy should correlate with a proportional change in ACP4/5 analogue RD₂₅.

ACP4/5 and analogues were built using ChemBio3D Ultra 14.0 and minimized using the MMFF force field. Molecular docking was performed on

EcClpP (PDB: 3MT6) and carried out with AutoDock Vina 1.1.2. Docking results were analysed with AutoDock 4.2.6. Torsions of the σ -bonds between the phenyl ring, the hydroxyl group, the dichlorovinyl group, the ester and the cyclohexanone were allowed, in addition to the ester bond, in order to perform flexible docking of the ligand.

To dock ACP4/5 analogues with the Schrödinger suite of computational tools, the companion graphical user interface Maestro was utilized. EcClpP (PDB: 3MT6) was preprocessed by Schrodinger's Prime. Solvent molecules were removed from the crystallographic structure, since water molecules are not involved in ACP4/5•EcClpP interactions. The most stable conformation of ligands was obtained with the conformational search tool using OPLS3 force field in water and the mixed torsional/low-mode sampling method. The compounds were then docked in EcClpP using Schrodinger's Glide and the binding affinities per residue were calculated. The ACP4/5•EcClpP distances and angles within the docking results were calculated with Maestro.

2.1.3. ***Results and Discussion***

As we hypothesized, when docked to the ADEP pocket, ACP5 binds EcClpP with the *para*-bromophenyl ring (orange) in the same sub-pocket as the ADEP phenylalanine fragment (green, Figure 13). The ACP5 binding conformation was considered an arbitrary reference for analogue docking, in order to evaluate the accuracy of analogue binding conformations. Besides some analogues with important structural differences (denoted with a star in Figure 15), all analogues followed the same docking pattern as ACP5. Although the predicted docking pose of ACP5 to EcClpP seems to be relevant due to positioning of the aromatic anchor and space filling models of the binding pocket, the *in silico*

predicted binding affinities (K_{pred}) of ACP4/5 analogues do not show any correlation with experimental compound activity (Figure 14), whether docked with AutoDock or Glide (Figure 15). The unsatisfactory results can be attributed to the scoring functions of the software that consider every interaction, between the ligand and the residues of the binding pocket, to have a similar influence on the activity. However, not every residue of a binding site is essential for the molecular recognition. Although many factors may contribute to the lack of correlation between K_{pred} and RD_{25} , we hypothesized that the lack of residue weighting is a key contributor to this discrepancy.

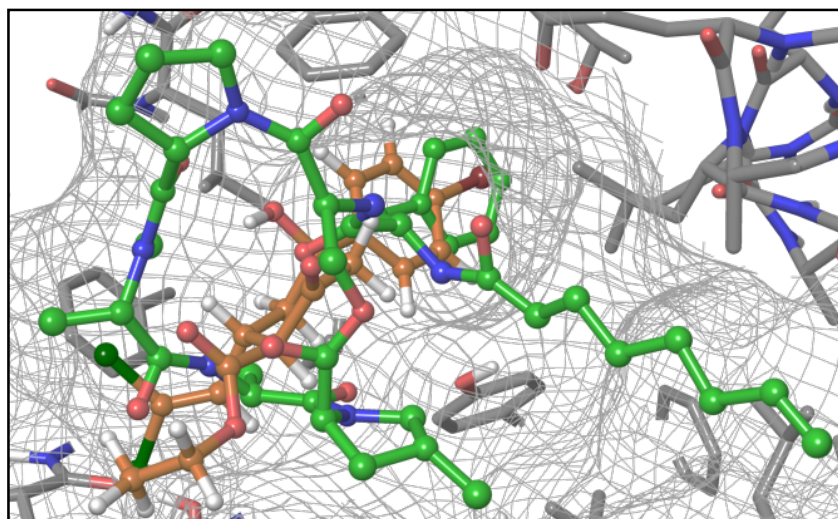


Figure 13. Superimposition of ADEP1 (green) and ACP5 (7) (orange) bound to EcClpP. ACP5 binding pose was predicted by Glide. Results were overlaid with the EcClpP·ADEP1 co-crystal structure (PDB: 3MT6).

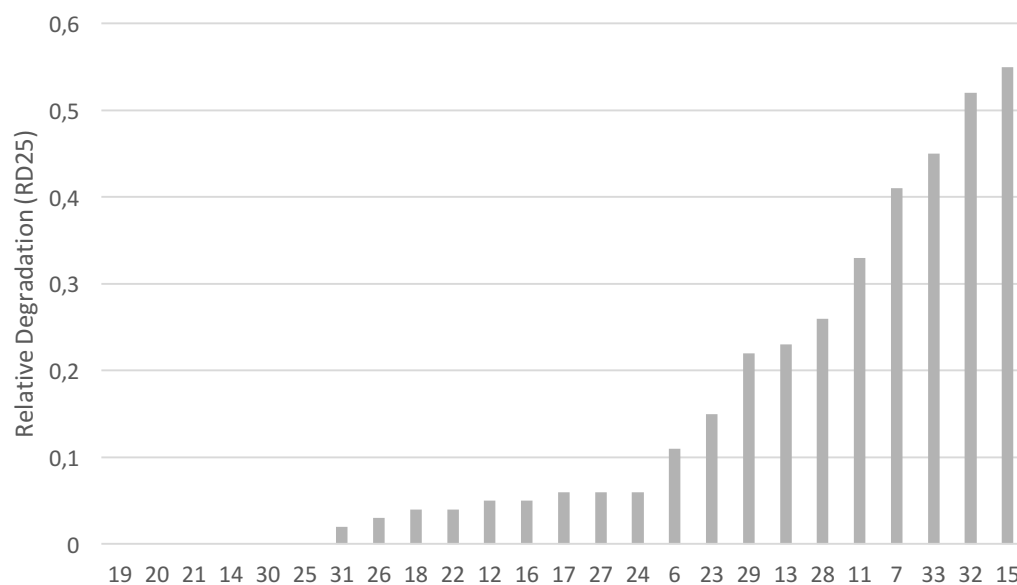


Figure 14. Experimentally determined ClpP activation activity of ACP4/5 analogues.

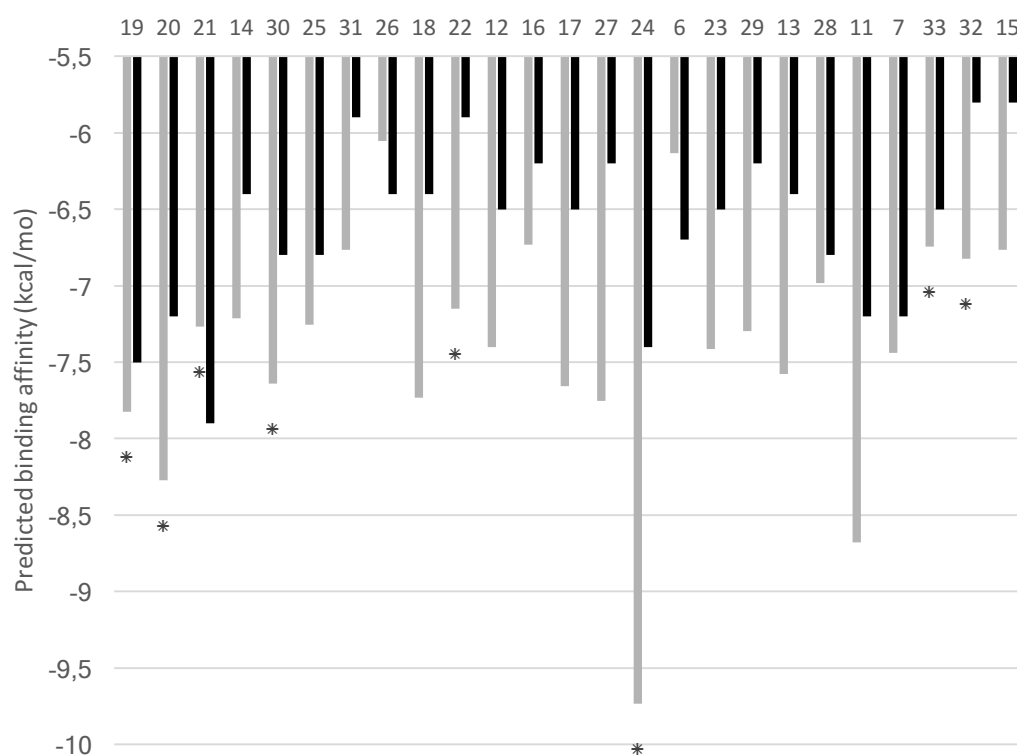


Figure 15. Predicted binding affinities of ACP4/5 analogues calculated by Glide (grey) and AutoDock (black). Compounds denoted with a star exhibited binding modes different that ACP5.

Glide, however, calculates binding energy per residue and analysis of this data also revealed no apparent correlation between specific residue involvement and activity. This could be explained partially by the fact that the receptor is treated as rigid during docking and only the ligands are flexible. As a result, the K_{pred} values are not as realistic as one desires. Furthermore, the binding site used for the docking studies of ACP5 is from the co-crystal structure of ADEP1 bound to EcClpP. With ADEP1 being substantially larger than ACP5, it is not surprising that the docking of ACP5 is less accurate.

Although the docking of ACP4/5 analogues lacks correlation with experimental activity, interactions between the ligand and binding site can be qualitatively evaluated. Furthermore, the docking results provided a relevant binding conformation of ACP4/5 scaffold because structurally comparable analogues adopted the same docking conformation with both AutoDock and Glide. Therefore, we can use the docking conformations to assess the different ACP4/5•EcClpP interactions.

Observation of the binding conformation (Figure 16) revealed that the phenyl ring, the dihalovinyl moiety and the ester are in the vicinity of previously noted key residues. Previously, we discussed the substituent-dependent nature of ClpP activation by ACP4/5 (e.g. halogens favor ClpP activation over H-bond acceptor or electron donating groups on the phenyl ring moiety). Thus, some interactions between ACP4/5 moieties and EcClpP residues are favored, suggesting that a docking analysis can provide further understanding of ACP4/5•EcClpP interactions. However, the ketone and hydroxyl moiety are further away from the pocket, leading us to conclude these moieties may indirectly impact ACP4/5 analogue activity, such as correctly orienting substituents in the pocket. Therefore,

analysis of analogue binding poses will only be focused on the phenyl ring, the dihalovinyl moiety and the ester.

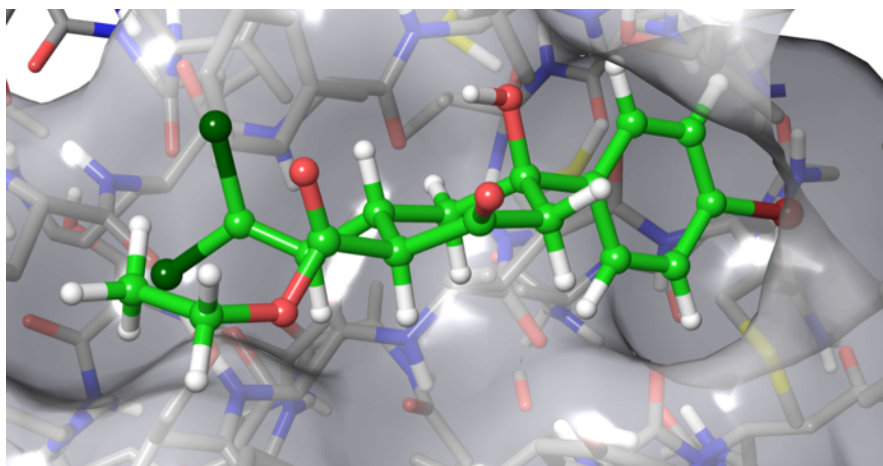


Figure 16. Predicted binding conformation of ACP5 (7) in EcClpP•ADEP binding pocket, calculated by Glide.

In our analysis, the ACP4/5 phenyl ring moiety was examined first. This motif is anchored in a hydrophobic pocket consisting of Leu48, Tyr62, Phe82, Ile90, Leu114 and Leu189 as shown in Figure 17. As mentioned previously, most of the ACP4/5 analogues are predicted to bind EcClpP in a similar fashion with the phenyl ring positioned in this pocket. As such, the aforementioned residues should interact in a similar fashion with every analogue. Upon inspection of the docked structures, different types of protein-ligand interactions with the phenyl ring are observed. For instance, for any of the docked ACP4/5 analogues, the EcClpP residues Leu48, Ile90 and Leu189 are positioned 3.84–4.64 Å (Table 5), which is consistent for weak alkyl- π interactions.⁵⁸ This observation coincides with Leung and co-workers' mutation studies, which demonstrate a loss in activity for ACP4/5 when a Leu189Glu mutation is made, demonstrating the importance of this alkyl- π interaction. The change from non-polar to polar residue likely reduces the hydrophobicity of the binding pocket and limits the ability of ligand binding. In addition to alkyl- π interactions, EcClpP Tyr62 and Phe82 provide π - π stacking

interactions with ACP4/5 ligands. As shown in Table 5, both Tyr62 (5.13 Å) and Phe82 (4.68 Å) are located at acceptable distances from ACP4/5 ligands to interact through π - π stacking interactions.⁵⁹

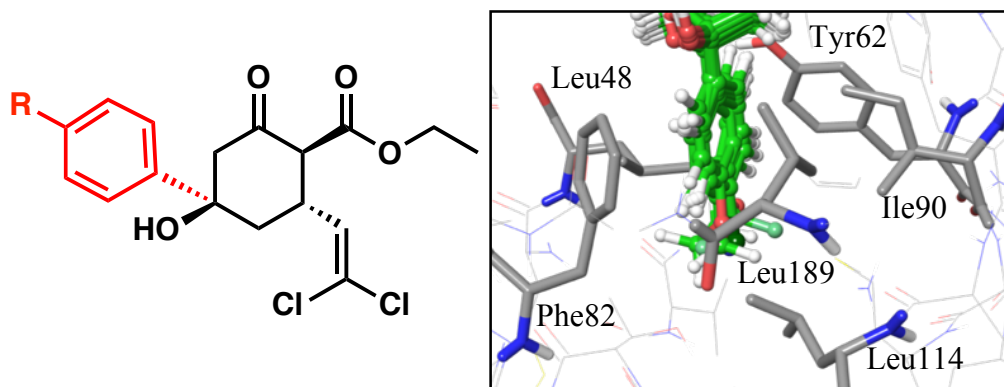


Figure 17. Close up view of superimposed phenyl ring moieties of compounds 6, 7, 11, 12, 13, 15, 16 and 18, and the surrounding residues.

Type of Interaction	Alkyl- π			π - π	
Residue	Leu48	Ile90	Leu189	Tyr62	Phe82
Average Calculated Distance (Å)	4.64	3.84	4.12	5.13	4.68

Table 5. Calculated distance between ACP5 phenyl ring moiety and surrounding residues.

The importance of the *para*-phenyl substituents was emphasized previously. The nature of the substituent greatly influences the capacity of the entire molecule to activate ClpP; therefore, a specific type of interaction may predominate in governing the activity. Interestingly, the *para*-substituent is close to two residues with heteroatom containing side chains, Thr79 and Met92 (Figure 18), suggesting that an interaction stronger than a simple hydrophobic interaction may contribute to the phenyl motif binding interactions.

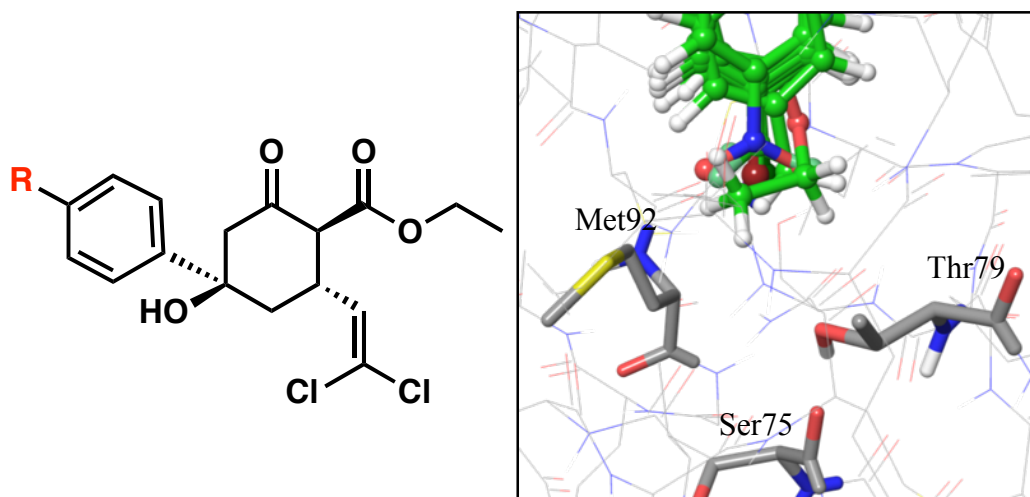


Figure 18. Close up view of superimposed phenyl ring moieties of compounds 6, 7, 11, 12, 13, 15, 16 and 18, and surrounding residues.

A hydrogen bond with the Thr79 side chain hydrogen seems unlikely, since the nitro (**6**), ethoxy (**12**), cyano (**18**) and methoxy (**16**) provide H-bond acceptor capabilities, but lack sufficient activity. Furthermore, the Thr79 hydroxyl proton is already involved in a H-bond with the Ser75 backbone oxygen. On the account of the low or moderate activity of **6**, **12**, **16**, and **18**, the formation of a competitive H-bond seems unlikely to occur. In addition, the methoxy (**16**), and particularly, the ethoxy (**12**) moiety seem to suffer from steric clashes with the residues of the pocket, as they are further away from Thr79 and/or Met92 (Table 6).

Compound	Calculated Distance R...O-Thr79 (Å)	Calculated Distance R...S-Met92 (Å)	Angle C-R...O-Thr79	Angle C-R...S-Met92
6	3.6	3.7	n/a	n/a
7	3.63	4.08	149.5°	120.9°
11	3.49	3.63	115.1°	114.9°
12	4.58	5.25	n/a	n/a
13	3.68	4.1	142.3°	117.2°
15	3.42	3.92	144.9°	117.9°
18	3.19	3.88	145.5°	114°
16	3.5	4.43	n/a	n/a

Table 6. Calculated distance between ACP4/5 analogues *para*-substituent and surrounding residues.

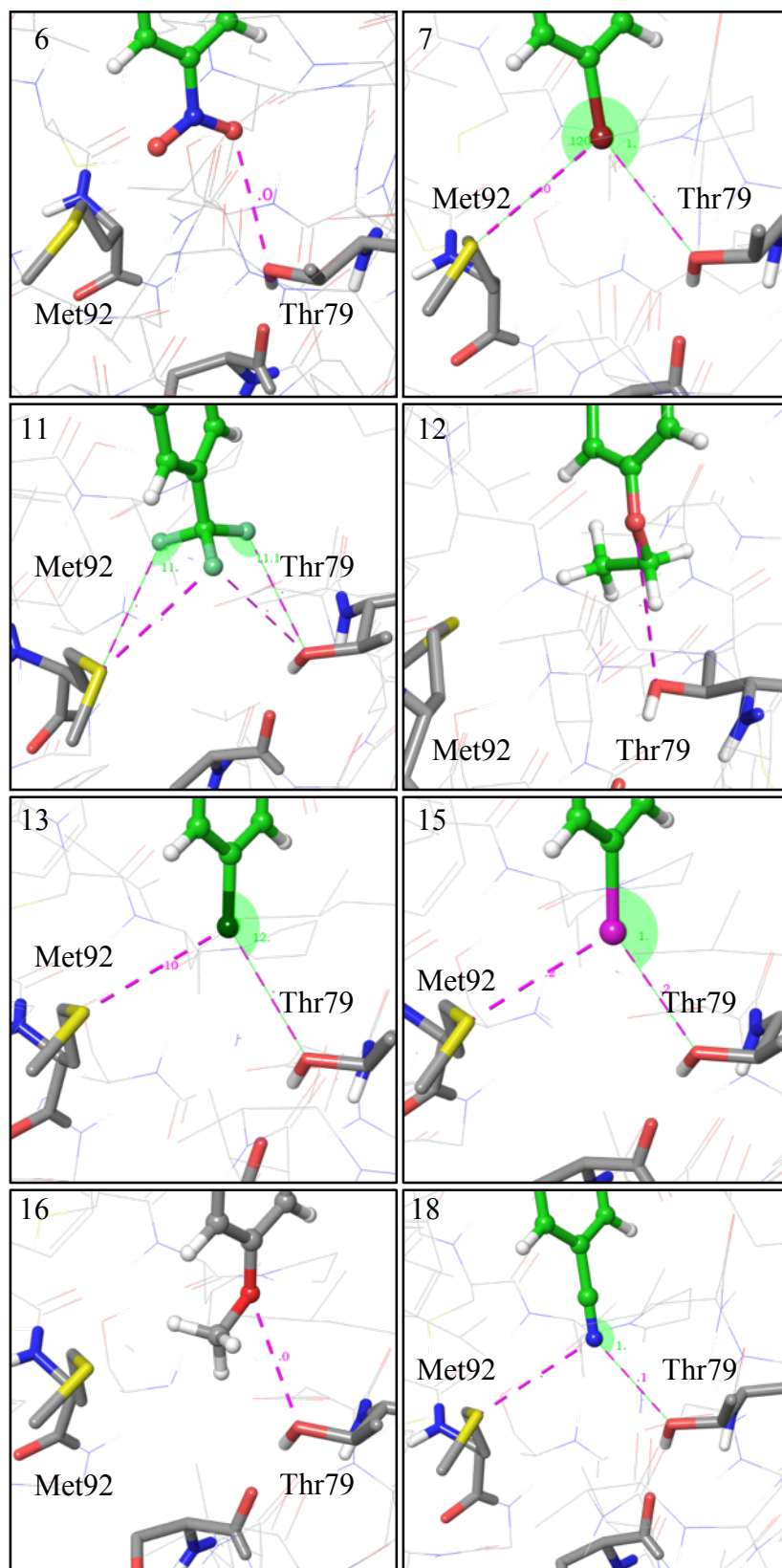


Figure 19. Predicted binding interactions of 6, 7, 11, 12, 13, 15, 16 and 18 with the surrounding residues Thr79 and Met92.

Upon further analysis of the phenyl motif, it was noticed that halogen containing analogues (**7**, **13**, **15**) are not only the most active, but also dock in such a way that positions the halogen atom in close proximity to Thr79 and Met92 (Figure 19). This suggests that halogen bonding, a relatively new concept in ligand-protein interactions, may be a key contributor in ACP4/5 binding. For a long time, halogens were considered only as hydrophobic moieties and good electron-withdrawing groups. Not until recently has the analysis of crystal structures unveiled this new type of non-covalent interaction.⁶⁰ Indeed, the electronic density on the halogen was first believed to be isotropic (Figure 20, left) but this representation has recently been refuted and a new charge distribution model proposed (Figure 20, right). Instead of a negative charge surrounding the entire halogen substituent, a positively charged region is located on the opposite end of the C-X σ bond and is called a σ -hole. A negative charge is then orthogonally distributed around the halogen to form an electron-rich belt.



Figure 20. Traditional (left) and current (right) electrostatic representation of a halobenzene.

Historically, one would have considered halogens to be engaged in a charge transfer-type interaction as electron donors toward an electron acceptor atom. However, it has been observed that in typical halogen bonds, the donor-acceptor model is reversed. Electrons located on a heteroatom side chain such as a hydroxyl group of serine, threonine or tyrosine; carboxylate groups in aspartate and glutamate; sulfurs in cysteine and methionine; and nitrogens in histidine, donate density toward the σ -hole of a halogen to form a non-covalent halogen interaction.

This type of electronic distribution confers halogens a dual function, as they can behave as electron donors when the contact is made on the side of the halogen or as electron acceptors when the approach is head-on. Furthermore, the σ -hole character of halogens depends on the size of the element, with iodine making the strongest halogen bond and fluorine the weakest.

Indeed, halogen introduction to exploit this interaction has improved the potency of known drugs. For instance, Hardegger *et al.* studied halogen bonding for inhibitors of human cathepsin L (hcatL) and MEK1 kinase. In both cases, substitution of *para*-aromatic hydrogen by iodine resulted in a significant decrease of the half-maximal inhibitory concentration (IC_{50}), 45-fold and 26-fold improvement was noted for hcatL and MEK1 inhibitors, respectively. Furthermore, potency improved with the halogen bonding capability of the halogen, demonstrating the importance of halogen bonding and the powerful use of halogens in drug design.⁶¹

Halogen	Oxygen	Sulfur
Fluorine	2.99	3.27
Chlorine	3.27	3.55
Bromine	3.37	3.65
Iodine	3.5	3.78

Table 7. Standard distances between halogen and halogen bond acceptors (\AA).⁶²

In the context of our study, the possibility of **7**, **13** and **15** forming a halogen bond between the EcClpP Thr79 side chain oxygen and the Met92 side chain sulfur was evaluated. As presented in Table 6, the iodine (**15**) is closer to the two heteroatom side chains 3.42 \AA (Thr79) and 3.92 \AA (Met92), than chlorine (**13**) and bromine (**7**), respectively 3.68/4.1 \AA and 3.63/4.08 \AA . In addition, the iodine is the closest to the optimal distance C-I...O-Thr79 compared to the chlorine and the bromine (Table 7). All C-X...S-Met92 distances, however, are out of the range of

optimal bond lengths. Thus, the iodo-analogue (**15**) seems to be at the right distance to make a meaningful halogen bond with Thr79. Acceptable angles (C-X...Y, Y=N, O, S) to make a halogen bond range from 180° (ideal angle) to 140°. Docked poses of **7**, **13** and **15** display C-X...O-Thr79 angles between 142.3° and 149.5°, and C-X...S-Met92 angles between 117.2° and 120.9° (Table 6). Hence, a halogen bond with Thr79 seems more probable than with Met92. In summary, halogenated compounds **7**, **13** and **15** are predicted to make favorable halogen bond interactions with the oxygen side chain of Thr79 and the correlation between the strength of the iodine-oxygen interaction and the high activity of **15** is consistent with the halogen bond model. Although, as previously stated, the docking method does not allow flexibility of the binding pocket, and one could envision an accommodation (distance/angle) of Thr79 to form a more favorable halogen bond.

In regards to the trifluoromethyl-analogue **11**, identification of the role of CF₃ in molecular recognition by the pocket is more difficult. Despite the high electronegativity of fluorine, it is not known to make strong interactions, as fluorine is a weak halogen bond donor. And it behaves as a poor hydrogen bond acceptor due its low polarizability and the tightness of its electron shell.⁶³ Over the years, it has been debated whether fluorine could participate hydrogen bonds or not, as fluorine fails to compete with other hydrogen bond acceptors (oxygen and nitrogen) and because of its low occurrence in biological systems. The current consensus can be summarized by the title of Dunitz and Taylor's study on the subject: "Organic fluorine hardly ever accepts hydrogen bonds."⁶⁴ Nevertheless, when fluorine does make H-bonds, the strength of that bond is close to a van der Waals interaction and it will be significant only in the absence of any other competing intermolecular forces.

The docking conformation of **11** seems to invalidate both halogen and hydrogen-bond interactions (Figure 19). None of the fluorines are close enough to Thr79 or Met92, and the C-F...O/S angles are lower than 140° (Table 6 and 7), well outside the accepted angles to suggest a meaningful interaction. Moreover, H-bond between a fluorine and Thr79 is unlikely to happen, because of the competition with Ser75. Therefore, the activity observed for CF₃-analogue **11** cannot be explained by a direct interaction of the binding pocket with the functional group or at least, our docking study fails to provide any meaningful insight.

Another moiety of ACP4/5 analogues that may benefit from halogen bonding is the dihalovinyl group. As shown in Figure 21, the dichlorovinyl and dibromovinyl of compound **7** and **23** respectively are in the vicinity of Tyr60, Ser88 and Phe112. However, it is noticeable, in Figure 22, that **23** is displaced compared to **7**, potentially explaining the decrease in activity of **23** and demonstrating that an increase of halogen size for this substituent is deleterious to ClpP activation capabilities. Despite the evident decrease in the RD₂₅, from 0.41 to 0.15 for **7** to **23**, respectively, the dibromovinyl analogue is still active, indicating that favorable interactions occur. A halogen-Ser88 oxygen bond can be then envisioned, albeit at the cost of other potentially more meaningful interactions. As presented in Table 8, the C-X...O-Ser88 distance is more favorable for **23** than for **7**, although both C-X...O-Ser88 angles are below 140°, potentially invalidating halogen bonding. However, as stated earlier, the lack of protein-flexibility during docking studies can skew these angles. Therefore, we can only hypothesize that a halogen bond with Ser88 may explain the activity dihalovinyl moiety.

Besides halogen bonding, a halogen- π interaction can be considered because of the proximity of the dihalovinyl moiety with Tyr60 and Phe112. Based

on the Leung *et al.* mutation study, the involvement of Phe112 must not be neglected, since the Phe112Ala mutation resulted in the loss of ACP4/5 activity. Thus, in addition to hydrophobic interactions, the dihalovinyl halogen is postulated to interact with Phe112 aromatic ring in a halogen- π fashion. Nevertheless, further computational analysis is required to assess the relevance of this interaction.⁶⁵

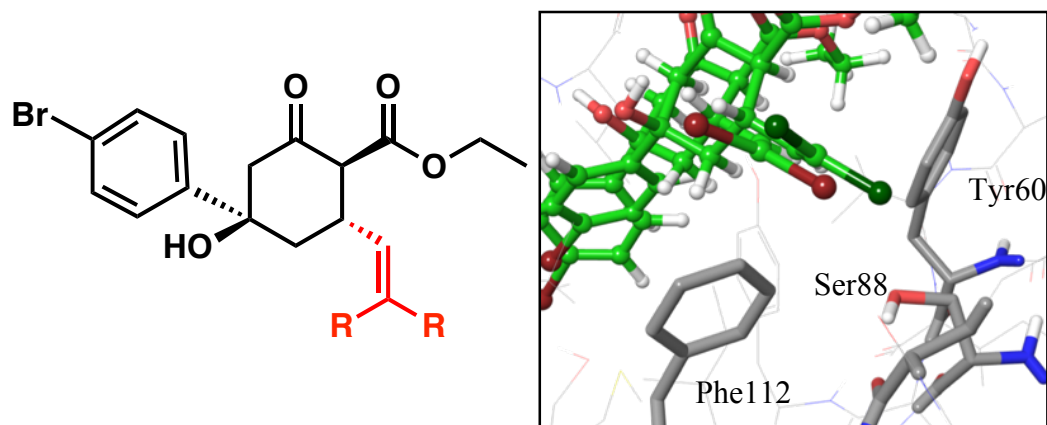


Figure 21. Close up view of superimposed dihalovinyl moieties of compounds 7 and 23, and the surrounding residues Phe112, Ser88 and Tyr60.

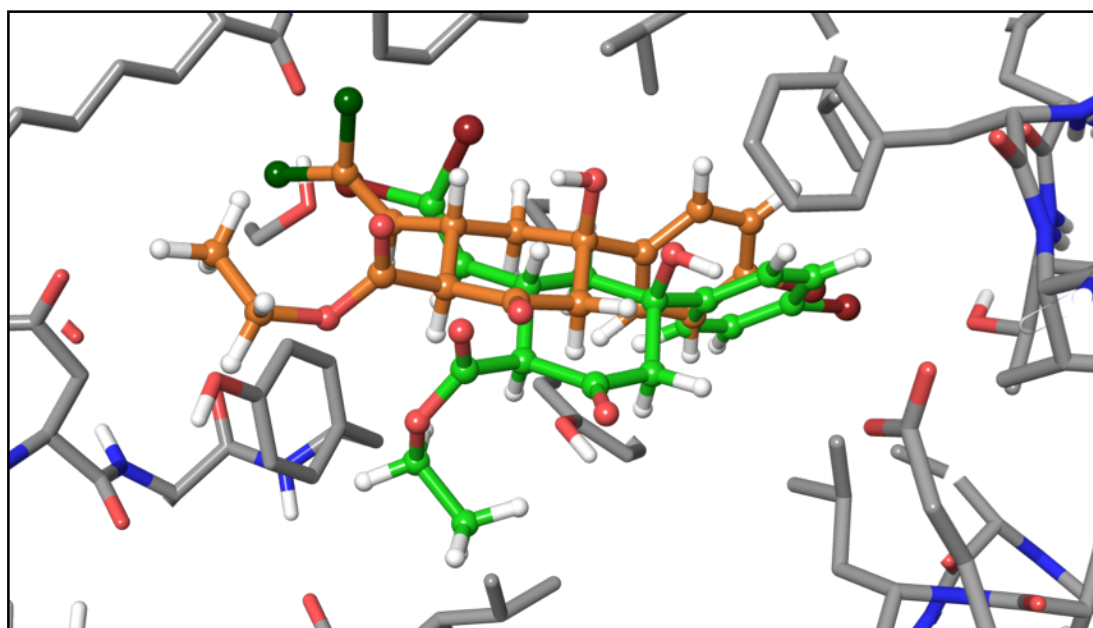


Figure 22. Superimposition of predicted docking conformations of 7 (orange) and 23 (green).

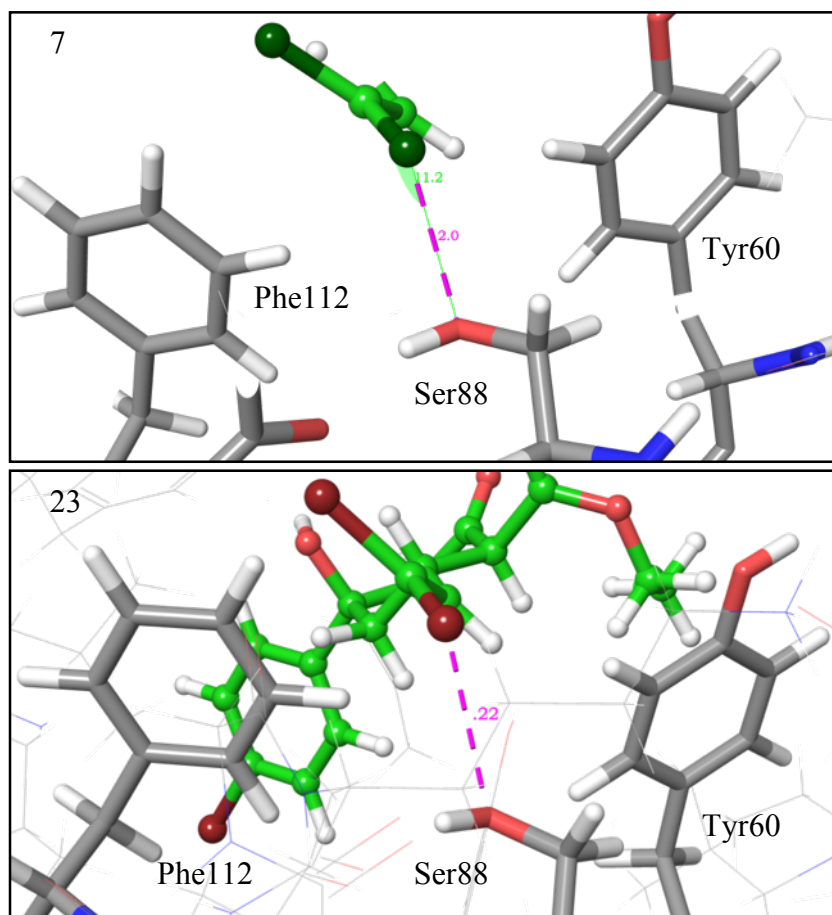


Figure 23. Binding conformation of compounds 7 and 23, and surrounding residues Phe112, Ser88 and Tyr60.

Compound	Calculated Distance R...O-Ser88 (Å)	Angle C-R...O-Ser88
7	2.9	117.2°
23	3.22	133.2°

Table 8. Calculated distances and angles between dihalovinyl moiety of compounds 7 and 23, and Ser88.

Finally, the proximity of the ester moiety to Tyr60 indicates a possible H-bond between the alkyl oxygen and the Tyr60 polar hydrogen, as shown in Figure 24. Even though Tyr60 hydrogen is oriented away from the molecule in the model, it is not involved in another H-bond, and thus capable of free rotation for hydrogen bonding. Furthermore, the docking conformation predicts a bond length between 3.39 and 3.48 Å (Table 9), the range of weak/moderate H-bonds.⁶⁶ Although the ester may form an H-bond with Tyr60, compounds 7, 27, 28 and 29 do not display

the same activity, suggesting that the size of the ester substituent may play a significant role in the H-bond formation.

As mentioned, esters can adopt *s-cis/trans* conformations depending on the size of the pendant alkyl group and steric interactions with the protein binding pocket. As presented in Figure 25, the methyl ester analogue **27** (less bulky) is predicted to adopt an *s-trans* conformation upon binding whereas **7**, **28** and **29** are predicted to adopt *s-cis* conformations, to avoid any steric clash with the rest of the molecule. Computational analyses of the conformational energies for **7**, **27**, **28** and **29** revealed a lower energy difference between the *s-cis* and *s-trans* conformations of the methyl ester than the other analogues (Table 10). Therefore, transition between *s-cis* and *s-trans* conformation is more facile for **27**. As previously mentioned binding of ligands is a dynamic process, as both ligand and protein are in a constant motion, possible steric clashes can occur. Therefore, an increase in the population of *s-trans* **27** conformers lowers the probability of forming an H-bond with Tyr60, as the methyl group blocks the interaction, possibly providing some insight into its low activity. Furthermore, the difference in relative EcClpP activation of **7**, **28** and **29**, 0.41, 0.26 and 0.22 respectively, may be attributed to steric clashes with Tyr60 that are more prevalent with both an iso-propyl and tert-butyl group than an ethyl group. In conclusion, **7** is the most active of ester analogues because of its high *s-cis/trans* energy difference, locking the ester in *s-cis* conformation, and also because the ethyl group induces less steric interactions than bulkier groups.

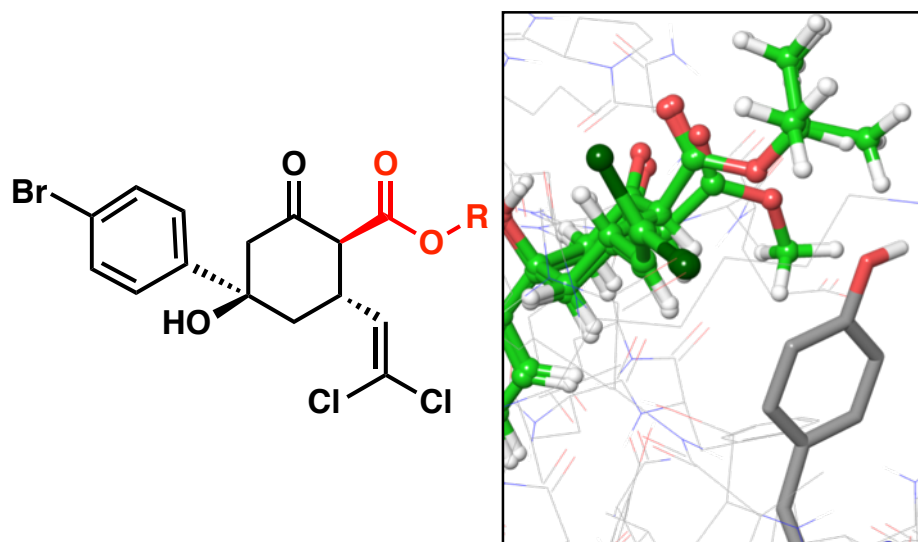


Figure 24. Close up view of the superimposed ester moieties of compounds 7, 27, 28 and 29, and the surrounding EcClpP residue Tyr60.

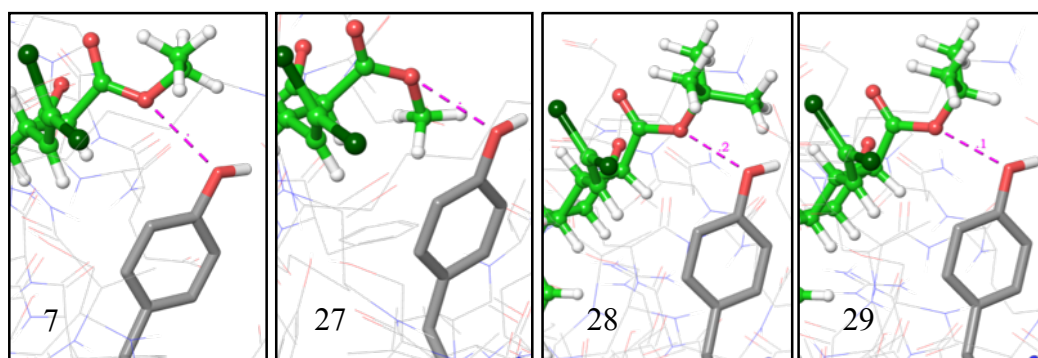


Figure 25. Predicted binding conformation of compounds 7, 27, 28 and 29

Compound	7	27	28	29
Calculated Distance R-O...O-Tyr60 (Å)	3.39	3.48	3.42	3.41

Table 9. Calculated distances between ACP4/5 ester moiety and Tyr60.

Compound	7	27	28	29
Energy Differences Between <i>cis/trans</i> Ester Conformation (kcal/mol)	7.698	5.920	8.061	8.630

Table 10. Calculated energy differences between *cis/trans* ester conformation.

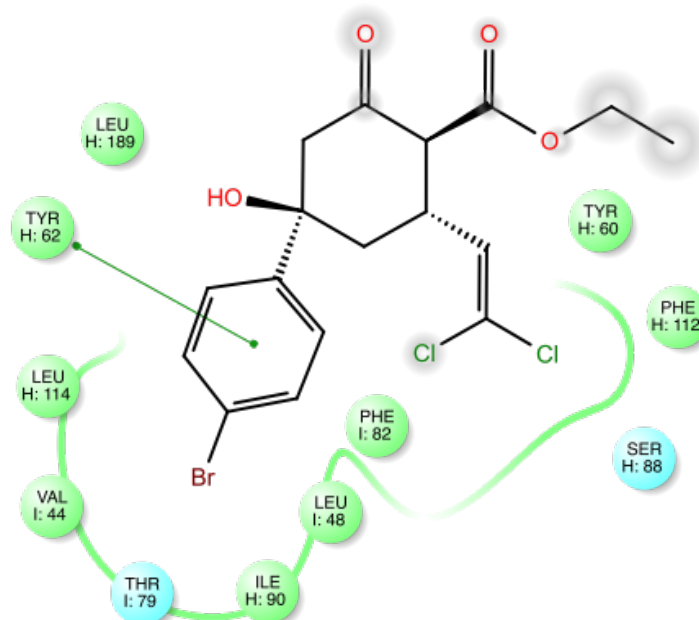


Figure 26. Docking studies summary of ACP5.

In summary, this is the first time a docking analysis of ClpP activators has been reported. Although predicted binding energies fail to correlate with experimental activity data, the docking analysis provides some insight into the potentially dominant interactions responsible for ACP4/5•EcClpP binding. For instance, the alkyl- π (Leu48, Ile90 and Leu189) and π - π stacking (Tyr62, Phe82) made with the phenyl ring moiety and the halogen bond (Thr79) made with the *para*-substituent appear to be essential for optimal ACP4/5 binding affinity. This is an observation not readily noted through predicted binding affinities and only arises from detailed inspection of computational results. In addition, this is coherent with our hypothesis that ADEP pharmacophore (i.e. the N-acylphenylalanine fragment) binds in the same subpocket than ACP4/5 analogues. Additionally, the H-bond (Tyr60) and the halogen bond (Ser88) formed respectively by the ester and the

dihalovinyl seem to be important to a lesser extent for EcClpP activation, since the orientation of these moieties is not optimal and the binding of these two moieties is not tightly enclosed between residues like the phenyl ring is. Therefore, analysis of our results brings us to the first flaw of the docking methods: The lack of residue flexibility may prohibit a proper accommodation of the ligand, possibly resulting in erroneous binding energies and contacts with residues. Second, no parallel was made between the binding energy and RD25 of ACP4/5 analogues, which prevents any quantitative correlation of the predicted binding affinity with the structure. However, we were able to qualitatively identify the possible interactions between the different moieties of ACP4/5 scaffold and the residues of the binding pocket. Therefore, the docking study provided some rationale for ACP4/5 derivative activities, but more detailed computational studies are needed. To clarify the activity difference of some compounds we aimed to provide additional insight into ACP4/5•ClpP interactions by analyzing the congruency between ligand and protein frontier molecular orbitals.

2.2. The Frontier Molecular Orbital Theory: A Tool to Enhance Molecular Recognition

2.2.1. Introduction

In 1982, Fukui introduced the revolutionary concept of Frontier Molecular Orbitals (FMOs) and their significant role in chemical reactions.⁶⁷ He theorized that the electron delocalization from a Highest Occupied Molecular Orbital (HOMO) toward a Lowest Unoccupied Molecular Orbital (LUMO) was responsible for the formation or the breaking of chemical bonds. Fukui also emphasized the importance of orbital symmetry in electron delocalization between FMOs, as they need to be complementary to overlap. The FMO theory can be exemplified by the

cycloaddition of butadiene and ethylene, where the interaction between the HOMO of the diene and the LUMO of the dienophile is essential for the occurrence of the reaction.⁶⁸ The concept of HOMO/LUMO interaction is not only limited to the formation of covalent bonds, but can also be applied to the understanding of ligand-protein interactions in molecular recognition. As such, the FMO theory has recently been introduced to the field of medicinal chemistry as a tool to enhance the understanding of ligand binding.

With the development of computational methods, quantum chemistry has become a useful tool available to medicinal chemists to design more active molecules. Although FMO theory has been integrated into quantitative SAR (QSAR) studies, applications remain limited to a ligand-based analysis. For example, some studies focus only on ligand HOMO and LUMO, neglecting the requirement for binding site complementarity in molecular recognition.⁶⁹ Another common approach is to calculate electronic properties of a molecule (i.e. HOMO energy, LUMO energy, or the energy gap between the HOMO and LUMO) in order to evaluate the “reactivity” of a molecule.⁷⁰ Considering only energies does not provide the location nor the symmetry of MOs and, as a result, the analysis of the electronic properties is incomplete. Nevertheless, some researchers utilize these incomplete FMO models to explain protein-ligand interactions.⁷¹ Inspired by the current status of FMO approaches, we sought to investigate FMO on both the ligand and protein levels to better understand ACP4/5•EcClpP interactions and thus provide insight into the design of improved ACP4/5 derivatives.

Our previous studies provided the binding poses of ACP4/5 analogues bound to the EcClpP•ADEP binding pocket and as a result of these studies we were able to identify potentially important ACP4/5•EcClpP interactions. However, the

lack of correlation between experimental compound activity and predicted binding affinities prohibited us from quantifying the gain of activity as a function of the related structural change. Furthermore, docking studies do not easily provide depiction of non-covalent interactions. Therefore, to further rationalize ACP4/5 activity we needed to develop a tool capable of accurately describing ACP4/5•EcClpP binding and the resulting interactions. For this reason, we are interested in using the FMO theory to interpret protein-ligand interactions.

Similar to the Fukui theory that describes covalent bond formation, we hypothesize that electron complementarity between interacting HOMOs and LUMOs plays an important role in the non-covalent interactions between ligands and proteins. Thus, a HOMO from a residue in the binding site can overlap with a LUMO from the ligand, or similarly a HOMO of the ligand with a LUMO of the pocket (Figure 27). From docking studies, it is evident that more than one interaction between the ligand and protein occurs; therefore, we need to take into account more than one HOMO/LUMO couple. However, the further away a MO is from the frontier, the weaker or the less relevant the interaction is.

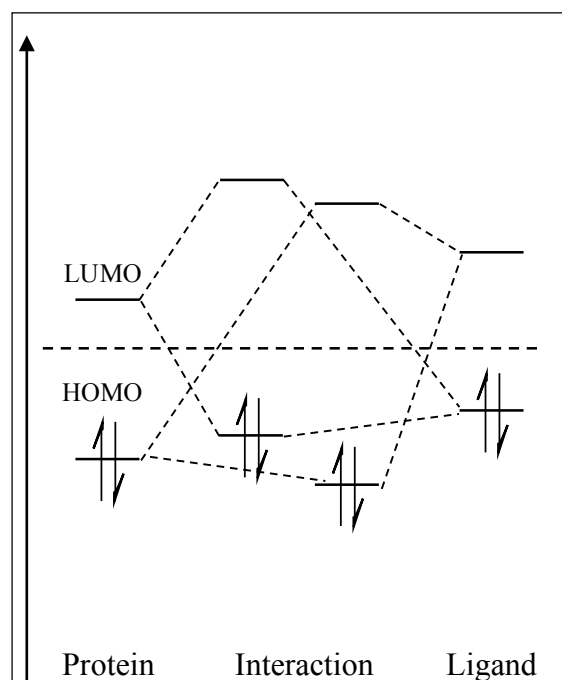


Figure 27. Diagram of frontier molecular orbital interactions.

As a proof-of-concept, we used the FMO model on ACP4/5 analogues to further characterize the non-covalent interactions identified in our docking studies. By combining our docking studies with the FMO model, the goal of these studies is to quantitatively describe ACP4/5•EcClpP interactions in order to predict the effect of structural modification on new ACP4/5 analogue activity. We postulated that only the MOs close to frontier are involved in major non-covalent interactions with the protein. Thus, the first ten LUMOs and the last ten HOMOs of each compound were calculated using Gaussian 09, providing MO energy levels and electronic distributions of each MO. In order to interpret RD_{25} differences between similar analogues, we compared the energy levels and the electronic distribution of MOs on a moiety. For instance, the electronic density of each MO displays the probability of electron distribution within the molecule indicating the atoms or group of atoms more likely to contribute to non-covalent interactions. Along with the electronic distribution, calculated MOs present orbital symmetries that must be complemented by the interacting partner to provide a positive interaction.

2.2.2. *Methods*

Calculations were performed using the Gaussian 09 suite.⁷² Geometry optimizations were conducted using the hybrid DFT, M06-2X/def2-TZVP basis set. This basis set is designed to represent non-covalent interactions with high accuracy and reasonable computational cost.⁷³ To afford structures with conformations close to a global minimum, every molecule was built using the ACP5 crystal structure.⁷⁴ The minimization calculation was confirmed by tight convergence optimization criteria and vibrational frequency analysis was achieved so that only real frequency (i.e., no imaginary frequencies) values were obtained for all geometries.

Throughout the study, MOs are represented as red and green lobes to visualize the electronic properties of the compounds. Population analysis was used to quantify the electronic distribution of each MO on molecules.

Since calculation of EcClpP MOs would be very computationally expensive and time intensive with Gaussian 09, we could not obtain whole protein EcClpP FMOs. However, we calculated the FMOs of individual residues involved in interactions to illustrate MO complementarity. This represents a first approximation approach to test our hypothesis.

2.2.3. *Results and Discussion*

2.2.3.1. *Phenyl Moiety Analysis*

2.2.3.1.1. *Halogen Bonding*

As previously discussed, the interaction between the *para*-substituent and the Thr79 side chain oxygen appears to be most favorable when a halogen bond is possible. In order to understand the selectivity towards halogens, the electronic properties of the 4-halobenzene analogues (**7**, **13**, **15**) were first studied. As

discussed previously and shown in more detail in Figure 28, the electrostatic potential (ESP) isosurfaces of halobenzenes illustrates the anisotropy of halogens. The σ -hole (red) noticeably increases with the halogen size, whereas the surrounding negative charge (blue) is constant independently of the halogen size.

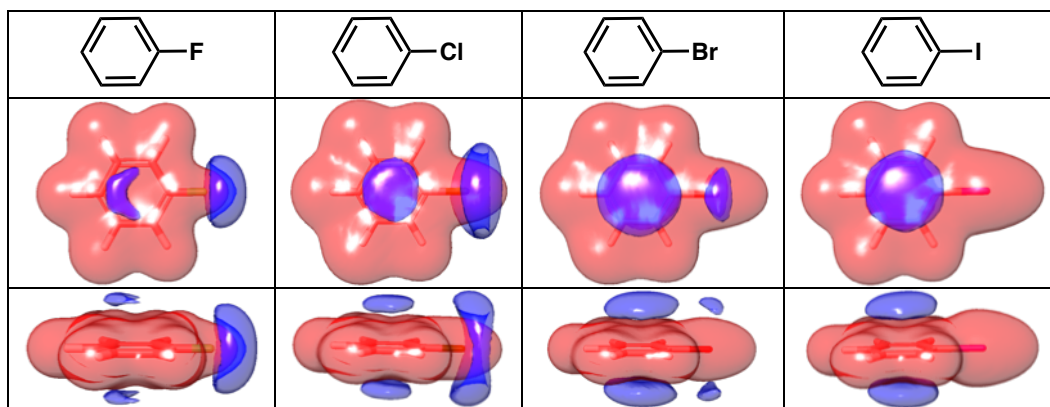


Figure 28. Electrostatic potential (ESP) isosurfaces of fluorobenzene, chlorobenzene, bromobenzene and iodobenzene. Positive ESP isosurfaces are represented in red and negative ESP isosurfaces in blue. The electrostatic potential surfaces for the representative aromatic units were plotted from DFT calculations (B3LYP using 6-31G**+) with Jaguar.

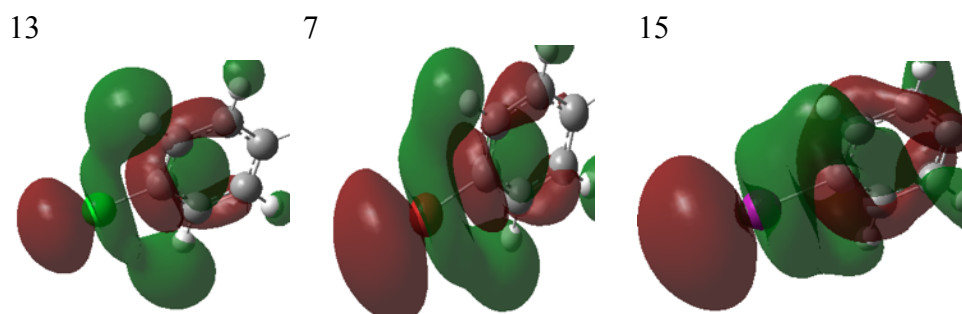


Figure 29. LUMOs of the phenyl portion of analogues 13, 7 and 15. The structures were minimized with the basis set M06-2X/Def2-TZVP in Gaussian 9.

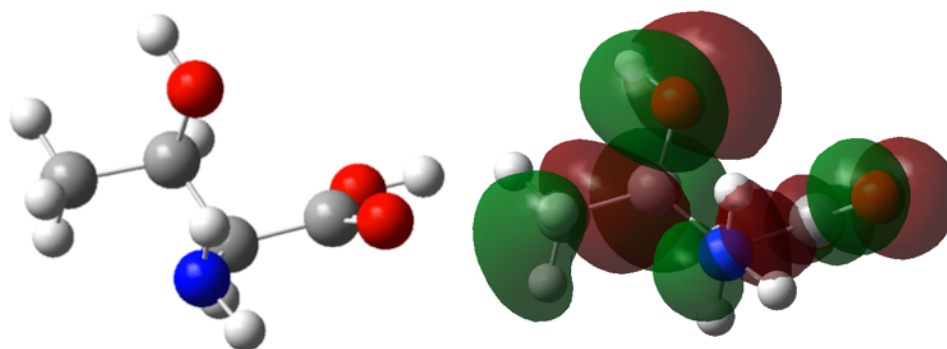


Figure 30. HOMO of threonine. The structure was minimized with the basis set M06-2X/Def2-TZVP in Gaussian 9.

In a qualitative fashion, the electronic distribution can also be observed in MOs; HOMOs displaying negative charges and LUMOs positive charges. With regards to halobenzenes, the positive ESP isosurfaces characterizing the σ -hole (red isosurfaces in Figure 28), correlates well to the calculated LUMOs on the halogens (red lobes on halogen in Figure 29). Thus, using LUMOs to depict the σ -hole of halogens may provide an opportunity to evaluate the halogen bond donor capacity of a halogen via the LUMO energy and the electronic density on halogen.

Based on our docking studies, the Thr79 side chain oxygen is the halogen bond acceptor, therefore the HOMO on the oxygen (Figure 30) corresponds to the oxygen lone pairs of electrons. An overlap between one of the HOMO lobes of the oxygen and the LUMO of the halogen can be envisioned as the lobes are compatible. As previously discussed, an increase in the size of the pendant halogen correlates with a gain of an ACP4/5 analogue activity. This trend may be explained by the fact that the electronic density of the halogen LUMO increases with the size of the halogen (Figure 32): 12% on the chlorine **13**, 34% on the bromine **7** and 43% on the iodine **15**. With a more prominent LUMO on the halogen, the overlap with the HOMO of Thr79 oxygen will be more significant, hence a stronger halogen bond is possible. In addition, the energy of the LUMO is inversely proportional to the size of the halogen: 1.809 eV for **13**, 0.937 eV for **7** and 0.044 eV for **15**. As a result, the “reactivity” of LUMO increases, as the energy gap between the LUMO of the halogen and the HOMO of the Thr79 oxygen (depicted in Figure 30) decreases.

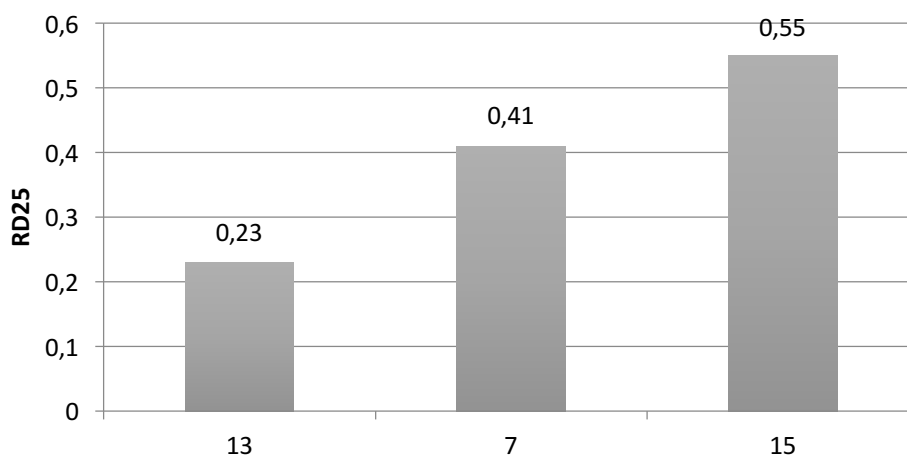


Figure 31. Relative EcClpP activation of compounds 13, 7 and 15.

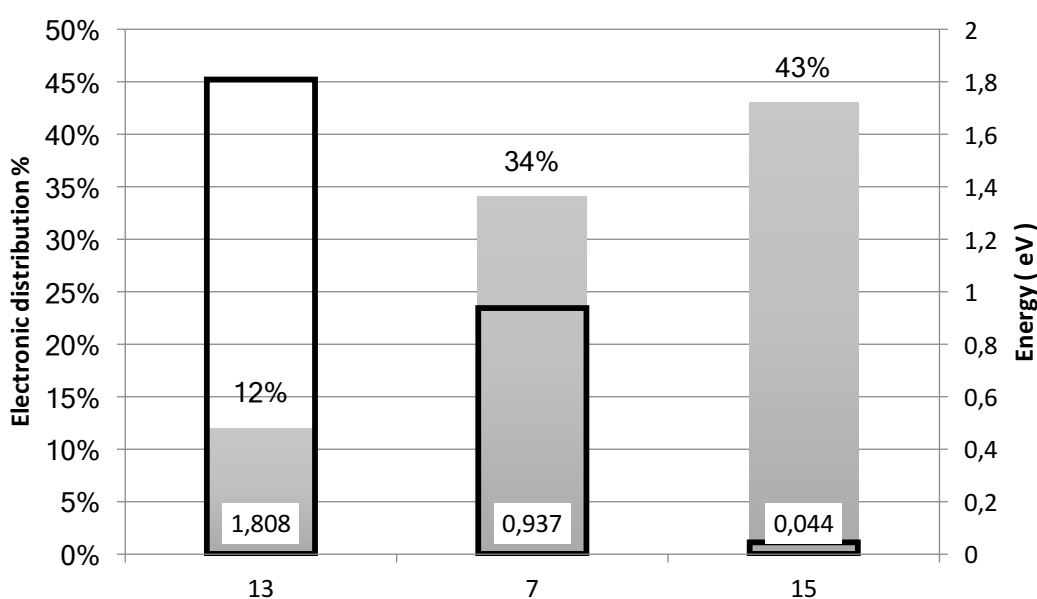


Figure 32. Correlation of LUMO energy and halogen electron density for 13, 7 and 15. The energy of the unoccupied molecular orbital in eV (in black) is represented with the percentage of electronic density on the halogen (in grey).

2.2.3.1.2. Phenyl Ring

The nature of the phenyl substituent not only contributes to interactions made with the surrounding residues, it also affects the electronic distribution of the phenyl ring. Generally, aromatic π electrons are polarized in a such way that a partial negative charge (blue, Figure 33) is centered on the ring and a partial positive charge (red, Figure 33) is distributed on the periphery. If we consider π - π stacking interactions as a charge-transfer fashion, π electrons from one ring (central

partial negative charge) are delocalized toward the peripheral partial positive charge of another ring. Therefore, the perpendicular T-shaped and parallel displaced geometries are favored for aromatic π - π stacking interactions (Figure 33).⁷⁵ In regards to electronic distribution, electron withdrawing groups create an π electron deficiency on the phenyl ring; whereas electron donating groups make the ring electron-rich. Therefore, the polarizing character of substituents influence the strength of interactions that involve π electrons, such as π - π stacking and alkyl- π interactions.⁷⁶

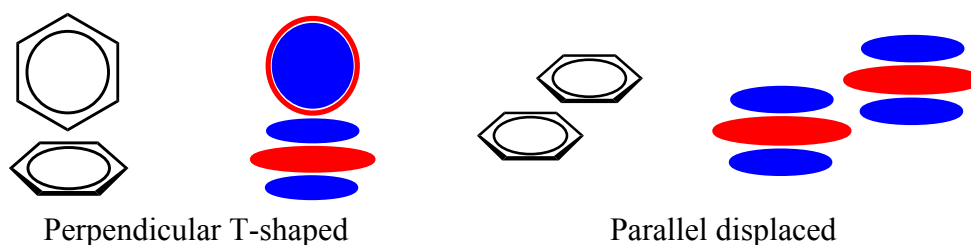


Figure 33. Favorable aromatic stacking arrangements and schemes representing the partial negative charge (blue) and the partial positive charge (red).

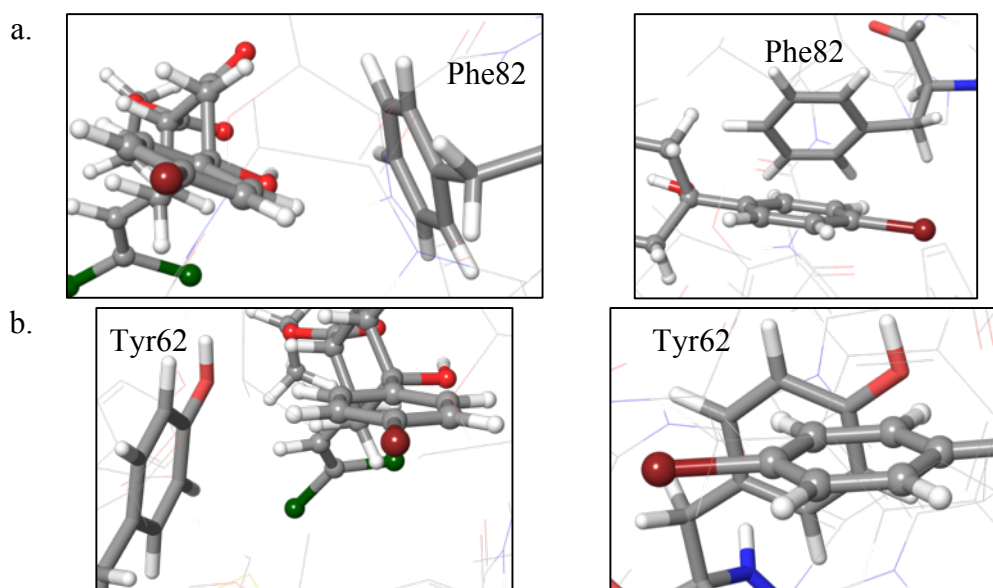


Figure 34. ACP5 (7) phenyl ring and predicted interactions with (a) Phe82 and (b) Tyr62.

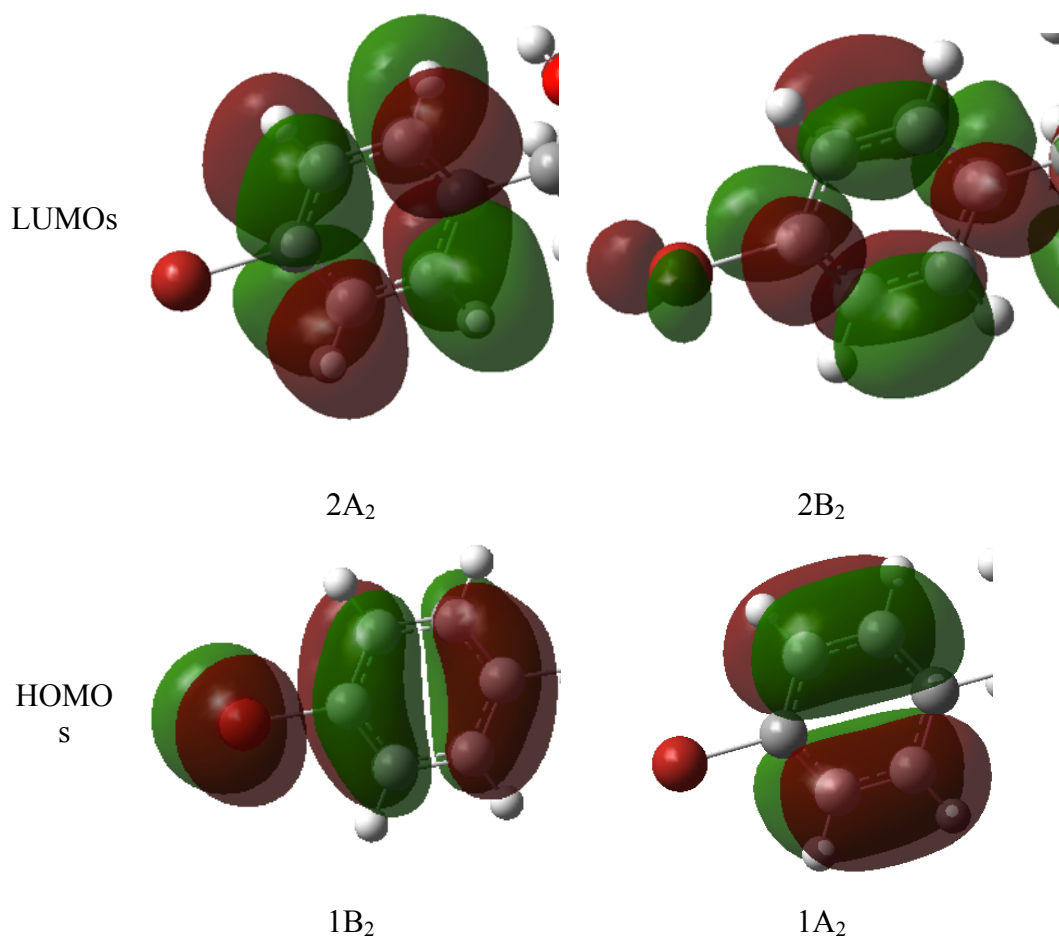


Figure 35. HOMOs and LUMOs of ACP5 (7) phenyl ring. ACP5 was minimized with the basis set M06-2X/Def2-TZVP in Gaussian 9.

Based on our docking studies, we can envision a charge-transfer from the central partial negative charges from Phe82 and Tyr62 (Figure 34) toward the peripheral positive charge of ACP5 (7) phenyl ring. To further evaluate the π - π stacking interaction, we examined FMOs of the phenyl ring of compound **6**, **7**, **11-18**. We can foresee electron delocalization from HOMOs of Tyr62 and Phe82 toward LUMOs of the phenyl ring moiety.

As presented in Figure 35, within the first ten HOMOs and LUMOs, we observed two symmetries of MOs on the phenyl ring for both occupied and unoccupied MOs. Interestingly, no other symmetries throughout the studied analogues (**6**, **7**, **11-18**) were noted. Despite the MO similarity, the phenyl substitution noticeably induces differences in MO energy levels. We present, in Figure 36, the MO energy levels of different *para*-substituted ACP4/5 analogues along with the corresponding activity. Substituents can promote π - π stacking interactions by bringing LUMO energy levels of the phenyl ring closer to HOMO energy levels of Tyr62 and Phe82 and conversely impede π - π stacking interactions by moving LUMO energy levels away. However, we do not notice an evident trend between MO energy levels (Figure 36) and experimental EcClpP activation, even though some substituents seem to have a greater influence on MOs than others and therefore, affect the corresponding compound's activity.

As shown in Figure 36b, the energy levels of LUMOs are lower, compared to **14**, in compounds bearing electron withdrawing groups (EWG), such as analogues **6**, **7**, **11**, **15** and **18**. This tendency is significant for compounds **6** and **18**, which contain the electron withdrawing nitro and nitrile groups, respectively. On the contrary, electron donating groups (EDG) increase the LUMO energy levels of **12** and **16**.

Interestingly, a parallel can be made between lower LUMO energy levels and moderate/good activity (**6**, **7**, **11** and **15**) and conversely for higher LUMO energy levels (**12**, **16**) and poorer activity. This trend corroborates that a more favorable charge-transfer interaction can occur between the phenyl ring LUMO and the protein residue HOMO due to a lower intermolecular HOMO-LUMO energy gap. However, the fact that lower HOMO-LUMO energy gap correlates only with **6**, **7**, **11** and **15** (Figure 36b) suggests that π - π stacking interactions are not a major determinant in ACP activity, but are rather secondary contributors, if we consider charge-transfer interaction as the sole contributor. Even though it helps us rationalize the activity of ACP4/5 analogues, we are not able explain the difference in activity of **6**, **11** and **18**.

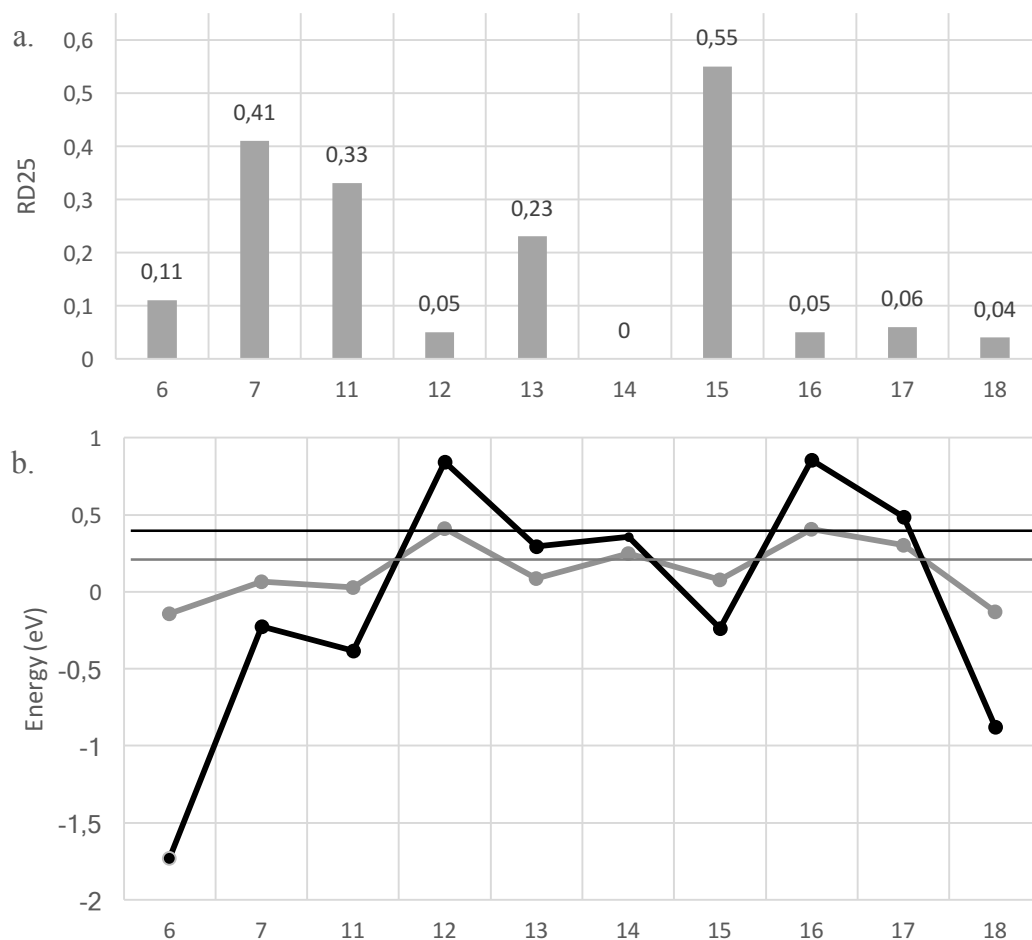


Figure 36. a. RD₂₅ of ACP4/5 analogues; b. phenyl ring LUMO energies of ACP4/5 analogues. Each color refers to a MO symmetry as follows, grey for 2A₂, black for 2B₂. Given the absence of substituent compound **14** is used as a reference, the different lines represent energy levels of corresponding MOs of **14**.

2.2.3.2. Dihalovinyl Moiety

In our docking studies of compounds **7** and **23**, we hypothesized that a halogen bond between the dihalovinyl moiety and Ser88 plays a role in ligand binding, however, due to unfavorable angles and distances, we cannot confirm nor deny this claim. Moreover, our FMO model, as it is, does not provide any more insight.

On the other hand, the dihalovinyl moiety of ACP4/5 analogues **7** and **23** is envisioned to interact with Tyr60 and Phe112 via halogen- π bonds. In order to

evaluate the probability of these interactions, FMOs of the dihalovinyl moiety were analyzed.

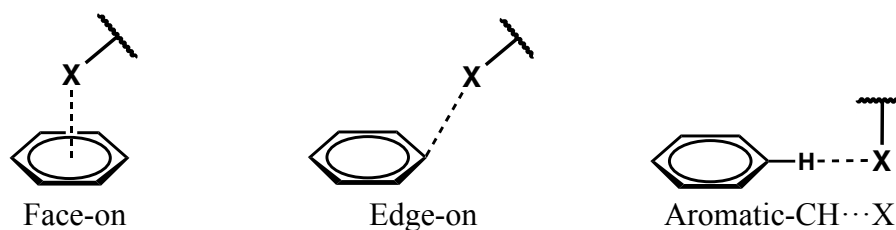


Figure 37. Different geometries of halogen(X)-aromatic interactions.

Our docking studies of the dihalovinyl moiety presented the *trans*-halogen of **7** and **23** in the vicinity of Tyr60 and Phe112, revealing a halogen- π interaction. Halogens are known to interact in several ways with π -systems: 1) the halogen is face-on or edge-on and the aromatic and dispersion forces are mostly engaged;⁷⁷ or 2) an aromatic-CH-halogen bond is formed and charge-transfer interactions are predominant (Figure 37).^{78,79} The orientation of the halogen on the same plane as the aromatic rings of both Tyr60 and Phe112, (Figure 23), suggests a charge-transfer interaction. Therefore, we can envision the halogen electron-rich belt interacting with the peripheral positive charge of the aromatic rings. In other words, halogen HOMOs (Figure 38) will overlap with aromatic ring LUMOs of Tyr60 and Phe112. Thus, a halogen- π interaction may occur between the halogen of the dihalovinyl moiety and, Tyr60 and Phe112, as a HOMO-LUMO interaction is plausible.

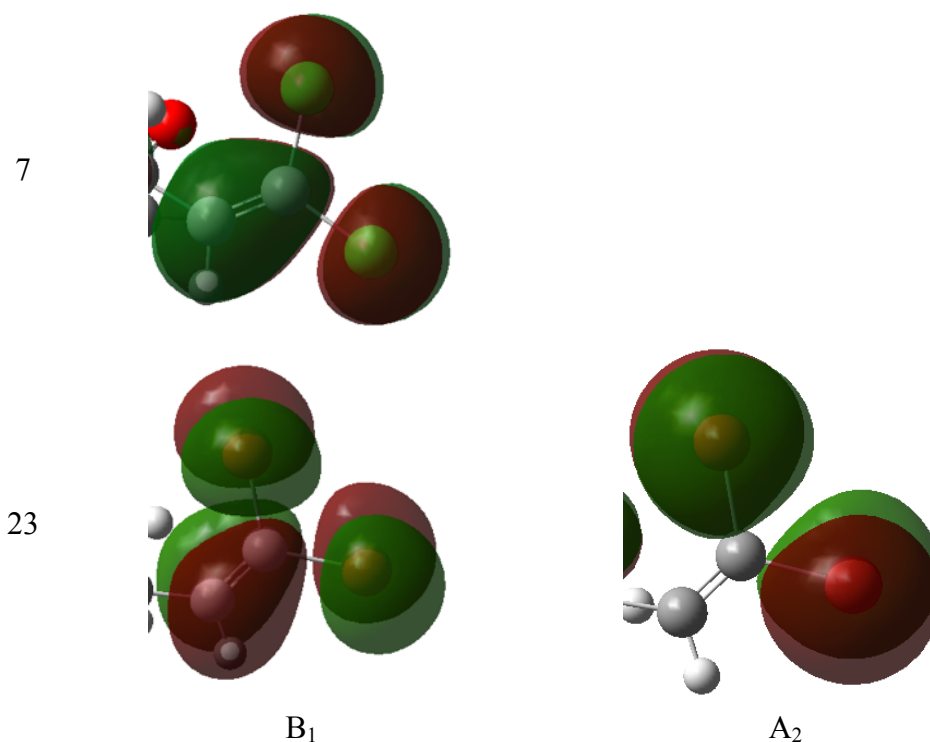


Figure 38. HOMOs of compound 7 and 23. The structure was minimized with the basis set M06-2X/Def2-TZVP in Gaussian 9.

2.2.3.3. Ester Moiety

Finally, the ester moiety is predicted to make an H-bond with Tyr60 and, as previously discussed, steric clashes, caused by ester substituent bulkiness, and ester conformational equilibrium may be responsible for the difference in activity of compounds **27**, **7**, **28** and **29**. However, it is interesting to further study the effect of ester substituents on the electronic character of the moiety. In Figure 39, energy levels of ester alkyl oxygen HOMO increases with the substituent size. Therefore, FMO analysis does not enhance our understanding on the difference in activity of the compounds, suggesting docking studies may be sufficient for interpreting this interaction.

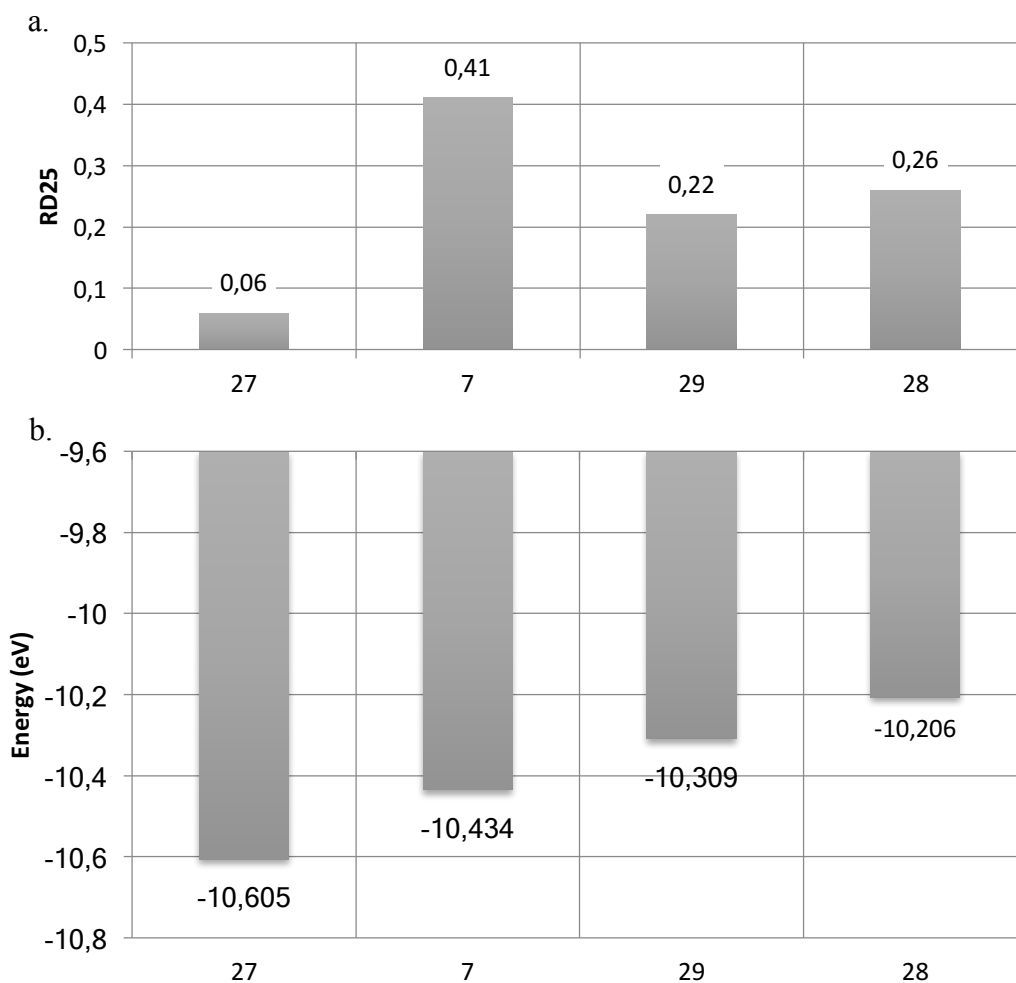


Figure 39. Energies of HOMOs of compounds 27, 7, 28 and 29.

3. Future Directions

In these studies, we utilized computational approaches to provide more insight into the binding mode of ACP derivatives with EcClpP. FMOs provided a description of the charge-transfer capabilities of both the halogen and phenyl motifs. We were able to rationalize the π - π stacking and halogen- π interactions, involving the phenyl ring and the dihalovinyl moieties respectively. However, the difference in activity could not be explained with FMOs for compounds **6**, **11** and **18**, bearing nitro, trifluoromethyl and nitrile groups. Furthermore, our FMO model did not provide a better understanding of the interaction of the ester moiety with the pocket. Analysis of FMOs throughout the ACP4/5 analogue library suggests

that substitution on a specific functionality will affect its electronic character, and consequently will affect interaction with residues in its vicinity.

In conclusion, this computational study revealed that the ACP4/5 scaffold activity is capable of interacting favorably with EcClpP and that attention to molecular orbital complementarity and non-covalent interactions may provide more insight than predicted binding affinities.

The intent of developing a computational model for ligand-ClpP binding is to provide a better understanding of intermolecular interactions than docking or SAR studies alone. An improved understanding will allow for rationale design of more potent derivatives. Moreover, coupling FMO model with docking results allowed us to visualize and predict ligand-protein interactions on a more detailed level. The challenge of this type of analysis is to accurately characterize the electronic properties of a molecule with a reasonable computational cost so it can be implemented in high-throughput screenings. Although FMOs may provide meaningful insight, a useful interpretation depends upon accurate docking conformations. Thus, if the resulting docking conformation is not accurate enough, interpretations may be misleading. As previously discussed, the lack of protein flexibility during the docking limits some aspects of analysis. Therefore, we hope to include molecular dynamic (MD) simulations in our computational platform to address the flexibility issue and obtain better ligand orientations within the binding pocket. Since directionality is critical in non-covalent interactions, MD simulation could orient both ligand and protein to a more accurate binding conformation. Therefore, evaluation of ligand-protein interactions should be then facilitated.

This computational study revealed interactions essential for activation of ClpP, however only the ACP4/5 scaffold was examined. By studying other ClpP

activator classes (e.g. ADEPs), we can expect to unveil more interactions; thus, we will be able to determine crucial residues for activation of ClpP and the type of molecular functionality that induces favorable interactions. Therefore, expanding this type of computational analysis to different chemotypes would lead to a better understanding in the binding mechanism and could lead to the design of potent ClpP activators. Although small in scale, these first-generation studies have been insightful and have allowed us to design new analogues, which will be presented in Chapter 3.

Chapter 3

Design and Synthesis of ACP Analogues

4. Rationale Design of New ACP Analogues

4.1. Introduction

As described previously, our initial focus was to utilize a computational approach to improve our understanding of ClpP chemo-activation and the key ligand-residue interactions involved. With 14 binding pockets and large conformational shifts required for activation, typical docking methods have failed to provide useful data to enable rational structure-based design of improved ClpP activators. To date, our results represent the first reported attempt to correlate SAR to specific ligand-residue interactions and thus provide a foundation for which we can begin to rationally design new ClpP activators. Although empirical approaches, like the Topliss tree, are powerful tools for drug design, they are typically only ligand-focused and fail to take into account the targeted receptor. The insight provided by our FMO coupled docking studies may allow for a more rational structure-based approach for ligand-receptor interactions that are too complicated to be analyzed with typical Gibbs free energy based docking approaches.⁸⁰ From our evaluation of the ACP4/5 library, we hypothesize that specific ligand-receptor interactions can be rationally optimized to improve the potency of the scaffold. To test this hypothesis, we have designed a small collection of new ACP analogues and will synthesize and evaluate these new analogues for ClpP activation activity. The efforts towards the synthesis of these new analogues are reported in this chapter.

4.2. Rationale and Design of New Phenyl Substituted ACP Analogues

Our computational SAR studies indicated that the ACP4/5 phenyl ring has a prominent role in ClpP activation. Therefore, we chose to focus first on this moiety and drew structural inspiration from the more potent ADEP and ACP1 families of ClpP activators.

4.2.1. Design of ADEP-inspired Analogues

ADEP derivatives are potent ClpP activators that exhibit at least a two-fold improvement in efficacy over ACP4/5 (Leung *et al.*). The efficient ClpP activation of ADEPs is attributed the N-acyl 3,5-difluorophenylalanine fragment (red in Figure 40), which prompted us to design ACP4/5 analogues that integrate the 3,5-difluorophenyl (**34**) and 3,5-difluorobenzyl moieties (**35**) (Figure 41).⁸¹

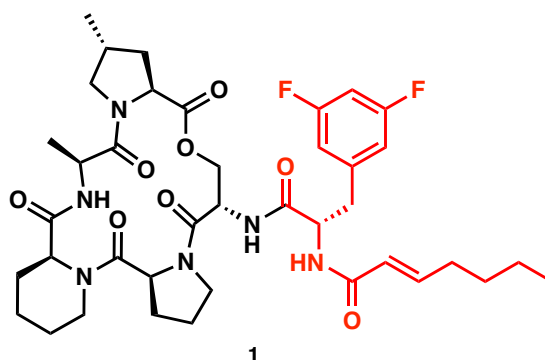


Figure 40. Chemical structure of ADEP4.

Our docking studies suggest that ADEP and ACP4/5 analogues bind to the same pocket and orient their respective phenylalanine and phenyl moieties into the same hydrophobic cavity within the pocket. Therefore, interactions involved between ADEP pharmacophore and EcClpP binding pocket should be mimicked with **34** and **35** and result in an increase of activity of ACP4/5 scaffold.

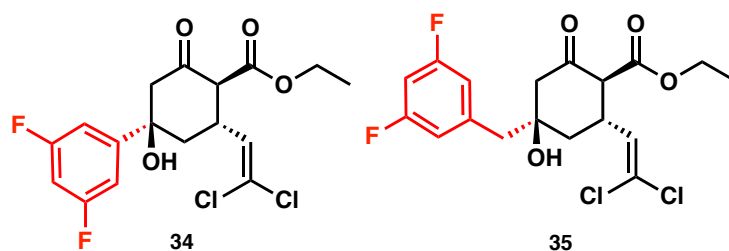


Figure 41. ADEP-inspired ACP analogues.

4.2.2. Design of ACP1-Inspired Analogues

Leung and co-workers extensively studied the 2-sulfonyl-pyridine scaffold, and discovered that **3** (ACP1) activates ClpP at the same extent than the representative ADEP (**37**) at 25 μ M.

Structure	Analogue	RD ₂₅
	37	0.6
	3 (ACP1)	0.53 (\pm 0.02)
	36	0.85 (\pm 0.01)
	38	0.03
	39	0.82 (\pm 0.04)

Table 11. Subset of ACP1 analogues and ADEP derivative.

Although ACP4/5 and ACP1 are structurally different, we can make a parallel between the subset of ACP1 derivatives presented in Table 11 and ACP4/5 analogues. For example, substitution of 3-trifluoromethylpyridine (**3**) to 3-bromopyridine (**39**) significantly improves the activity, similar to the activity increase from *para*-trifluoromethyl ACP4/5 analogue (**11**) to the *para*-bromo derivative ACP5 (**7**), 0.33 and 0.41 respectively (Table 1). From our docking studies, we attributed the gain of activity to the formation of a halogen bond with Thr79 within the EcClpP binding site. Furthermore, in Wilcken's halogen bond analysis, substitution of the core halobenzene scaffold to a 3-halopyridine was found to increase the halogen σ -hole of halogens to provide an improved halogen bonding capability. Therefore, assuming that ACP1 binds to the same pocket as ADEPs and ACP4/5 (an assumption supported by Leung's mutation study), we hypothesize that ACP1 forms a halogen bond with Thr79. Similar to ACP4/5 analogues, removing the bromine to give the unsubstituted pyridyl ring results in the abolishment of activity (**38**). This suggests that the pyridine is not likely involved in any other important interactions with the pocket and further supports the σ -hole enhancing effect of the pyridyl moiety. In our efforts to improve the halogen bonding capacity of the ACP4/5 phenyl motif, we designed two 3-halopyridyl analogues (**40**, **41**, Figure 42), bromine and iodine were chosen because of their significant halogen bonding capacity and the ability to make direct comparisons with the bromobenzene and iodobenzene derivatives previously tested by Leung and co-workers.

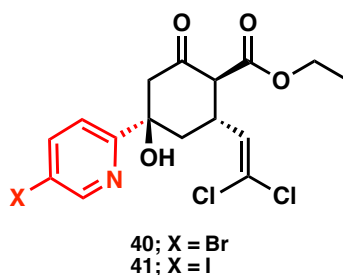


Figure 42. ACP1-Inspired ACP analogues.

4.3. Rationale and Design of New Dihalovinyl Substituted ACP Analogues

Our computational studies indicate that substitution of the dichlorovinyl motif with a dibromovinyl moiety will result in a decreased ClpP activation profile. The decreased predicted binding affinity is likely due to the steric demands of the bromine atoms, which results in ligand displacement within the pocket, disrupting optimal binding interactions. As such, substitution of the dihalovinyl motif with a smaller halogen containing substituent may be more favorable, and thus we designed the difluorovinyl analogue **42** (Figure 43).

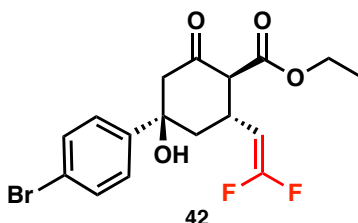


Figure 43. Difluorovinyl ACP analogue.

This analogue will be critical in determining if steric hindrance is the key determinant for this portion of the binding pocket, or if halogen bonding plays a larger role. Ideally, one will eventually want to design new analogues that lack the halovinyl moiety, as these substituents are known to be metabolic liabilities.⁸²

4.4. Rationale and Design of New Ester Substituted ACP Analogues

The small subset of ester analogues prepared and tested by Leung prompted us to further explore the SAR profile of this group (Figure 44), especially

considering our *in silico* identification of a possible H-bond opportunity with ClpP Tyr60.

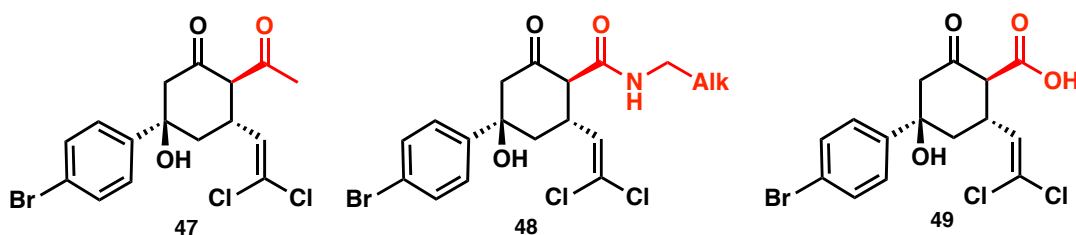


Figure 44. Keto-, amido- and carboxyl ACP analogues.

First, substitution of the ester to a ketone (**47**) is expected to reveal the role of steric interactions and provide insight as to which oxygen of the ACP4/5 ester may be involved with a Tyr60 H-bond. Second, an amide (**48**) would replace a H-bond acceptor (O-alkyl) to a H-bond donor. From a medicinal chemistry perspective, an amide provides additional features of interest: 1) the rigid character of an amide may lock substituents in more favored binding conformation as compared to the ester;⁸³ 2) amides are more stable than esters to cleavage mechanisms and thus **48** is predicted to be more stable;⁸⁴ 3) amides are more polar than esters and this could be beneficial to increasing the spectrum of ACP4/5 analogues;⁸⁵ and 4) an amide can exhibit higher substitution levels than esters, providing an increased area of interaction with the binding pocket. Finally, the carboxylic acid derivative (**49**) can aid in the determination of H-bond characteristics and will also reveal the ClpP activation capability of analogues that succumb to ester hydrolysis.

Although the newly designed analogues represent only a small pool of new ACP analogues, these derivatives have been strategically designed to aid in the experimental validation of our computational hypotheses while simultaneously answering important SAR questions surrounding the ACP4/5 scaffold.

5. Synthesis of ACP Analogues

The goal of the synthetic approach was to develop a robust and flexible route to afford not only the designed compounds, but also future generations. Following is a description of several approaches we explored towards the synthesis of new ACP analogues.

5.1. Robinson Annulation

To synthesize the general ACP4/5 scaffold **52**, we began with a procedure published by Woznesensky that consists of a Robinson annulation reaction between the requisite dichlorovinyl chalcone **51** and ethyl acetoacetate **50** in the presence of sodium ethoxide at room temperature in pure ethanol (Figure 45).

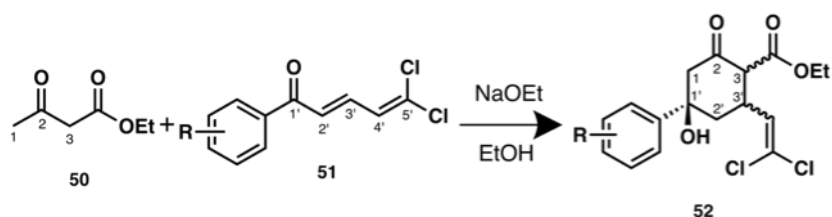


Figure 45. Synthetic route to ACP4/5 analogues

This initial approach, however, was problematic in that **52** was obtained along with a side product that significantly hindered the ability to purify **52** due to similar polarities ($\Delta R_f = 0.1$, 10% ethyl acetate in hexane). We solved this issue by running the annulation reaction at colder temperatures, which eliminated the formation of the side-product and provided **52** in un-optimized yields ranging from 8% to 51%.

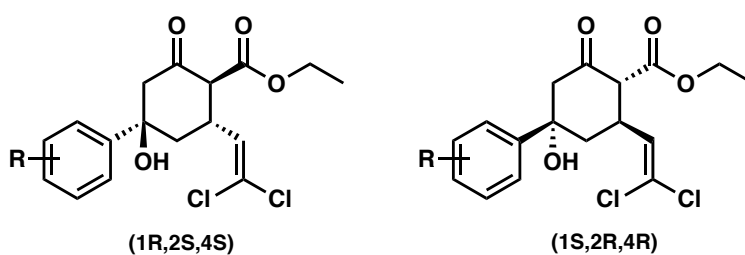


Figure 46. Expected enantiomers of synthesized ACP4/5 analogues.

We expected a racemic mixture of the synthesized compounds (Figure 46), since the synthetic route does not induce stereoselectivity. Even though the final product **52** contains three stereocenters, only one diastereomer was reported by Woznesensky. However, when we conducted the synthesis of ACP4/5 analogues, a diastereomeric mixture was usually produced. As exemplified in Figure 47, ^1H NMR analysis of synthesized compounds revealed peak duplications of the dichlorovinyl hydrogen (H^1), methylene hydrogen (H^2), and the β -ketoester α -hydrogen (H^3). The similarity of the splittings suggests that, throughout the series of synthesized ACP4/5 analogues, at least three diastereomers are produced. In addition, the peak integrations of H^1 (Figure 47) enable us to quantify the diastereomeric ratio, in average the ratio is 0.13 : 0.59 : 0.28 (1:4:2). However, we have not yet been able to isolate the different diastereomers, which has prohibited us from assigning absolute or relative stereochemistry of each diastereomer.

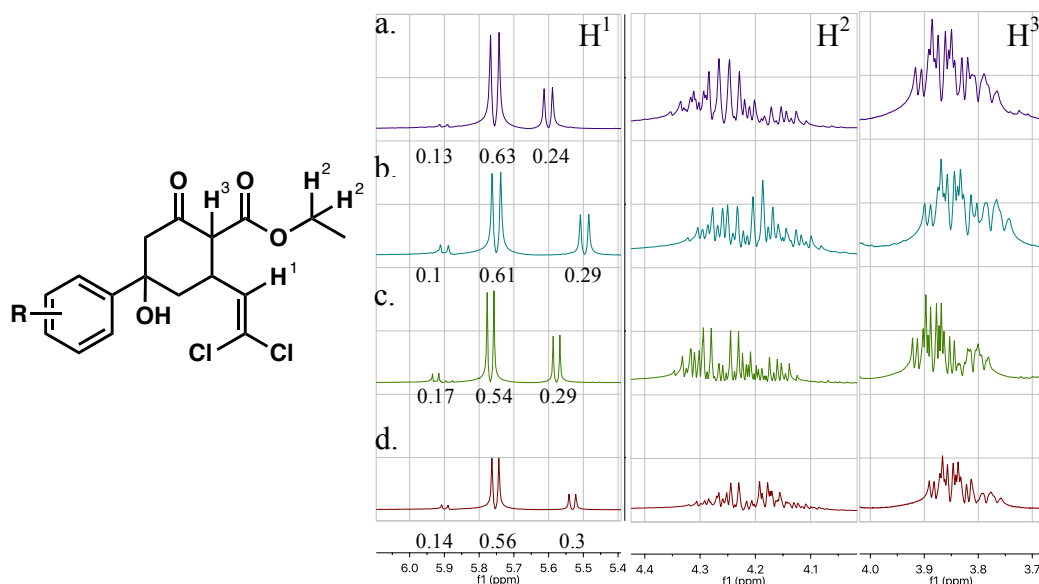


Figure 47. ^1H NMR spectra of compounds (a) **34**, (b) **59**, (c) **72**, (d) **73**.

To further understand the formation of diastereomers via this synthetic route, we analyzed the postulated mechanism of the reaction. Mechanistically, the reaction is believed to proceed, first, by a Michael addition achieved by the

formation of the enolate form of **50** (via deprotonation of C-3), followed by the nucleophilic attack of C-3 onto C-3' of **51** (Figure 48). We can assume the nucleophilic attack on C-3' is favored over C-1' because the enolate form of **50** is more compatible with the hard/soft profile of the C-3' electrophile, the C-5' position is more sterically hindered (negatively affecting the Bürgi-Dunitz trajectory), and no products from C-5' addition were ever isolated during our synthetic efforts.

The stereochemistry of the Michael adduct depends on the approach of the enolate **50**, as presented in Figure 48, which can be determined through analysis of the nucleophile approach. Both reactants are planar, so we can envision four different approaches, hence four possible diastereomers. The formation rate of **(2S, 3S)-53** and **(2R, 3R)-53** are predicted to be slow due to the steric clashes between the phenyl ring and the ethyl ester and between the methyl and the dichlorovinyl during the initial approach. This is speculative, however, as the Michael addition products could not be isolated due to the spontaneous nature of the proceeding cyclization.

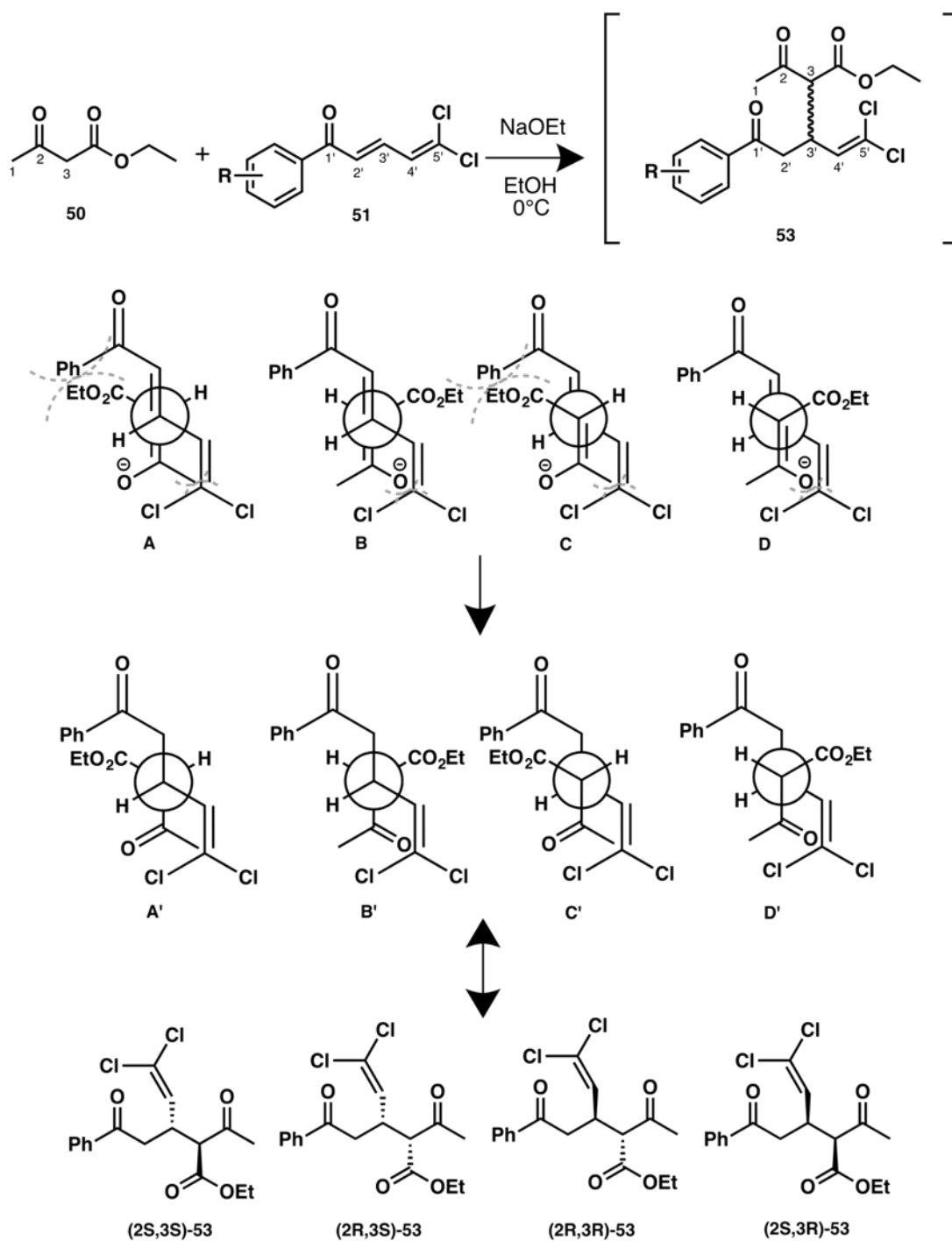


Figure 48. Analysis of Michael addition of 50 with 51 via steric approach control.

The resulting Michael adducts were directly converted to **52**, through an intramolecular condensation between C-1 and C-1' (Figure 48). The crude products were obtained after quenching the reaction mixture with saturated aqueous solution of ammonium chloride and typical organic extraction.

Steric approach control and chelation control were employed to evaluate the stereochemistry of the final products and predict the major product. As shown in Figure 49, steric approach control represents the intermediary state. Depending on the stereochemistry of **53**, the ethyl ester and dichlorovinyl motifs have different staggered conformations. From this approach, we can assume that **(1S*, 2R*, 4R*)** will be the major product, since ethyl ester and dichlorovinyl are anti, whereas these groups in the other intermediates are gauche. The chelation control intermediate can be described as a bicyclo[3.3.1]nonane with sodium coordinating both the enolate oxygen and the ketone oxygen. Similar to the steric approach control, ethyl ester and dichlorovinyl are orientated differently depending on their stereochemistry. The **(1R*, 2S*, 4R*)** intermediate has both of these groups in the equatorial orientation, suggesting this diastereomer will be the major product, due to higher stability of the intermediate, contrary to the steric control analysis. Therefore, assuming that both the steric and chelation mechanisms are at play, we can hypothesize that **(1S*, 2R*, 4R*)** and **(1R*, 2S*, 4R*)** will be the major products, with the **(1S*, 2S*, 4R*)** and **(1R*, 2R*, 4R*)** diastereomers being formed to a lesser extent.

Michael adduct	Steric approach control	Chelation control	Product
(2S,3S)-53			 Major product (Steric control) (1S*,2R*,4R*)
(2R,3S)-53			 (1R*,2R*,4R*)
(2R,3R)-53			 Major product (Chelation control) (1R*,2S*,4R*)
(2S,3R)-53			 (1S*,2S*,4R*)

Figure 49. Cyclisation analysis via steric approach control and chelation control. Final products are denoted with a star to indicate racemic mixture.

5.2. Dichlorovinyl Chalcone Synthesis

The dichlorovinyl chalcone was prepared in three steps from vinyl ethyl ether **54**. Treatment of **54** with benzoyl peroxide and carbon tetrachloride resulted in a radical mediated chlorination of vinyl ethyl ether to provide 1,1,1,3-tetrachloropropyl ether **55** (Figure 50). Under strongly acidic conditions, **55** decomposes via an E1 elimination mechanism and acidic cleavage of the ether affords the requisite dichloro-acrolein **55''** *in situ*.⁸⁶ Exposure of **55''** to enolized

56 results in a condensation reaction, which yields dichlorovinyl chalcones in decent yields (>50%) over 3-steps.

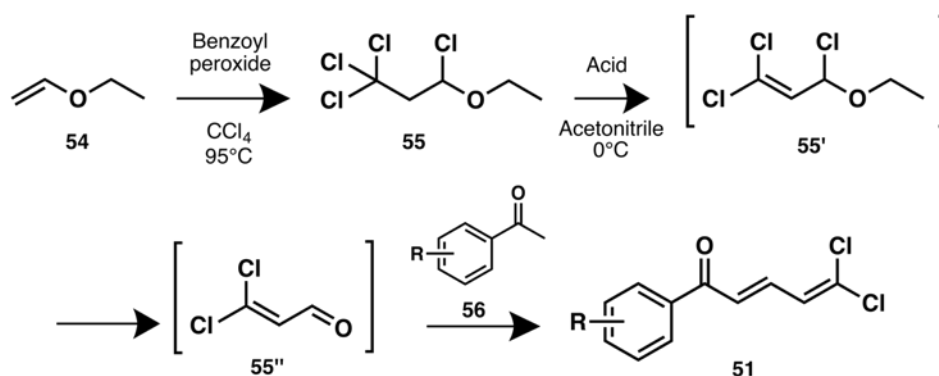


Figure 50. Synthetic route to dichlorovinyl chalcones.

As shown in Table 12, the formation of **55** from **51** required some optimization, as the transformation was strongly dependent upon the acid catalyst. In fact, only trifluoromethanesulfonic acid provided substantive amounts of product, suggesting that a very strong acid ($pK_a \geq -14$) is optimal for acetophenone enolization and subsequent formation of the dichloroacrolein.

Condition	Reaction time	Yield
CH ₃ COOH	72h	No reaction
HCl (conc.)	24h	No reaction
TFA	24h	No reaction
CF ₃ SO ₃ H	1h	66%

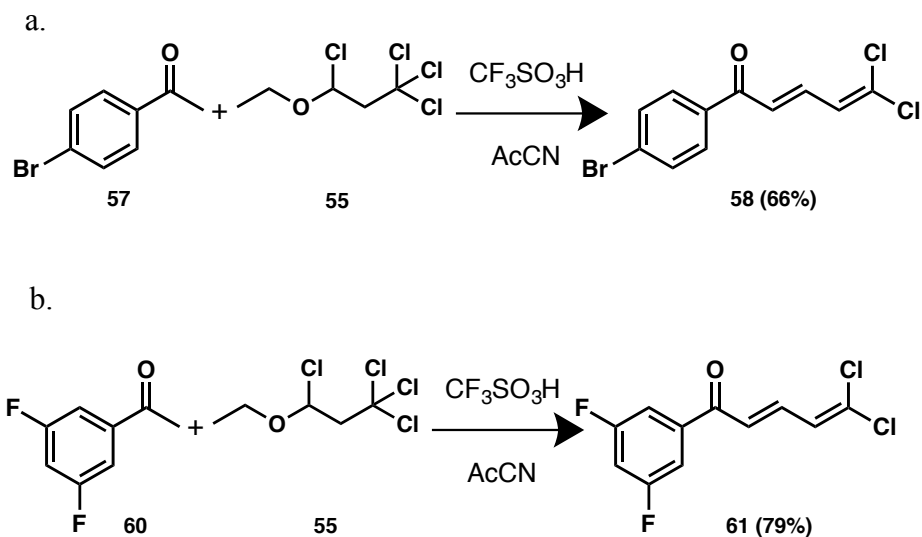
Table 12. Conditions explored to synthesize dichlorovinyl *para*-bromo-chalcone **58.**

Formation of the dichloro-acrolein **55''** was the biggest challenge in this synthetic approach, as **55''** is not stable and spontaneously polymerizes when formed. As such, a large excess of **55** was needed in order to afford **51** in large enough quantities to enable the synthesis of the desired analogues.

5.3. Synthesis

Utilizing the routes depicted in Figures 51 and 52, we successfully synthesized **34**, **47**, and **59** as a diastereomeric mixtures. In order to compare the activity of new ACP4/5 analogues we first prepared ACP5 (**59**), as a positive

control. From the dichlorovinyl bromochalcone **58**, afforded in 66% yield, we obtained compound **59** in 32% yield. The Robinson annulation reaction between the chalcone **58** and acetylacetone yielded compound **47** in 8% yield. Synthesis of **34** was achieved in 32% yield from the corresponding chalcone **61**, which was produced in 79% yield from **60**.



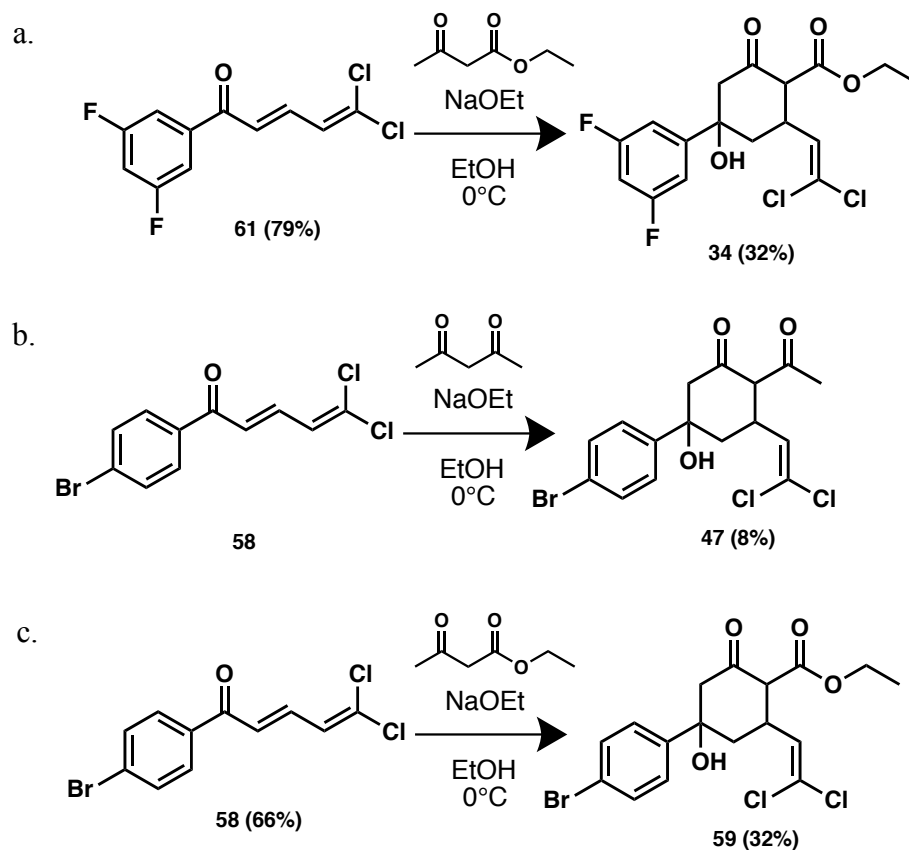


Figure 52. Synthetic routes to compounds (a) 34, (b) 47 and (c) 59.

Unfortunately, our first attempts to separate diastereomers have not been successful with common purification processes (i.e. flash column chromatography and preparative thin layer chromatography), and more advanced methods (e.g. HPLC methods) are needed to isolate single diastereomers. Upon the isolation of single diastereomers we will be able to assign the absolute stereochemistry of derivatives and evaluate pure diastereomers for biological evaluation. Purification by HPLC is ongoing and represents the immediate focus of this project. Furthermore, ^1H NMR spectra of **34**, **59**, **72** and **73** showed a peak at 12.5 ppm integrating for 0.3, suggesting enolization of the β -ketoester.

5.4. Alternate Route to Dichlorovinyl Chalcone

As previously mentioned, access to dichloro-acrolein is challenging, the instability of the molecule and the necessity of strong acidic conditions do not allow flexibility in the synthesis of dichlorovinyl chalcone. Several synthetic routes have been explored to remedy this issue but were unfortunately unsuccessful.

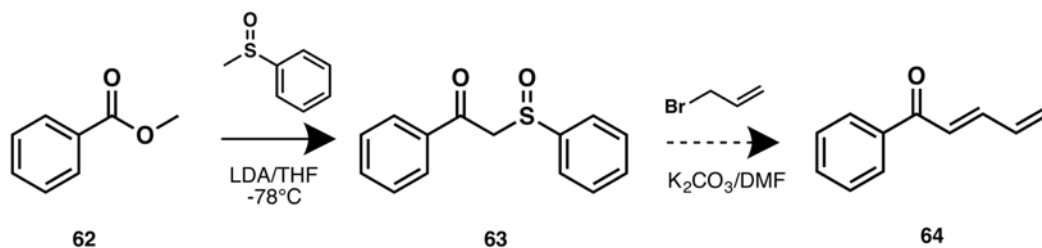


Figure 53. Dichlorovinyl chalcone synthesis via β-ketosulfoxide addition.

We first pursued the synthesis of a phenyl dienone **64** by using methyl phenyl sulfoxide (Figure 53). Even though the phenyl dienone is not the intended product, it represents a good model system to test the chemistry. Condensation of methyl benzoate **62** with the carbanion of methyl phenyl sulfoxide gave the β-ketosulfoxide **63**.⁸⁷ However, the alkylation step with allyl bromide did not yield product **64**. This route was being pursued in parallel to that shown in Figure 50, and was abandoned upon successful execution of the original route. This method however, is worth noting as its optimization would allow for the rapid generation of new chalcones that may provide interesting SAR in the future. Furthermore, the method in Figure 53 would provide a more robust way to generate chalcones in a controlled and scalable manner, rather than entrusting *in situ* generation of key intermediates.

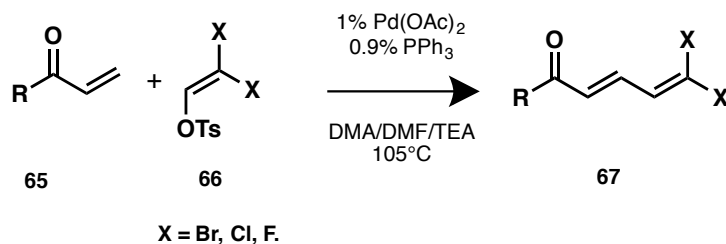


Figure 54. Dichlorovinyl chalcone generation via Heck coupling reaction.

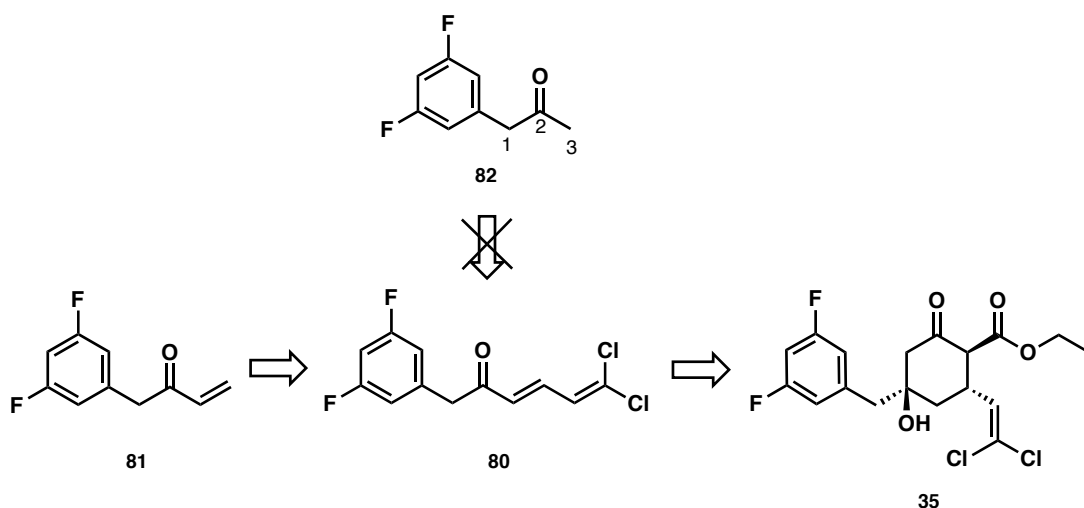


Figure 55. Retrosynthetic scheme of compound 35.

We also considered using the Heck cross coupling reaction between the Michael acceptor **65** and dihalovinyl tosylate **66** to afford dihalovinyl chalcones **67** (Figure 54).⁸⁸ The advantage of this synthetic route is the possibility to use different tosylates **66** which would open the door to new derivatives.⁸⁹

We assessed this approach by attempting to synthesize **80**, which cannot be easily afforded using the synthetic route described in Figure 50 because equilibrium favors enolization on C-1 over C-3 (Figure 55). Therefore, we expected to produce the dichlorovinyl chalcone **80** from **81**. However, we were unable to synthesize **81**, and thus we cannot make any conclusions on the viability of this route. As this project progresses however, the implementation of this Heck-coupling mediated chalcone formation will be a major focus.

6. Determination of ACP4/5 Binding Pocket via Photo Affinity Labelling

6.1. Introduction

One of the critical elements to an advanced SAR study is knowing the ligand binding pocket with certainty. Without this crucial information, rational design of improved compounds is extremely difficult. The previous chapter demonstrates the value of being able to visualize the ligand-protein interactions.

Although the mutational studies by Leung and co-workers identified the ADEP binding pocket as a possible ACP4/5 binding domain, their study also revealed a potential second binding pocket. Even though residue mutation studies provide the first indication of ligand binding location, we lack experimental data that provides any clues regarding the ligand orientation in the pocket. Our docking studies suggest ACP4/5 to bind with the aromatic motif buried in the same hydrophobic pocket that accommodates the phenylalanine moiety in ADEPs, but we would like to confirm these results experimentally.

Several methods exist to identify the binding site and the residues that interact with the ligand, such as co-crystallization, binding pocket site-directed mutagenesis, 2D protein NMR, and photo-affinity labelling. For the sake of our study and the time limitations, we chose to investigate photoaffinity labelling (PAL) as a method to identify the binding pocket of ACP4/5 molecules and provide a clue as to their orientation within the binding pocket. A photoaffinity probe is used to conduct a PAL experiment. This probe generally contains the pharmacophore – the fragment necessary for protein binding - and a photo reactive group. The purpose of the probe is to covalently cross-link the ligand to a residue of the target protein within the binding site. Cross-linking is achieved by irradiation of the reactive species.⁹⁰ In order to determine the cross-linking site, denaturation

conditions are employed on the cross-linked protein, followed by digestion (i.e. enzymatic or chemical cleavage of peptide bonds) to break down the protein. The fragments are then analyzed by MALDI-mass spectrometry. Therefore, a covalent bond is necessary to withstand these conditions and consequently yield the desired information.⁹¹ Benzophenone, aryl azide and diazirines are three of the most common photoreactive groups.

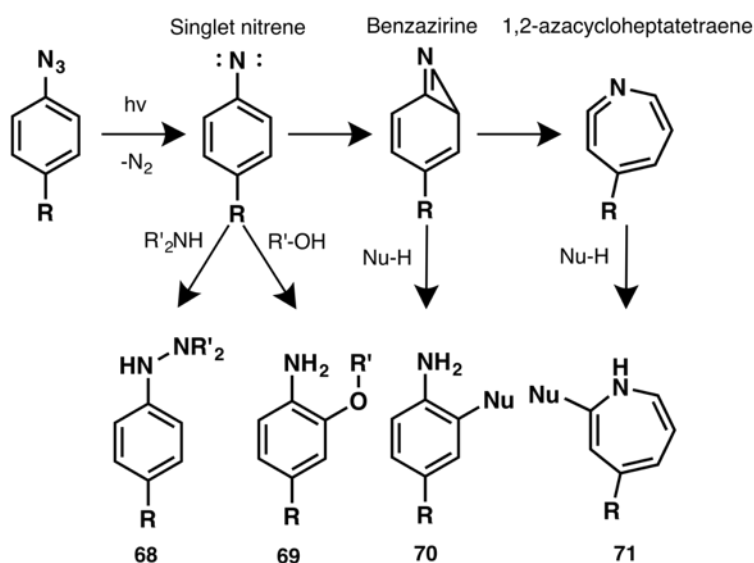


Figure 56. Photoactivation mechanism of aryl azides.

The most frequently used probes are aryl azides because of their small size, their synthetic accessibility, and their high photo-induced reactivity. Upon photoirradiation, the aryl azide generates a singlet nitrene, which can itself cross-link protein residues (**68**, **69**), or rearrange to form either a benzazirine or a 1,2-azacycloheptatetraene capable of protein cross-linking (**70**, **71**), as described in Figure 56.⁹²

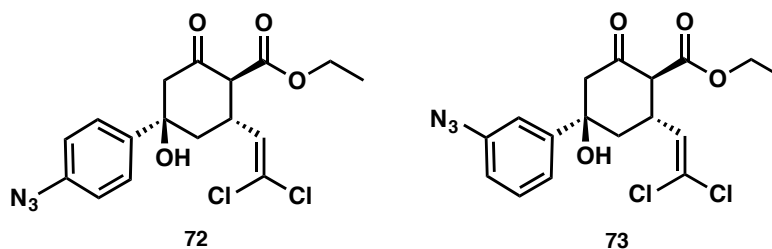


Figure 57. Target ACP4/5 azido-analogues.

By conducting PAL experiments on purified recombinant EcClpP, our goal is to validate the binding site of ACP4/5 analogues and elucidate the binding orientation of ACP4/5 analogues within the binding pocket. To determine the binding site along with the interacting residues, we designed and synthesized ACP4/5 azido-analogues **72** and **73** (Figure 57) bearing an azide moiety on the phenyl ring. As discussed earlier, the interaction of the phenyl moiety with ADEP's pocket is essential for activating ClpP and the tight binding of the moiety is expected to ensure a cross-linking with residues such as Thr79 or Met92. From the analysis of the ACP4/5 analogue library, we can hypothesize that a para-azido moiety will be accommodated in the binding pocket, as the azide group is relatively similar in size than iodine, as shown in Table 13. We are less certain about the ability of the 3-azido analogue to bind, however, we decided to generate this analogue in parallel to the 4-azido compound for comparison. Leung's hypothesis that a second ClpP binding pocket exists is intriguing as it 1) implies that some ClpP activators may have a different mechanism of action than the acyldepsipeptides and 2) ligands that exploit interactions in both ClpP binding pockets may present an opportunity to improve upon the activity of ClpP activators.

	Linear volume ^c	Non-linear volume ^d	Van der Waals volume ^d
Br	34.307	33.823	30.88
I	n/a	n/a	40.17
N ₃	41.334	42.853	38.31 ^e

Table 13. Linear and non-linear volumes of atom/group of atoms in Å³.

6.2. Results and Discussion

6.2.1. Synthesis of Azido-ACP4/5 Analogues

The synthesis of azido ACP4/5 analogues (**72**, **73**) was achieved by the cyclisation of the representative dichlorovinyl chalcones **78**, **79** with ethyl acetoacetate via a Robinson annulation reaction.

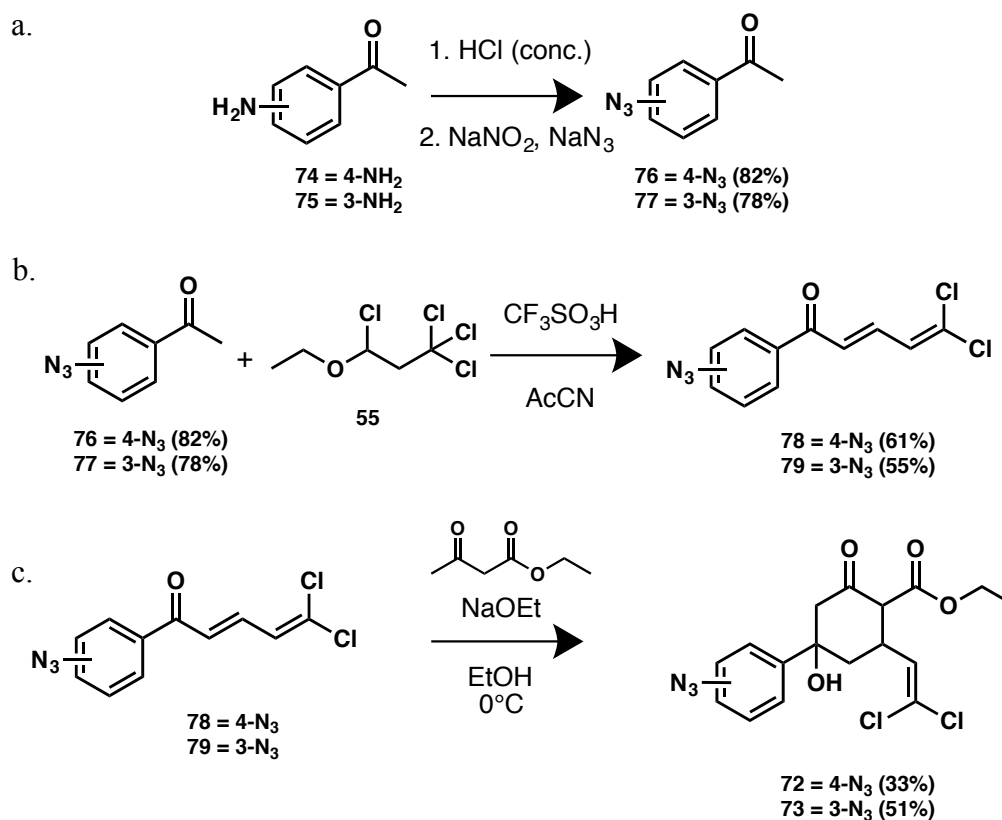


Figure 58. Synthetic route to analogues 3/4-azido ACP4/5 analogues.

The final analogues were prepared in un-optimized yields of 33% (**72**) and 51% (**73**, Figure 58). To afford chalcone **78**, 4-azido acetophenone **76** was first

^c Values from *Structural Chemistry*, 12(3/4), 205-212, 2001.

^d Values from *Chemical Physics Letters*, 116(5), 1985.

^e Calculated the method from *Chemical Physics Letters*, 116(5), 1985.

generated from the corresponding aromatic amine **74** at 82% yield. Acetophenone **76** was then condensed with 1,1,1,3-tetrachloropropyl ether **55** under strongly acid conditions to provide **78** in 61% yield. In a similar fashion, **79** was produced in two steps in 55% yield from the 3-amino acetophenone **75**.

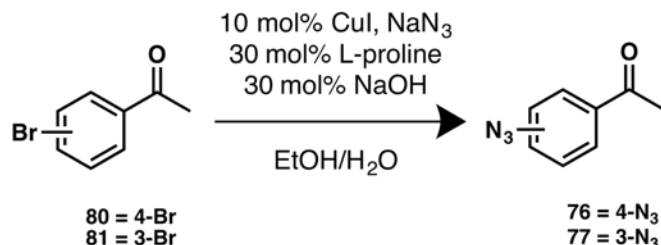


Figure 59. Generation of azido-acetophenones via proline-promoted CuI-catalyzed coupling reaction.

Another route to access azido acetophenones was explored in parallel (Figure 59) but was not as successful as the route presented in Figure 58 because of low conversion and difficulty in purification. Purification difficulties were due to a small difference in the retention factor between the bromo-acetophenone (**80**, **81**) and the azido acetophenone (**76**, **77**).⁹³

The azido ACP4/5 analogues were readily synthesized; however, as indicated with other ACP4/5 analogues, products were formed as a diastereomeric mixture. As such, prior to carrying out the photo crosslinking experiments, we need to separate the mixture.

7. Future directions

In conclusion, we utilized results from our computational analysis to rationally design and synthesize new ACP4/5 analogues. Synthetically, we have improved the conditions to obtain a higher yield than reported for the key intermediate, dichlorovinyl chalcone. However, this route lacks flexibility and further work is needed to stabilize the *in situ* generated dichloro acrolein. Although most of our target molecules were synthesized successfully, the key Robinson

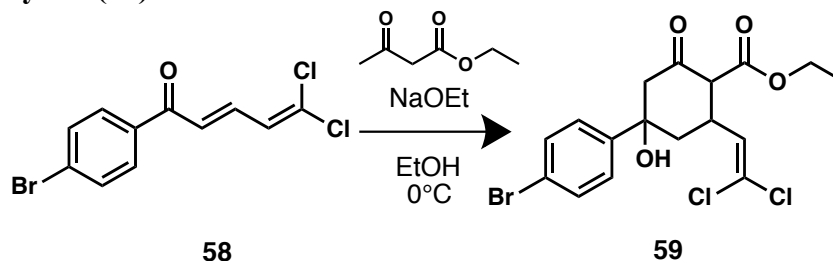
annulation step produced diastereomers, which has so far prohibited evaluation of the synthesized compounds for ClpP activation. Therefore, we need to introduce stereoselectivity or find a reliable purification process to allow us to obtain the derivatives as pure compounds. Only after evaluation will we know how informative our FMO coupled docking studies are to the field of ClpP modulation and future structure-based initiatives.

In addition, we synthesized two potential photo affinity labelling probes to aid in the identification of the ACP4/5•EcClpP binding site. By performing the photo affinity labelling experiments, we hope to validate the hypothesized binding pocket and provide the first evidence of the orientation of ACP4/5 analogues within the binding domain.

8. Experimental Section

8.1. Synthesis of ACP4/5 Analogues

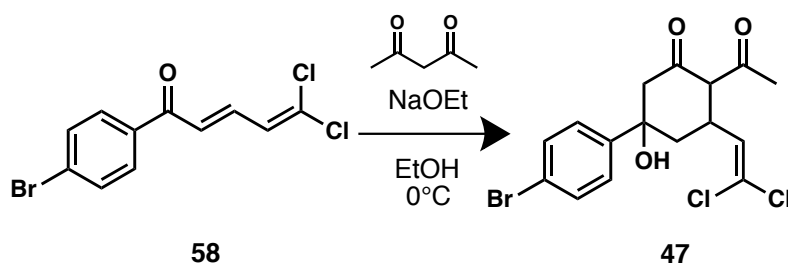
Ethyl-4-(4-bromophenyl)-2-(2,2-dichlorovinyl)-4-hydroxy-6-oxocyclohexane-1-carboxylate (59):



To a solution of dichlorovinyl chalcone **58** (0.40 mmol, 121 mg) in pure ethanol (4 mL) was added a 21% sodium ethoxide in ethanol solution (0.16 mmol, 61 μ L) and ethyl acetoacetate (2.26 mmol, 303 μ L). The reaction mixture was stirred overnight in an ice bath and then quenched with a solution of saturated aqueous ammonium chloride and the aqueous layer was extracted with ethyl acetate. The organic layers were combined, washed with H₂O and saturated aqueous NaCl before being dried over Na₂SO₄ and filtered. The filtrate was concentrated *in vacuo* and purified by

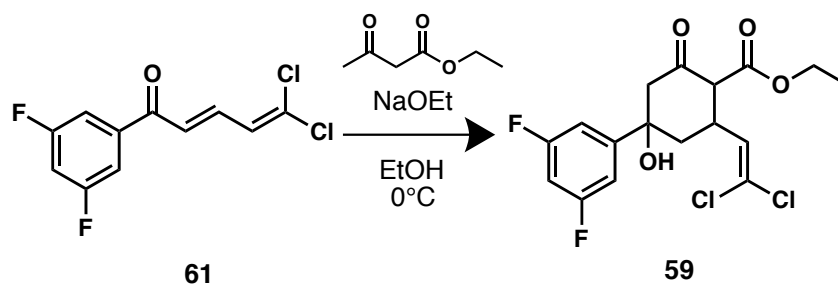
flash column chromatography (SiO₂, 1% methanol, 49% dichloromethane, 50% hexane) to yield **59** as a ~1:4:2 (A, B, C) diastereomeric mixture (55.7 mg, 32%). Yellow amorphous solid. Diastereomer A: ¹H NMR (500 MHz, CDCl₃) δ 7.51 – 7.47 (m, 2H), 7.37 – 7.33 (m, 2H), 5.90 (d, *J* = 9.1 Hz, 1H), 4.32 – 4.09 (m, 3H), 3.89 – 3.76 (m, 1H), 3.33 (d, *J* = 11.0 Hz, 1H), 2.94–2.87 (m, 1H), 2.64 (dd, *J* = 14.1, 2.5 Hz, 1H), 2.14–2.09 (m, 1H), 2.07–1.99 (m, 1H), 1.26 (m, 3H); ¹³C (125 MHz, CDCl₃) δ 202.1, 171.9, 144.8, 132.3 (2C), 131.2 (2C), 129.1, 126.7, 123.3, 75.8, 62.5, 61.6, 53.1, 41.7, 38.2, 14.2; Diastereomer B: ¹H NMR (500 MHz, CDCl₃) δ 7.51 – 7.47 (m, 2H), 7.37 – 7.33 (m, 2H), 5.75 (d, *J* = 9.7 Hz, 1H), 4.32 – 4.09 (m, 3H), 3.89 – 3.76 (m, 1H), 3.33 (d, *J* = 11.0 Hz, 1H), 2.94–2.87 (m, 1H), 2.64 (dd, *J* = 14.1, 2.5 Hz, 1H), 2.14–2.09 (m, 1H), 2.07–1.99 (m, 1H), 1.26 (m, 3H); ¹³C (125 MHz, CDCl₃) δ 202.1, 168.3, 144.8, 132.3 (2C), 131.2 (2C), 129.1, 125.6, 123.3, 75.8, 61.6, 60.7, 53.1, 41.7, 38.2, 14.2; Diastereomer C: ¹H NMR (500 MHz, CDCl₃) δ 7.51 – 7.47 (m, 2H), 7.37 – 7.33 (m, 2H), 5.53 (d, *J* = 9.5 Hz, 1H), 4.32 – 4.09 (m, 3H), 3.89 – 3.76 (m, 1H), 3.33 (d, *J* = 11.0 Hz, 1H), 2.94–2.87 (m, 1H), 2.64 (dd, *J* = 14.1, 2.5 Hz, 1H), 2.14–2.09 (m, 1H), 2.07–1.99 (m, 1H), 1.26 (m, 3H); ¹³C (125 MHz, CDCl₃) δ 202.1, 168.3, 144.8, 132.3 (2C), 131.2(2C), 129.1, 126.7, 123.3, 75.8, 61.6, 60.7, 53.1, 41.7, 38.2, 14.2; HRESI-TOF *m/z* 458.9563 (C₁₇H₁₇BrCl₂O₄ + Na⁺ requires 458.956).

2-Acetyl-5-(4-bromophenyl)-3-(2,2-dichlorovinyl)-5-hydroxycyclohexan-1-one (47):



To a solution of dichlorovinyl chalcone **58** (0.46 mmol, 140 mg) in pure ethanol (5 mL) was added a 21% sodium ethoxide in ethanol solution (0.19 mmol, 71 μ L) and acetylacetone (3.41 mmol, 350 μ L). The reaction mixture was stirred overnight in an ice bath and then quenched with a solution of saturated aqueous ammonium chloride and the aqueous layer was extracted with ethyl acetate. The organic layers were combined, washed with H₂O and saturated aqueous NaCl before being dried over Na₂SO₄ and filtered. The crude was concentrated *in vacuo* and purified by flash column chromatography (SiO₂, 50% toluene, 15% ethyl acetate, 35% hexane) to yield **47** (15.8 mg, 8%). Yellow amorphous solid. ¹H NMR (300 MHz, CDCl₃) δ 7.79 (d, J = 8.5 Hz, 2H), 7.62 (d, J = 8.5 Hz, 2H), 6.06 (d, J = 10.0 Hz, 1H), 4.19 (d, J = 7.1 Hz, 1H), 3.85 – 3.77 (m, 1H), 3.26 (dd, J = 17.6, 5.8 Hz, 1H), 3.13 (dd, J = 17.6, 6.2 Hz, 1H), 2.55 – 2.51 (m, 1H), 2.25 (s, 3H), 2.16 (d, J = 5.6 Hz, 1H); ¹³C NMR (75 MHz, CDCl₃) δ 203.3, 196.8, 135.0, 132.1 (2C), 129.6 (2C), 128.8, 123.0, 110.0, 77.2, 68.8, 39.7, 35.5, 30.4, 29.7. HRESI-TOF m/z 428.9455 (C₁₆H₁₅BrCl₂O₃ + Na⁺ requires 428.945).

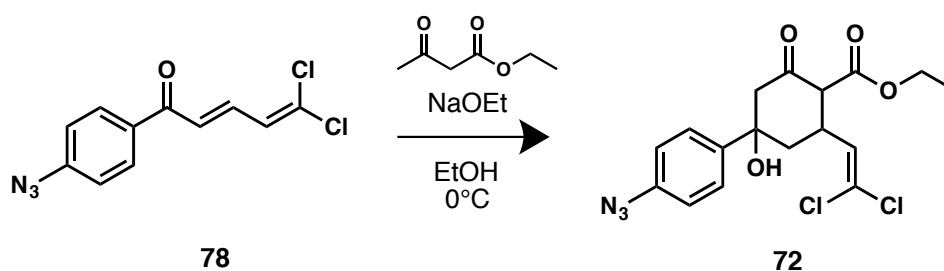
Ethyl-2-(2,2-dichlorovinyl)-4-(3,5-difluorophenyl)-4-hydroxy-6-oxocyclohexane-1-carboxylate (34):



To a solution of dichlorovinyl chalcone **61** (0.5 mmol, 130 mg) in pure ethanol (4 mL) was added a 21% sodium ethoxide in ethanol solution (0.17 mmol, 65 μ L) and ethyl acetoacetate (1.98 mmol, 250 μ L). The reaction mixture was stirred overnight in an ice bath and then quenched with a solution of saturated aqueous ammonium chloride and the aqueous layer was extracted with ethyl acetate. The organic layers were combined, washed with H₂O and saturated aqueous NaCl before being dried over Na₂SO₄ and filtered. The filtrate was concentrated *in vacuo* and purified by flash column chromatography (SiO₂, 1% methanol, 49% dichloromethane, 50% hexane) to yield **59** as a ~1:4:2 (A, B, C) diastereomeric mixture (58.1 mg, 32%). Yellow amorphous solid. Diastereomer A: ¹H NMR (400 MHz, CDCl₃) δ 7.04 – 6.97 (m, 2H), 6.74 (tt, *J* = 8.5, 2.2 Hz, 1H), 5.90 (d, *J* = 8.7 Hz, 1H), 4.35 – 4.11 (m, 2H), 3.92 – 3.77 (m, 1H), 3.33 (d, *J* = 12.0 Hz, 1H), 2.86 (d, *J* = 14.1 Hz, 1H), 2.67 (dd, *J* = 14.2, 2.5 Hz, 1H), 2.15 – 2.07 (m, 1H), 2.01 (dd, *J* = 14.0, 12.2 Hz, 1H), 1.35 – 1.24 (m, 3H); ¹³C (100 MHz, CDCl₃) δ 201.3, 170.0, 164.3 (2C), 150.1, 132.8, 123.5, 107.6 (2C), 103.3, 75.5, 61.3, 52.9, 42.8, 39.5, 33.4, 14.1; Diastereomer B: ¹H NMR (400 MHz, CDCl₃) δ 7.04 – 6.97 (m, 2H), 6.74 (tt, *J* = 8.5, 2.2 Hz, 1H), 5.76 (d, *J* = 9.9 Hz, 1H), 4.35 – 4.11 (m, 2H), 3.92 – 3.77 (m, 1H), 3.33 (d, *J* = 12.0 Hz, 1H), 2.86 (d, *J* = 14.1 Hz, 1H), 2.67 (dd, *J* = 14.2, 2.5 Hz, 1H), 2.15 – 2.07 (m, 1H), 2.01 (dd, *J* = 14.0, 12.2 Hz, 1H), 1.35 – 1.24 (m, 3H);

^{13}C (100 MHz, CDCl_3) δ 201.3, 168.1, 164.3 (2C), 150.1, 129.1, 123.5, 107.6 (2C), 103.3, 75.5, 61.3, 52.9, 41.6, 37.9, 33.4, 14.1; Diastereomer C: ^1H NMR (400 MHz, CDCl_3) δ 7.04 – 6.97 (m, 2H), 6.74 (tt, $J = 8.5, 2.2$ Hz, 1H), 5.60 (d, $J = 9.3$ Hz, 1H), 4.35 – 4.11 (m, 2H), 3.92 – 3.77 (m, 1H), 3.33 (d, $J = 12.0$ Hz, 1H), 2.86 (d, $J = 14.1$ Hz, 1H), 2.67 (dd, $J = 14.2, 2.5$ Hz, 1H), 2.15 – 2.07 (m, 1H), 2.01 (dd, $J = 14.0, 12.2$ Hz, 1H), 1.35 – 1.24 (m, 3H); ^{13}C (100 MHz, CDCl_3) δ 201.3, 168.1, 164.3 (2C), 150.1, 129.1, 123.5, 107.6 (2C), 103.3, 75.5, 61.3, 52.9, 41.6, 37.9, 33.4, 14.1; HRESI-TOF m/z 415.0288 ($\text{C}_{17}\text{H}_{16}\text{Cl}_2\text{F}_2\text{O}_4 + \text{Na}^+$ requires 415.029).

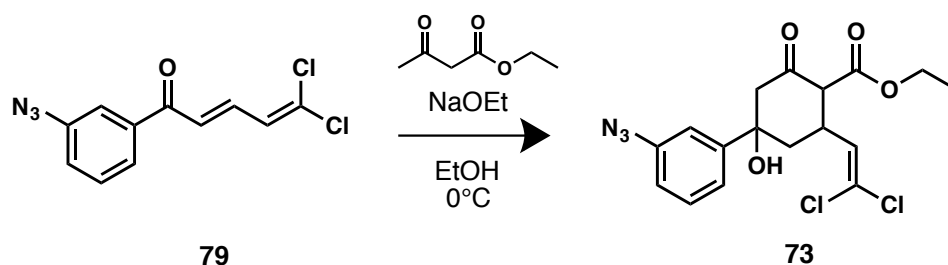
Ethyl-4-(4-azidophenyl)-2-(2,2-dichlorovinyl)-4-hydroxy-6-oxocyclohexane-1-carboxylate (72):



To a solution of dichlorovinyl chalcone **78** (0.47 mmol, 127 mg) in pure ethanol (4 mL) was added a 21% sodium ethoxide in ethanol solution (0.17 mmol, 64 μL) and ethyl acetoacetate (2.37 mmol, 318 μL). The reaction mixture was stirred overnight in an ice bath and then quenched with a solution of saturated aqueous ammonium chloride and the aqueous layer was extracted with ethyl acetate. The organic layers were combined, washed with H_2O and saturated aqueous NaCl before being dried over Na_2SO_4 and filtered. The filtrate was concentrated *in vacuo* and purified by flash column chromatography (SiO_2 , 1% methanol, 49% dichloromethane, 50% hexane) to yield **72** as a ~1:4:2 (A, B, C) diastereomeric mixture (61.8 mg, 33%). Orange amorphous solid. Diastereomer A: ^1H NMR (400 MHz, CDCl_3) δ 7.47 – 7.41 (m, 2H), 7.01 (dd, $J = 8.7, 2.4$ Hz, 2H), 5.90 (d, $J = 9.0$ Hz, 1H), 4.32 – 4.08

(m, 2H), 3.90 – 3.74 (m, 1H), 3.32 (d, $J = 11.8$ Hz, 1H), 2.90 (d, $J = 14.1$ Hz, 1H), 2.64 (dd, $J = 14.1, 2.5$ Hz, 1H), 2.16 – 2.09 (m, 1H), 2.03 (dd, $J = 14.0, 12.1$ Hz, 1H), 1.33 – 1.24 (m, 3H); ^{13}C (100 MHz, CDCl_3) δ 202.1, 171.9, 142.4, 139.7, 133.1 (2C), 129.3 (2C), 125.8, 123.3, 75.8, 61.3, 53.2, 42.9, 39.9, 33.5, 14.1; Diastereomer B: ^1H NMR (400 MHz, CDCl_3) δ 7.47 – 7.41 (m, 2H), 7.01 (dd, $J = 8.7, 2.4$ Hz, 2H), 5.75 (d, $J = 9.7$ Hz, 1H), 4.32 – 4.08 (m, 2H), 3.90 – 3.74 (m, 1H), 3.32 (d, $J = 11.8$ Hz, 1H), 2.90 (d, $J = 14.1$ Hz, 1H), 2.64 (dd, $J = 14.1, 2.5$ Hz, 1H), 2.16 – 2.09 (m, 1H), 2.03 (dd, $J = 14.0, 12.1$ Hz, 1H), 1.33 – 1.24 (m, 3H); ^{13}C (100 MHz, CDCl_3) δ 202.1, 168.3, 142.4, 139.7, 133.1 (2C), 129.3 (2C), 125.8, 119.2, 75.8, 61.3, 53.2, 41.8, 38.0, 33.5, 14.1; Diastereomer C: ^1H NMR (400 MHz, CDCl_3) δ 7.47 – 7.41 (m, 2H), 7.01 (dd, $J = 8.7, 2.4$ Hz, 2H), 5.50 (d, $J = 9.8$ Hz, 1H), 4.32 – 4.08 (m, 2H), 3.90 – 3.74 (m, 1H), 3.32 (d, $J = 11.8$ Hz, 1H), 2.90 (d, $J = 14.1$ Hz, 1H), 2.64 (dd, $J = 14.1, 2.5$ Hz, 1H), 2.16 – 2.09 (m, 1H), 2.03 (dd, $J = 14.0, 12.1$ Hz, 1H), 1.33 – 1.24 (m, 3H); ^{13}C (100 MHz, CDCl_3) δ 202.1, 170.5, 142.4, 139.7, 133.1 (2C), 129.3 (2C), 125.8, 123.3, 75.8, 61.3, 53.2, 42.9, 39.9, 33.5, 14.1; HRESI-TOF m/z 420.0493 ($\text{C}_{17}\text{H}_{17}\text{Cl}_2\text{N}_3\text{O}_4 + \text{Na}^+$ requires 420.049).

Ethyl-4-(3-azidophenyl)-2-(2,2-dichlorovinyl)-4-hydroxy-6-oxocyclohexane-1-carboxylate (73):



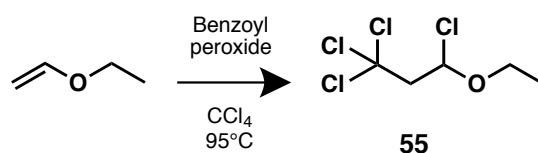
To a solution of dichlorovinyl chalcone **79** (0.097 mmol, 26 mg) in pure ethanol (4 mL) was added a 21% sodium ethoxide in ethanol solution (0.035 mmol, 13 μL) and ethyl acetoacetate (0.49 mmol, 65 μL). The reaction mixture was stirred

overnight in an ice bath and then quenched with a solution of saturated aqueous ammonium chloride and the aqueous layer was extracted with ethyl acetate. The organic layers were combined, washed with H₂O and saturated aqueous NaCl before being dried over Na₂SO₄ and filtered. The filtrate was concentrated *in vacuo* and purified by flash column chromatography (SiO₂, 1% methanol, 49% dichloromethane, 50% hexane) to yield **73** as a ~1:4:2 (A, B, C) diastereomeric mixture (19.8 mg, 51%). Orange amorphous solid. Diastereomer A: ¹H NMR (400 MHz, CDCl₃) δ 7.41 – 7.35 (m, 1H), 7.23 – 7.21 (m, 1H), 7.15 (dt, *J* = 13.8, 2.0 Hz, 1H), 7.02 – 6.98 (m, 1H), 5.92 (d, *J* = 8.8 Hz, 1H), 4.35 – 4.12 (m, 2H), 3.93 – 3.77 (m, 1H), 3.38 – 3.32 (m, 1H), δ 2.93 (d, *J* = 14.0 Hz, 1H), 2.67 (dd, *J* = 14.2, 2.6 Hz, 1H), 2.18 – 2.11 (m, 1H), 2.06 (dd, *J* = 14.1, 12.2 Hz, 1H), 1.36 – 1.25 (m, 3H); ¹³C (100 MHz, CDCl₃) δ 201.5, 168.1, 147.7, 140.7, 133.0, 130.2, 129.2, 120.7, 118.4, 115.2, 76.0, 61.5, 53.2, 42.9, 39.7, 33.4, 14.1; Diastereomer B: ¹H NMR (400 MHz, CDCl₃) δ 7.41 – 7.35 (m, 1H), 7.23 – 7.21 (m, 1H), 7.15 (dt, *J* = 13.8, 2.0 Hz, 1H), 7.02 – 6.98 (m, 1H), 5.77 (d, *J* = 9.7 Hz, 1H), 4.35 – 4.12 (m, 2H), 3.93 – 3.77 (m, 1H), 3.38 – 3.32 (m, 1H), δ 2.93 (d, *J* = 14.0 Hz, 1H), 2.67 (dd, *J* = 14.2, 2.6 Hz, 1H), 2.18 – 2.11 (m, 1H), 2.06 (dd, *J* = 14.1, 12.2 Hz, 1H), 1.36 – 1.25 (m, 3H); ¹³C (100 MHz, CDCl₃) δ 201.5, 168.1, 147.7, 140.7, 133.0, 130.2, 129.2, 120.7, 118.4, 115.2, 76.0, 61.5, 53.2, 41.8, 39.7, 33.4, 14.1; Diastereomer C: ¹H NMR (400 MHz, CDCl₃) δ 7.41 – 7.35 (m, 1H), 7.23 – 7.21 (m, 1H), 7.15 (dt, *J* = 13.8, 2.0 Hz, 1H), 7.02 – 6.98 (m, 1H), 5.58 (d, *J* = 9.7 Hz, 1H), 4.35 – 4.12 (m, 2H), 3.93 – 3.77 (m, 1H), 3.38 – 3.32 (m, 1H), δ 2.93 (d, *J* = 14.0 Hz, 1H), 2.67 (dd, *J* = 14.2, 2.6 Hz, 1H), 2.18 – 2.11 (m, 1H), 2.06 (dd, *J* = 14.1, 12.2 Hz, 1H), 1.36 – 1.25 (m, 3H); ¹³C (100 MHz, CDCl₃) δ 201.5, 168.1,

147.7, 140.7, 133.0, 130.2, 129.2, 120.7, 118.4, 115.2, 76.0, 61.5, 53.2, 41.8, 37.9, 33.4, 14.1; HRESI-TOF m/z 420.0494 ($C_{17}H_{17}Cl_2N_3O_4 + Na^+$ requires 420.049).

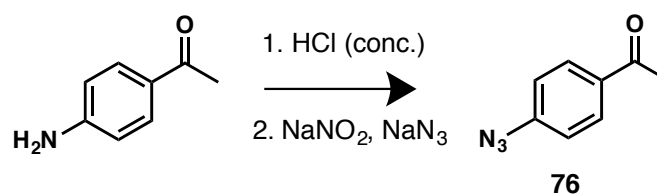
8.2. Synthesis of Dichlorovinyl Chalcones and Precursors

1,1,1,3-Tetrachloro-3-ethoxypropane (55):



A solution of dibenzoyl peroxide (245 mg, 1.01 mmol) in carbon tetrachloride (20 mL) was heated at 95°C for 30 min. Ethyl vinyl ether (9.04 g, 0.125 mol) was added dropwise to the reaction mixture and was stirred at 95°C for 4h. The crude reaction mixture was concentrated *in vacuo* and used without further purification. ^1H NMR (400 MHz, CCl_4 , crude) δ 5.96 (dt, $J = 7.3$ Hz, 1H), 4.04 – 3.94 (m, 1H), 3.69 – 3.60 (m, 1H), 3.53 (dd, $J = 15.2, 7.5$, 1H), 3.41 (d, $J = 14.6$ Hz, 1H), 1.30 (t, $J = 7.3$ Hz, 3H); ^{13}C (100 MHz, CCl_4 , crude) δ 95.0, 93.5, 66.6, 62.5, 14.5.

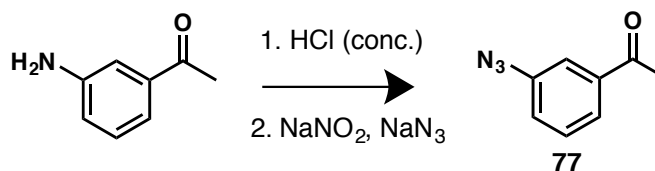
1-(4-Azidophenyl) ethan-1-one (76):



To a concentrated solution of HCl (6 mL, 11 N), 4-aminoacetophenone (4.30 mmol, 581 mg) was added and the reaction mixture was allowed to stir for 30 min. The reaction mixture was cooled in an ice bath and sodium nitrite (6.23 mmol, 430 mg) was added, followed by a solution of sodium azide (5.37 mmol, 349 mg) in distilled water (3 mL). The reaction mixture was extracted with toluene. The organic phase was washed with a saturated aqueous solution of NaHCO_3 followed by saturated aqueous solution of NaCl . After concentration *in vacuo* of the organic phase, the

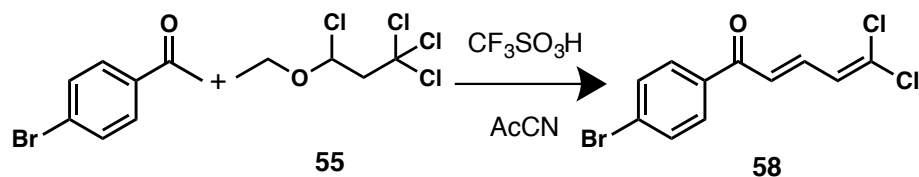
crude product was purified by flash column chromatography (SiO₂, 75% toluene in hexanes) to yield **76** as a light orange amorphous solid (568 mg, 82%). ¹H NMR (400 MHz, CDCl₃) δ 7.85 (d, *J* = 8.7 Hz, 2H), 6.96 (d, *J* = 8.3 Hz, 2H), 2.47 (s, 3H); ¹³C (100 MHz, CDCl₃) δ 196.3, 144.7, 133.7 (2C), 130.1 (2C), 118.8, 26.3.

1-(3-Azidophenyl) ethan-1-one (77):



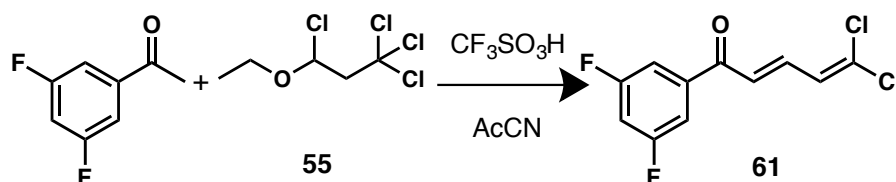
To a concentrated solution of HCl (6 mL, 11 N), 3-aminoacetophenone (3.7 mmol, 500 mg) was added and the reaction mixture was allowed to stir for 30 min. The reaction mixture was cooled in an ice bath and sodium nitrite (5.36 mmol, 370 mg) was added, followed by a solution of sodium azide (4.61 mmol, 300 mg) in distilled water (3 mL). The reaction mixture was extracted with toluene. The organic phase was washed with a saturated aqueous solution of NaHCO₃ followed by saturated aqueous solution of NaCl. After concentration *in vacuo* of the organic phase, the crude product was purified by flash column chromatography (SiO₂, 75% toluene in hexanes) to yield **77** as a light orange amorphous solid (471 mg, 79%). ¹H NMR (400 MHz, CDCl₃) δ 7.63 (d, *J* = 8.0 Hz, 1H), 7.50 (t, *J* = 1.8 Hz, 1H), 7.37 (t, *J* = 8.1 Hz, 1H), 7.12 (ddd, *J* = 8.0, 2.3, 0.9 Hz, 1H), 2.52 (s, 3H); ¹³C (100 MHz, CDCl₃) δ 196.9, 140.7, 138.5, 129.9, 124.8, 123.4, 118.3, 26.6.

(E)-1-(4-bromophenyl)-5,5-dichloropenta-2,4-dien-1-one (58):



To a solution of 4-bromoacetophenone (2.511 mmol, 500 mg) and crude **55** (2 mL) in acetonitrile (10 mL) at 0°C, was added dropwise trifluoromethanesulfonic acid (1.26 mmol, 116 μL). The reaction mixture was stirred for 2h and then quenched with a saturated aqueous solution of NaHCO_3 and concentrated *in vacuo*. The crude mixture was suspended in hexane and filtered through a silica plug. The filtrate was precipitated in acetonitrile to yield **58** as orange amorphous solid (509 mg, 66%). ^1H NMR (300 MHz, CDCl_3) δ 7.78 (d, $J = 8.5$ Hz, 2H), 7.60 (d, $J = 8.5$ Hz, 2H), 7.56 – 7.45 (m, 1H), 6.99 (d, $J = 15.2$ Hz, 1H), 6.67 (d, $J = 11.1$ Hz, 1H); ^{13}C (75 MHz, CDCl_3) δ 188.6, 137.6, 136.2, 132.0 (2C), 131.1 (2C), 129.9, 128.3, 127.5, 126.7.

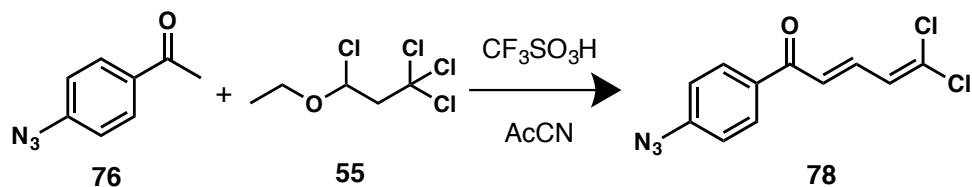
(E)-5,5-dichloro-1-(3,5-difluorophenyl) penta-2,4-dien-1-one (61):



To a solution of 3,5-difluoroacetophenone (0.64 mmol, 100 mg) and crude **55** (1.5 mL) in acetonitrile (8 mL) at 0°C, was added dropwise trifluoromethanesulfonic acid (0.51 mmol, 200 μL). The reaction mixture was stirred for 2h and then quenched with a saturated aqueous solution of NaHCO_3 and concentrated *in vacuo*. The crude mixture was suspended in hexane and filtered through a silica plug. The filtrate was precipitated in acetonitrile to yield **61** as yellow amorphous solid (132 mg, 79%). ^1H NMR (400 MHz, CDCl_3) δ 7.60 (dd, $J = 15.1, 11.1$ Hz, 1H), 7.41 –

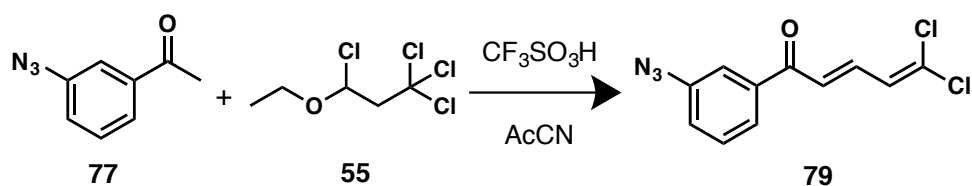
7.48 (m, 2H), 7.04 (tt, $J = 8.4, 2.4$ Hz, 1H), 6.95 (dd, $J = 15.1, 0.8$ Hz, 1H), 6.71 (dd, $J = 11.2, 0.8$ Hz, 1H); ^{13}C NMR (100 MHz, CDCl_3) δ 187.1, 164.3 (2C), 140.5, 138.5, 132.0, 127.3, 126.0, 111.5, 108.4 (2C).

(E)-1-(4-azidophenyl)-5,5-dichloropenta-2,4-dien-1-one (78):



To a solution of **76** (0.78 mmol, 125.71 mg) and crude **55** (2.5 mL) in acetonitrile (10 mL) at 0°C , was added dropwise trifluoromethanesulfonic acid (0.38 mmol, 150 μL). The reaction mixture was stirred for 2h and then quenched with a saturated aqueous solution of NaHCO_3 and concentrated *in vacuo*. The crude mixture was suspended in hexane and filtered through a silica plug. The filtrate was precipitated in acetonitrile to yield **78** as orange amorphous solid (127 mg, 61%). ^1H NMR (300 MHz, CDCl_3) δ 7.94 (d, $J = 8.5$ Hz, 2H), 7.53 (dd, $J = 15.1, 11.2$ Hz, 1H), 7.08 (d, $J = 8.8$ Hz, 2H), 7.02 (d, $J = 15.1$ Hz, 1H), 6.67 (d, $J = 11.2$ Hz, 1H); ^{13}C (75 MHz, CDCl_3) δ 187.8, 145.0, 137.2, 134.1 (2C), 130.7 (2C), 130.4, 127.5, 126.9, 119.1.

(E)-1-(3-azidophenyl)-5,5-dichloropenta-2,4-dien-1-one (79):



To a solution of **77** (0.35 mmol, 56.41 mg) and crude **55** (2 mL) in acetonitrile (7 mL) at 0°C , was added dropwise trifluoromethanesulfonic acid (0.20 mmol, 80 μL). The reaction mixture was stirred for 2h and then quenched with a saturated aqueous solution of NaHCO_3 and concentrated *in vacuo*. The crude mixture was suspended in hexane and filtered through a silica plug. The filtrate was precipitated in

acetonitrile to yield **79** as orange amorphous solid (52 mg, 55%). ^1H NMR (400 MHz, CDCl_3) δ 7.68 (ddd, $J = 7.7, 1.6, 1.0$ Hz, 1H), 7.60 – 7.58 (m, 1H), 7.57 (dd, $J = 15.0, 11.1$ Hz, 1H), 7.47 (t, $J = 7.8$ Hz, 1H), 7.23 (ddd, $J = 8.0, 2.4, 0.9$ Hz, 1H), 7.01 (dd, $J = 15.1, 0.8$ Hz, 1H), 6.70 (dd, $J = 11.1, 0.8$ Hz, 1H); ^{13}C (100 MHz, CDCl_3) δ 188.8, 141.1, 139.2, 137.8, 131.3, 130.1, 127.5, 126.8, 124.8, 123.5, 118.7.

References

-
- ¹ Gentry, E. J. (2012). Antibiotics and Antimicrobial Agents. Foye's Principles of Medicinal Chemistry: Wolters Kluwer Health., 1073-1124.
- ² Boucher, H. W., Talbot, G. H., Benjamin, D. K., Jr., Bradley, J., Guidos, R. J., Jones, R. N., Infectious Diseases Society of, A. (2013). 10 x '20 Progress--development of new drugs active against gram-negative bacilli: an update from the Infectious Diseases Society of America. *Clin. Infect. Dis.*, 56(12), 1685-1694.
- ³ Powers, J. H. (2004). Antimicrobial drug development--the past, the present, and the future. *Clin. Microbiol. Infect.*, 10 (Suppl 4), 23-31.
- ⁴ Center for Disease Dynamics, Economics & Policy. (2015). *State of the World's Antibiotics, 2015*. CDDEP: Washington, D.C.
- ⁵ Lewis, K. (2013). Platforms for antibiotic discovery. *Nat. Rev. Drug. Discov.*, 12(5), 371-387.
- ⁶ Baym, M., Stone, L. K., Kishony, R. (2016). Multidrug evolutionary strategies to reverse antibiotic resistance. *Science*, 351(6268), aad3292.
- ⁷ Yanling, J., Xin, L., Zhiyu, L. (2013). The Antibacterial Drug Discovery, Drug Discovery, Prof. Hany El-Shemy (Ed.), InTech, 289-307.
- ⁸ Aminov, R. I. (2010). A brief history of the antibiotic era: lessons learned and challenges for the future. *Front. Microbiol.*, 1, 134.
- ⁹ Wright, P. M., Seiple, I. B., Myers, A. G. (2014). The evolving role of chemical synthesis in antibacterial drug discovery. *Angew. Chem. Int. Ed. Engl.*, 53(34), 8840-8869.

¹⁰ Muciz C. C., Zelaya T. E. C., Esquivel G. R., Fernandez F. J. Penicillin and cephalosporin production: A historical perspective. *Rev. Latinoam. Microbiol.* 2007. Vol. 49. P. 88-98.

¹¹ O'Neill, J. (2016). Tackling Drug-Resistant Infections Globally: Final Report and Recommendations. *The Review on Antimicrobial Resistance*.

¹² Brown, D. (2015). Antibiotic resistance breakers: can repurposed drugs fill the antibiotic discovery void? *Nat. Rev. Drug. Discov.*, 14(12), 821-832.

¹³ Ruer, S., Pinotsis, N., Steadman, D., Waksman, G., Remaut, H. (2015). Virulence-targeted Antibacterials: Concept, Promise, and Susceptibility to Resistance Mechanisms. *Chem. Biol. Drug. Des.*, 86(4), 379-399.

¹⁴ Raju, R. M., Goldberg, A. L., Rubin, E. J. (2012). Bacterial proteolytic complexes as therapeutic targets. *Nat. Rev. Drug. Discov.*, 11(10), 777-789.

¹⁵ Turk, B. (2006). Targeting proteases: successes, failures and future prospects. *Nat. Rev. Drug. Discov.*, 5(9), 785-799.

¹⁶ Brotz-Oesterhelt, H., Sass, P. (2014). Bacterial caseinolytic proteases as novel targets for antibacterial treatment. *Int. J. Med. Microbiol.*, 304(1), 23-30.

¹⁷ Yu, A. Y., Houry, W. A. (2007). ClpP: a distinctive family of cylindrical energy-dependent serine proteases. *FEBS Lett.*, 581(19), 3749-3757.

¹⁸ Brotz-Oesterhelt, H., Beyer, D., Kroll, H. P., Endermann, R., Ladel, C., Schroeder, W., Labischinski, H. (2005). Dysregulation of bacterial proteolytic machinery by a new class of antibiotics. *Nat. Med.*, 11(10), 1082-1087.

¹⁹ Baker, T. A., Sauer, R. T. (2012). ClpXP, an ATP-powered unfolding and protein-degradation machine. *Biochim. Biophys. Acta.*, 1823(1), 15-28.

²⁰ Alexopoulos, J. A., Guarne, A., Ortega, J. (2012). ClpP: a structurally dynamic protease regulated by AAA+ proteins. *J. Struct. Biol.*, 179(2), 202-210.

-
- ²¹ Flynn, J. M., Neher, S. B., Kim, Y.-I., Sauer, R. T., Baker, T. A. (2003). Proteomic Discovery of Cellular Substrates of the ClpXP Protease Reveals Five Classes of ClpX-Recognition Signals. *Molecular Cell*, *11*(3), 671-683.
- ²² Kim, D. Y., Kim, K. K. (2003). Crystal structure of ClpX molecular chaperone from *Helicobacter pylori*. *J. Biol. Chem.*, *278*(50), 50664-50670.
- ²³ Kim, Y. I., Levchenko, I., Fraczkowska, K., Woodruff, R. V., Sauer, R. T., Baker, T. A. (2001). Molecular determinants of complex formation between Clp/Hsp100 ATPases and the ClpP peptidase. *Nat. Struct. Biol.*, *8*(3), 230-233.
- ²⁴ Martin, A., Baker, T. A., Sauer, R. T. (2007). Distinct static and dynamic interactions control ATPase-peptidase communication in a AAA+ protease. *Molecular Cell*, *27*(1), 41-52.
- ²⁵ Gersch, M., Famulla, K., Dahmen, M., Gobl, C., Malik, I., Richter, K., Sieber, S. A. (2015). AAA+ chaperones and acyldepsipeptides activate the ClpP protease via conformational control. *Nat. Commun.*, *6*, 6320.
- ²⁶ Kirstein, J., Hoffmann, A., Lilie, H., Schmidt, R., Rubsamen-Waigmann, H., Brotz-Oesterhelt, H., Turgay, K. (2009). The antibiotic ADEP reprogrammes ClpP, switching it from a regulated to an uncontrolled protease. *EMBO Mol. Med.*, *1*(1), 37-49.
- ²⁷ Goodreid, J. D., Janetzko, J., Santa Maria, J. P., Jr., Wong, K. S., Leung, E., Eger, B. T., Batey, R. A. (2016). Development and Characterization of Potent Cyclic Acyldepsipeptide Analogues with Increased Antimicrobial Activity. *J. Med. Chem.*, *59*(2), 624-646.
- ²⁸ Compton, C. L., Carney, D. W., Groomes, P. V., Sello, J. K. (2015). Fragment-Based Strategy for Investigating and Suppressing the Efflux of Bioactive Small Molecules. *ACS Infectious Diseases*, *1*(1), 53-58.

-
- ²⁹ Gominet, M., Seghezzi, N., Mazodier, P. (2011). Acyl depsipeptide (ADEP) resistance in *Streptomyces*. *Microbiology*, 157(Pt 8), 2226-2234.
- ³⁰ Goodreid, J. D., Janetzko, J., Santa Maria, J. P., Jr., Wong, K. S., Leung, E., Eger, B. T., Batey, R. A. (2016). Development and Characterization of Potent Cyclic Acyldepsipeptide Analogues with Increased Antimicrobial Activity. *J. Med. Chem.*, 59(2), 624-646.
- ³¹ Lavey, N. P., Coker, J. A., Ruben, E. A., Duerfeldt, A. S. (2016). Sclerotiamide: The First Non-Peptide-Based Natural Product Activator of Bacterial Caseinolytic Protease P. *J. Nat. Prod.*, 79(4), 1193-1197.
- ³² Gaillot, O., Pellegrini, E., Bregenholt, S., Nair, S., Berche, P. (2002). The ClpP serine protease is essential for the intracellular parasitism and virulence of *Listeria monocytogenes*. *Molecular Microbiology*, 35(6), 1286-1294.
- ³³ Robertson, G. T., Ng, W. L., Foley, J., Gilmour, R., Winkler, M. E. (2002). Global Transcriptional Analysis of *clpP* Mutations of Type 2 *Streptococcus pneumoniae* and Their Effects on Physiology and Virulence. *Journal of Bacteriology*, 184(13), 3508-3520.
- ³⁴ Frees, D., Qazi, S. N. A., Hill, P. J., Ingmer, H. (2003). Alternative roles of ClpX and ClpP in *Staphylococcus aureus* stress tolerance and virulence. *Molecular Microbiology*, 48(6), 1565-1578.
- ³⁵ Kirstein, J., Hoffmann, A., Lilie, H., Schmidt, R., Rubsamen-Waigmann, H., Brotz-Oesterhelt, H., Turgay, K. (2009). The antibiotic ADEP reprogrammes ClpP, switching it from a regulated to an uncontrolled protease. *EMBO Mol. Med.*, 1(1), 37-49.

-
- ³⁶ Bottcher, T., Sieber, S. A. (2009). Beta-lactones decrease the intracellular virulence of *Listeria monocytogenes* in macrophages. *ChemMedChem*, 4(8), 1260-1263.
- ³⁷ Bottcher, T., Sieber, S. A. (2008). Beta-lactones as specific inhibitors of ClpP attenuate the production of extracellular virulence factors of *Staphylococcus aureus*. *J. Am. Chem. Soc.*, 130(44), 14400-14401.
- ³⁸ Leung, E., Datti, A., Cossette, M., Goodreid, J., McCaw, S. E., Mah, M., Houry, W. A. (2011). Activators of cylindrical proteases as antimicrobials: identification and development of small molecule activators of ClpP protease. *Chem. Biol.*, 18(9), 1167-1178.
- ³⁹ Houry, W., Batey R., Cosette, M., Goodreid, J., Datti, A., Liu, J., Nhieu, A. J., Gray-Owen, S. D., Fai, E. F., Eger, B. T. (2012). Activators of Cylindrical Proteases. *US Patent 61,423,953*.
- ⁴⁰ Nhieu, A. (2014). Development of Small Molecule Activators of Caseinolytic Protease P. Retrieved from <http://hdl.handle.net/1807/65438>.
- ⁴¹ Huheey, J. E. (1966). The Electronegativity of Multiply Bonded Groups. *J. Phys. Chem.*, 70(7), 2086-2092.
- ⁴² Gilli, P., Pretto, L., Bertolasi, V., Gilli, G. (2009). Predicting hydrogen-bond strengths from acid-base molecular properties. The pK(a) slide rule: toward the solution of a long-lasting problem. *Acc. Chem. Res.*, 42(1), 33-44.
- ⁴³ Zhao, Y. H., Abraham, M. H., Zissimos, A. M. (2003). Fast calculation of van der Waals volume as a sum of atomic and bond contributions and its application to drug compounds. *J. Org. Chem.*, 68(19), 7368-7373.
- ⁴⁴ Jones, G. I. L., Owen, N. L. (1973). Molecular structure and conformation of carboxylic esters. *Journal of Molecular Structure*, 18(1), 1-32.

-
- ⁴⁵ Söderhjelm, P. (2009). A first-principles approach to protein–ligand interaction. <http://lup.lub.lu.se/record/1276785>.
- ⁴⁶ Du, X., Li, Y., Xia, Y. L., Ai, S. M., Liang, J., Sang, P., Liu, S. Q. (2016). Insights into Protein-Ligand Interactions: Mechanisms, Models, and Methods. *Int. J. Mol. Sci.*, 17(2).
- ⁴⁷ Chiu, S. H., Xie, L. (2016). Toward High-Throughput Predictive Modeling of Protein Binding/Unbinding Kinetics. *J. Chem. Inf. Model.*, 56(6), 1164-1174.
- ⁴⁸ Mahadevi, A. S., Sastry, G. N. (2016). Cooperativity in Noncovalent Interactions. *Chem. Rev.*, 116(5), 2775-2825.
- ⁴⁹ Bissantz, C., Kuhn, B., Stahl, M. (2010). A medicinal chemist's guide to molecular interactions. *J. Med. Chem.*, 53(14), 5061-5084.
- ⁵⁰ Gilson, M. K., Zhou, H. X. (2007). Calculation of protein-ligand binding affinities. *Annu. Rev. Biophys. Biomol. Struct.*, 36, 21-42.
- ⁵¹ Young, D. C. (2009). Docking. *Computational Drug Design: A Guide for Computational and Medicinal Chemists*, 133-160.
- ⁵² Trott, O., Olson, A. J. (2010). AutoDock Vina: improving the speed and accuracy of docking with a new scoring function, efficient optimization, and multithreading. *J. Comput. Chem.*, 31(2), 455-461.
- ⁵³ Forli, S., Huey, R., Pique, M. E., Sanner, M. F., Goodsell, D. S., Olson, A. J. (2016). Computational protein-ligand docking and virtual drug screening with the AutoDock suite. *Nat. Protoc.*, 11(5), 905-919.
- ⁵⁴ Michel F. Sanner, M. F. (1999). Python: A Programming Language for Software Integration and Development. *J. Mol. Graphics Mod.*, 1999, Vol 17(1), 57-61.

⁵⁵ Friesner, R. A., Banks, J. L., Murphy, R. B., Halgren, T. A., Klicic, J. J., Mainz, D. T., Shenkin, P. S. (2004). Glide: a new approach for rapid, accurate docking and scoring. 1. Method and assessment of docking accuracy. *J. Med. Chem.*, 47(7), 1739-1749.

⁵⁶ Halgren, T. A., Murphy, R. B., Friesner, R. A., Beard, H. S., Frye, L. L., Pollard, W. T., Banks, J. L. (2004). Glide: a new approach for rapid, accurate docking and scoring. 2. Enrichment factors in database screening. *J. Med. Chem.*, 47(7), 1750-1759.

⁵⁷ Friesner, R. A. M., Repasky, M. P., Frye, L. L., Greenwood, J. R., Halgren, T. A., Sanschagrin, P. C., Mainz, D. T. (2006). Extra Precision Glide: Docking and Scoring Incorporating a Model of Hydrophobic Enclosure for Protein-Ligand Complexes. *J. Med. Chem.*, 49(21), 6177–6196.

⁵⁸ Ribas, J., Cubero, E., Luque, F. J., Orozco, M. (2002). Theoretical Study of Alkyl- π and Aryl- π Interactions. Reconciling Theory and Experiment. *J. Org. Chem.*, 67(20), 7057-7065.

⁵⁹ Tsuzuki, S., Honda, K., Uchimaru, T., Mikami, M., Tanabe, K. (2002). Origin of Attraction and Directionality of the π/π Interaction: Model Chemistry Calculations of Benzene Dimer Interaction. *J. Am. Chem. Soc.*, 124(1), 104-112.

⁶⁰ Wilcken, R., Zimmermann, M. O., Lange, A., Joerger, A. C., Boeckler, F. M. (2013). Principles and applications of halogen bonding in medicinal chemistry and chemical biology. *J. Med. Chem.*, 56(4), 1363-1388.

⁶¹ Hardegger, L. A., Kuhn, B., Spinnler, B., Anselm, L., Ecabert, R., Stihle, M., Diederich, F. (2011). Halogen bonding at the active sites of human cathepsin L and MEK1 kinase: efficient interactions in different environments. *ChemMedChem*, 6(11), 2048-2054.

-
- ⁶² Sirimulla, S., Bailey, J. B., Vegesna, R., Narayan, M. (2013). Halogen interactions in protein-ligand complexes: implications of halogen bonding for rational drug design. *J. Chem. Inf. Model.*, 53(11), 2781-2791.
- ⁶³ Panini, P., Chopra, D. (2015). Understanding of Noncovalent Interactions Involving Organic Fluorine. *Lecture Notes in Chemistry*, 87, 37-67.
- ⁶⁴ Dunitz, J. D., Taylor, R. (1997). Organic fluorine hardly ever accepts hydrogen bonds. *Chem. Eur. J.*, 3(1), 89-98.
- ⁶⁵ Imai, Y. N., Inoue, Y., Nakanishi, I., Kitaura, K. (2008). Cl- π interactions in protein-ligand complexes. *Protein Sci.*, 17(7), 1129-1137.
- ⁶⁶ Jeffrey, G. A., Takagi, S. (1978). Hydrogen-bond structure in carbohydrate crystals. *Acc. Chem. Res.*, 11(7), 264-270.
- ⁶⁷ Fukui, K. (1982). Role of frontier orbitals in chemical reactions. *Science*, 218(4574), 747-754.
- ⁶⁸ Fujimoto, H., Inagaki, S., Fukui, K. (1976). On the donor-acceptor relationship in cyclic additions. *J. Am. Chem. Soc.*, 98(9), 2670-2671.
- ⁶⁹ (a) Arooj, M., Thangapandian, S., John, S., Hwang, S., Park, J. K., Lee, K. W. (2011). 3D QSAR pharmacophore modeling, in silico screening, and density functional theory (DFT) approaches for identification of human chymase inhibitors. *Int. J. Mol. Sci.*, 12(12), 9236-9264; (b) Raya, A., Barrientos-Salcedo, C., Rubio-Poo, C., Soriano-Correa, C. (2011). Electronic structure evaluation through quantum chemical descriptors of 17 β -aminoestrogens with an anticoagulant effect. *Eur. J. Med. Chem.*, 46(6), 2463-2468; (c) Banavath, H. N., Sharma, O. P., Kumar, M. S., Baskaran, R. (2014). Identification of novel tyrosine kinase inhibitors for drug resistant T315I mutant BCR-ABL: a virtual screening and molecular dynamics simulations study. *Sci. Rep.*, 4, 6948; (d) de Carvalho, L.

L., Maltarollo, V. G., de Lima, E. F., Weber, K. C., Honorio, K. M., da Silva, A. B. (2014). Molecular features related to HIV integrase inhibition obtained from structure- and ligand-based approaches. *PLoS One*, 9(1), e81301.

⁷⁰ (a) Zheng, Y., Zheng, M., Ling, X., Liu, Y., Xue, Y., An, L., Ji, M. (2013). Design, synthesis, quantum chemical studies and biological activity evaluation of pyrazole-benzimidazole derivatives as potent Aurora A/B kinase inhibitors. *Bioorg. Med. Chem. Lett.*, 23(12), 3523-3530; (b) Matysiak, J. (2007). Evaluation of electronic, lipophilic and membrane affinity effects on antiproliferative activity of 5-substituted-2-(2,4-dihydroxyphenyl)-1,3,4-thiadiazoles against various human cancer cells. *Eur. J. Med. Chem.*, 42(7), 940-947; (c) Jesudason, E. P., Sridhar, S. K., Malar, E. J., Shanmugapandiyan, P., Inayathullah, M., Arul, V., Jayakumar, R. (2009). Synthesis, pharmacological screening, quantum chemical and in vitro permeability studies of N-Mannich bases of benzimidazoles through bovine cornea. *Eur. J. Med. Chem.*, 44(5), 2307-2312.

⁷¹ X. Pang, L. Z., Lily Zhang, L. Xu, X. Zhang. (2008). Two Rules on the Protein-Ligand Interaction. *Nature Precedings*.

⁷² Gaussian 09, M. J. Frisch, G. W. Trucks, H. B. Schlegel, G. E. Scuseria, M. A. Robb, J. R. Cheeseman, G. Scalmani, V. Barone, B. Mennucci, G. A. Petersson, H. Nakatsuji, M. Caricato, X. Li, H. P. Hratchian, A. F. Izmaylov, J. Bloino, G. Zheng, J. L. Sonnenberg, M. Hada, M. Ehara, K. Toyota, R. Fukuda, J. Hasegawa, M. Ishida, T. Nakajima, Y. Honda, O. Kitao, H. Nakai, T. Vreven, J. A. Montgomery, Jr., J. E. Peralta, F. Ogliaro, M. Bearpark, J. J. Heyd, E. Brothers, K. N. Kudin, V. N. Staroverov, R. Kobayashi, J. Normand, K. Raghavachari, A. Rendell, J. C. Burant, S. S. Iyengar, J. Tomasi, M. Cossi, N. Rega, J. M. Millam, M. Klene, J. E. Knox, J. B. Cross, V. Bakken, C. Adamo, J. Jaramillo, R. Gomperts,

R. E. Stratmann, O. Yazyev, A. J. Austin, R. Cammi, C. Pomelli, J. W. Ochterski, R. L. Martin, K. Morokuma, V. G. Zakrzewski, G. A. Voth, P. Salvador, J. J. Dannenberg, S. Dapprich, A. D. Daniels, Ö. Farkas, J. B. Foresman, J. V. Ortiz, J. Cioslowski, D. J. Fox, Gaussian, Inc., Wallingford CT, 2009.

⁷³ a) Zhao, Y., Truhlar, D. G. (2006). A new local density functional for main-group thermochemistry, transition metal bonding, thermochemical kinetics, and noncovalent interactions. *J. Chem. Phys.*, 125(19), 194101; b) Weigend, F., Ahlrichs, R. (2005). Balanced basis sets of split valence, triple zeta valence and quadruple zeta valence quality for H to Rn: Design and assessment of accuracy. *Phys. Chem. Chem. Phys.*, 7(18), 3297-3305; c) Kozuch, S., Martin, J. M. (2013). Halogen Bonds: Benchmarks and Theoretical Analysis. *J. Chem. Theory Comput.*, 9(4), 1918-1931.

⁷⁴ Woznesensky, S. A., Dudinov, A. A., Belenkii, L. I., Struchkova, M. I., Nesterov, V. N., Krayushkin, M. M., Struchkov, Y. T. (1997). Synthesis of carbonyl compounds based on the products of addition of polyhaloalkanes to unsaturated systems. Reactions of 1-aryl-5,5-dichloropenta-2,4-dien-1-ones with ethyl acetoacetate. *Russian chemical bulletin*, 46(3), 501-506.

⁷⁵ Arendorf, J. R. T.; (2011) A study of some non-covalent functional group π interactions. Doctoral thesis, UCL (University College London).

⁷⁶ Martinez, C. R., Iverson, B. L. (2012). Rethinking the term “pi-stacking”. *Chemical Science*, 3(7), 2191-2201.

⁷⁷ Imai, Y. N., Inoue, Y., Nakanishi, I., Kitaura, K. (2008). Cl- π interactions in protein-ligand complexes. *Protein Sci.*, 17(7), 1129-1137.

⁷⁸ Ramasubbu, N., Parthasarathy, R., Murray-Rust, P. (1986). Angular preferences of intermolecular forces around halogen centers: preferred directions

of approach of electrophiles and nucleophiles around carbon-halogen bond. *J. Am. Chem. Soc.*, 108(15), 4308-4314.

⁷⁹ Swierczynski, D., Luboradzki, R., Dolgonos, G., Lipkowski, J., Schneider, H.-J. (2005). Non-Covalent Interactions of Organic Halogen Compounds with Aromatic Systems – Analyses of Crystal Structure Data. *Eur. J. Org. Chem.*, 2005(6), 1172-1177.

⁸⁰ Topliss, J. G. (1972). Utilization of operational schemes for analog synthesis in drug design. *J. Med. Chem.*, 15(10), 1006-1011.

⁸¹ Hinzen, B., Raddatz, S., Paulsen, H., Lampe, T., Schumacher, A., Habich, D., Brotz-Oesterhelt, H. (2006). Medicinal chemistry optimization of acyldepsipeptides of the enopeptin class antibiotics. *ChemMedChem*, 1(7), 689-693.

⁸² Kazius, J., McGuire, R., Bursi, R. (2005). Derivation and validation of toxicophores for mutagenicity prediction. *J. Med. Chem.*, 48(1), 312-320.

⁸³ Barlow, R. B., Bremner, J. B., & Soh, K. S. (1978). The Effects of Replacing Ester by Amide on the Biological Properties of Compounds Related to Acetylcholine. *British Journal of Pharmacology*, 62(1), 39-50.

⁸⁴ McGrath, N. A., Raines, R. T. (2011). Chemoselectivity in chemical biology: acyl transfer reactions with sulfur and selenium. *Acc. Chem. Res.*, 44(9), 752-761.

⁸⁵ Prasad, C. V., Sundaram, K. (1979). On the polarity of the amide group and its impact on dipeptide conformation. *Int. J. Quant. Chem.*, 15(6), 783-792.

⁸⁶ Schroth, W. S., D., Jahn, U., Spitzner, R. (1989). Eine vereinfachte Herstellung von Bis(2,2-dichloro-vinyl)keton. *Z. Chem*, 29.

⁸⁷ Chun, J., Li, G., Byun, H.-S., Bittman, R. (2002). Synthesis of New Trans Double-Bond Sphingolipid Analogues: $\Delta^4,6$ and Δ^6 Ceramides. *J. Org. Chem.*, 67(8), 2600-2605.

⁸⁸ Fu, X., Zhang, S., Yin, J., McAllister, T. L., Jiang, S. A., Tann, C.-H., Zhang, F. (2002). First examples of a tosylate in the palladium-catalyzed Heck cross coupling reaction. *Tetrahedron Letters*, 43(4), 573-576.

⁸⁹ Gogsig, T. M., Sobjerg, L. S., Lindhardt, A. T., Jensen, K. L., Skrydstrup, T. (2008). Direct vinylation and difluorovinylation of arylboronic acids using vinyl- and 2,2-difluorovinyl tosylates via the Suzuki-Miyaura cross coupling. *J. Org. Chem.*, 73(9), 3404-3410.

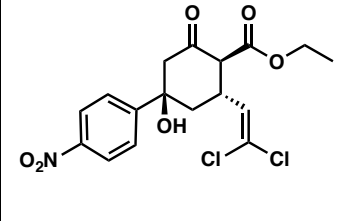
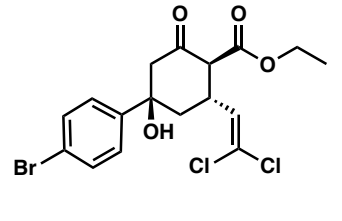
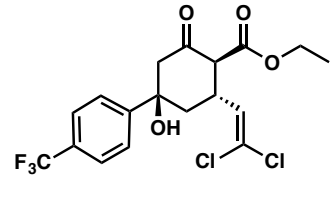
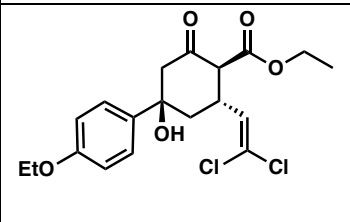
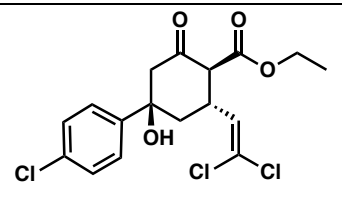
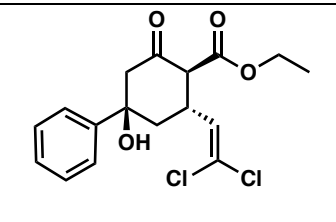
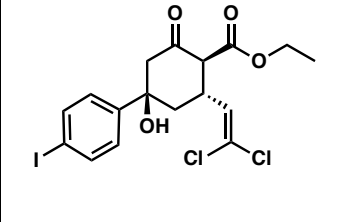
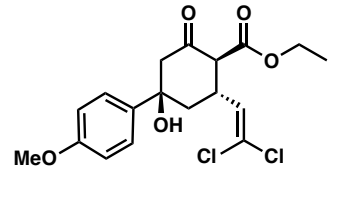
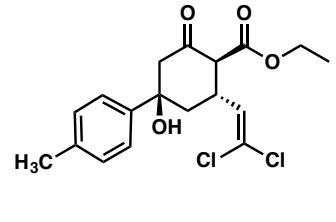
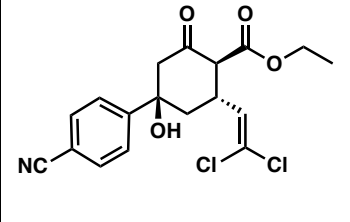
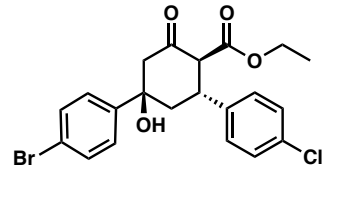
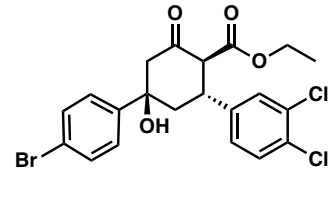
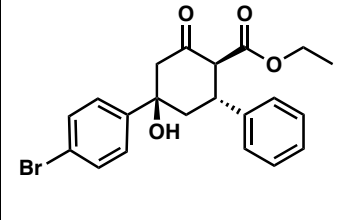
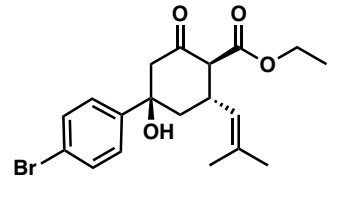
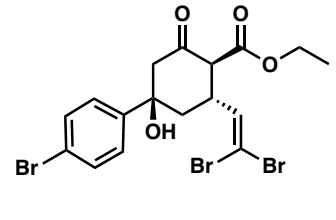
⁹⁰ Sumranjit, J., Chung, S. J. (2013). Recent advances in target characterization and identification by photoaffinity probes. *Molecules*, 18(9), 10425-10451.

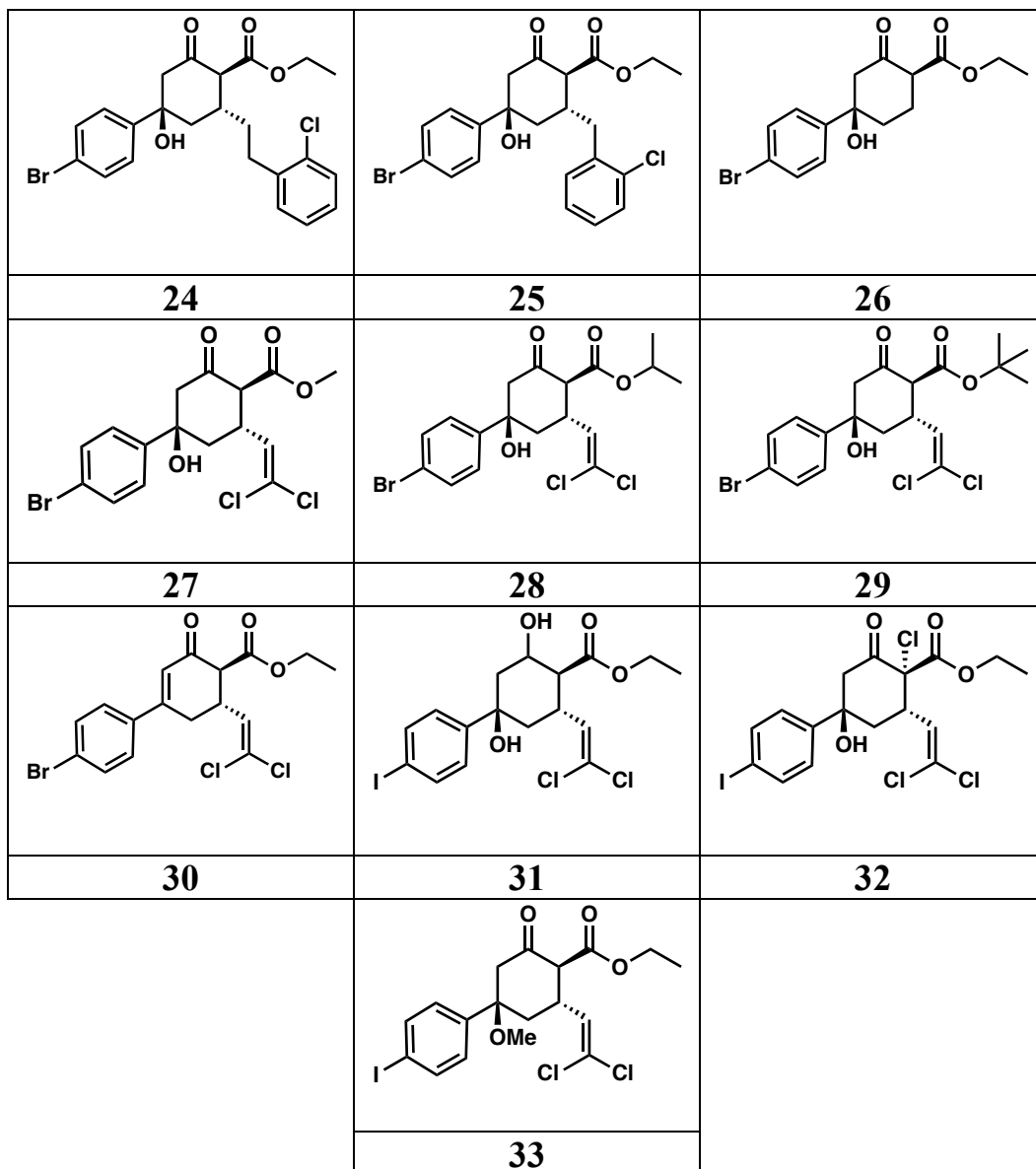
⁹¹ Sadakane, Y., Hatanaka, Y. (2006). Photochemical Fishing Approaches for Identifying Target Proteins and Elucidating the Structure of a Ligand-binding Region Using Carbene-generating Photoreactive Probes. *Analytical Sciences*, 22(2), 209-218.

⁹² Voskresenska, V., Wilson, R. M., Panov, M., Tarnovsky, A. N., Krause, J. A., Vyas, S., Hadad, C. M. (2009). Photoaffinity labeling via nitrenium ion chemistry: protonation of the nitrene derived from 4-amino-3-nitrophenyl azide to afford reactive nitrenium ion pairs. *J. Am. Chem. Soc.*, 131(32), 11535-11547.

⁹³ Zhu, W., Ma, D. (2004). Synthesis of aryl azides and vinyl azides via proline-promoted CuI-catalyzed coupling reactions. *Chem. Commun.*, 7, 888-889.

Appendix
Compound key

		
6	7	11
		
12	13	14
		
15	16	17
		
18	19	20
		
21	22	23



Spectral Data for All Identified Compounds and Intermediates

